Multiphysics Performance and Safety Analysis for High Temperature Advanced Reactors

A Dissertation Presented for the
Doctor of Philosophy
Degree
The University of Tennessee, Knoxville

Edward Matthew Duchnowski
December 2023

Copyright © 2023 by Edward Matthew Duchnowski
All rights reserved.

DEDICATION

This dissertation is dedicated to my father, Edward Duchnowski Jr., and my mother, Krystina Duchnowska, who immigrated from Poland to provide me and my siblings with an opportunity for a prosperous life.

ACKNOWLEDGEMENTS

I would like to thank my advisor Professor Nicholas Brown for tremendous support and mentorship throughout my years in graduate school. I would also like to thank my committee members, Professor Jason Trelewicz, Professor Brian Wirth, and Professor Vladimir Sobes, for all of their invaluable feedback and guidance during the graduate process. Thank you to Dr. Gerhard Strydom, Dr. Aaron Epiney, Dr. Bin Cheng, Dr. Xunxiang Hu, Professor Lance Snead, Dr. Volkan Seker, and Professor Tomas Downar for the insightful discussions and information on the technical aspects of this work. I would like to thank all of my collaborators and colleagues, Dr. Nader Satvat, Dr. Jacob Gorton, Dr. Robert Kile, Dr. Veronica Karriem, Khian Skidmore, and Kenny Bott, for their contributions. Finally, I would like to express my gratitude for all of the support from my family and friends during my time in graduate school.

ABSTRACT

A global initiative on mitigating the use of fossil fuels and transitioning to a more sustainable and cleaner energy source has brought the potential of nuclear energy to the forefront of the conversation. The modular, high temperature, particle fueled reactor platform has become the leading candidate for advanced nuclear reactors because of its robust safety features, enhanced fuel utilization, and the potential of high-quality heat for industrial applications. This particular reactor platform may take on various forms depending on the specific application, but all designs are centered around the use of particle fuel embedded into a solid moderating material and operate at a considerably higher temperature than more conventional nuclear reactors. The particular reactor concepts that are presented in this dissertation are 1) prismatic high temperature gas cooled microreactors, 2) pebble bed fluoride salt cooled high temperature reactors, and 3) pebble bed high temperature gas cooled reactors. The goals and approaches on the various studies for these concepts differ but each study has the underlying theme of evaluating performance and safety to enhance the knowledge of various high temperature reactor technologies/concepts through the use of multiphysics assessment for the enhancement of nuclear power safety, competitiveness, and efficiency.

Results from these studies demonstrate the performance and safety potential of various high temperature reactor concepts as well as highlight some areas for modeling development. A preconceptual high temperature gas cooled microreactor was developed to provide a basis for comparing moderators alternative to graphite for the objective of enhancing reactor performance without compromising safety. The results from the microreactor study demonstrated the higher reactor performance of two-phase composite

moderators relative to the industry standard, graphite without compromising intrinsic safety features. A coupled reactor physics and thermal-hydraulics model was used to assess the safety response for a generic pebble bed fluoride salt cooled pebble bed reactor under a set of different transient conditions, demonstrating the resilience of the reactor concept to accidents. Finally, the severe accident and consequence modeling code, MELCOR, was used for verification and validation of steady state and transient conditions for a high temperature gas cooled pebble bed reactor.

TABLE OF CONTENTS

CHAPTER 1 INTRODUCTION 1
1.1 High Temperature Advanced Reactors 1
1.2 Motivation and Key Questions to Answer 3
1.3 Contributions and Outline 7
CHAPTER 2 LITERATURE REVIEW 10
2.1 High Temperature Gas Cooled Microreactors 10
2.2.1 BWX Technologies, Incorporated 12
2.2.2 X-energy, LLC 13
2.2.3 Ultra Safe Nuclear Corporation 14
2.2.4 HolosGen, LLC 14
2.2 Two-phase Composite Moderators 15
2.3 Fluoride Salt Cooled Reactors 19
2.3 Pebble Bed High Temperature Reactors 22
2.4 Computational Simulating Tools for High Temperature Advanced Reactors 27
CHAPTER 3 TWO-PHASE COMPOSITE MODERATOR HIGH TEMPERATURE GAS COOLED MICROREACTOR: DESIGN AND NEUTRONICS PERFORMANCE 31
3.1 Motivation for Microreactors 31
3.2 Design Constraints, Launching Point, and Coarse Changes 33
3.3 Neutronics Model 38
3.3.1 Fuel Type 38
3.3.2 Moderators and Assembly 42
3.3.3 Reactor Core 44
3.4 Lattice Pitch Study 44
3.5 Power Study 60
3.6 Natural Resource Utilization and Fuel Cycle Cost 65
3.7 Discussion 71
CHAPTER 4 74
TWO-PHASE COMPOSITE MODERATOR HIGH TEMPERATURE GAS COOLED MICROREACTOR: SAFETY CHARACTERISTICS AND THERMAL-HYDRAULIC DESIGN SPACE 74
4.1 Motivation for Design Space and Safety Analysis 74
4.2 Thermal-Hydraulic Model 75
4.3 Design Space 85
4.4 Reactivity Temperature Coefficient 99
4.5 Emergency Planning Zone 100
4.6 Depressurized Loss of Forced Coolant 107
4.7 Discussion 114
CHAPTER 5 117
NEUTRONIC AND THERMAL-HYDRAULIC CALCULATIONS UNDER STEADY STATE AND TRANSIENT CONDITIONS FOR A GENERIC PBBLE BED FLUORIDE SALT COOLED HIGH TEMPERATURE REACTOR 117
5.1 Background 117

5.2 Model Development 119
5.2.1 The generic FHR 120
5.2.2 Serpent Model 124
5.2.3 KP-AGREE Model 129
5.3 Steady State Results 135
5.3.1 Standalone Neutronics 137
5.3.1 Steady State Coupled Neutronics and Thermal-Hydraulics 146
5.4 Transient Results 151
5.4.1 Loss of Flow Accident 151
5.4.2 Overcooling 156
5.4.3 Control Rod Withdrawal 159
5.5 Discussion 162
CHAPTER 6 166
VERIFICATION AND VALIDATION OF MELCOR FOR THE HTR-10 STEADY STATE AND TRANSIENT BENCHMARK 166
6.1 Background 166
6.1 HTR-10 Design Description and Benchmark Problem 168
6.3 The MELCOR Model 173
6.3 Steady State Results 183
6.4 Transient Results 185
6.4.1 Pressurized Loss of Forced Coolant 191
6.4.2 Control Rod Withdrawal 194
6.4 Discussion 197
CHAPTER 7 CONCLUSION 200
7.1 Microreactor Performance 200
7.2 Microreactor Safety and Design Space 201
7.3 Multiphysics Modeling of a Pebble Bed Fluoride Salt Cooled Reactor 203
7.4 Verification and Validation of MELCOR for the HTR-10 Steady State and Transient Benchmark 204
7.5 Review of Key Questions 205
References 209
VITA 221

LIST OF TABLES

Table 1. High temperature pebble bed reactor concepts 25
Table 2. Constraints inspired by Project Pele [90] 34
Table 3. Justification of minimal micro assembly size based on Figure 7 41
Table 4. Summary of AGR TRISO fuel, FCM TRISO fuel used for this study 43
Table 5. Volume fraction of considered moderating materials 45
Table 6. Unchanged parameters of fuel assembly within this study [22] 46
Table 7. Unchanged parameters of the reactor core within this study 47
Table 8. Costs associated with TRISO fuel fabrications [106] 69
Table 9. List of components for the nodalization diagram. 82
Table 10. Sources for thermophysical properties of the moderators. 87
Table 11. Upper and lower bounds of parameters used for identifying the design space. 88
Table 12. Constraints applied to the design space. 89
Table 13. Key isotopes contributing to EPZ size. 105
Table 14. Key parameters of the gFHR used in generating the multiphysics models [18] 122
Table 15. Thermophysical properties used in the KP-AGREE model 136
Table 16. 2, 4, and 7 energy group structures [84] [169] 139
Table 17. Predicted k_{eff} and power profile comparison in KP-AGREE to Serpent for various energy group structures. Fuel temperature set to 959 K and all other component temperatures set to 900 K. *Serpent reference k_{eff} is 1.01467± 0.00091 142
Table 18. k_{eff} and reactivity temperature coefficients between Serpent, KP-AGREE with 7 energy groups and benchmark reference [20]. Fuel temperature set to 959 K and all other component temperatures set to 900 K 144
Table 19. Design feature of the HTR-10 [64] 171
Table 20. Zones in conduction model [182] 174
Table 21. Zones in Convection model [182] 175
Table 22. Power profile for the CRP-5 HTR-10 in W/cc [182] 176
Table 23. RMSE between measure and calculated side reflector temperatures for CRP-5 participants and this study. Ranked from lowest to highest RMSE. 187
Table 24. RMSE between measure and calculated nominal power during the first 300 seconds of the PLOFC for CRP-5 participants and this study. Ranked from lowest to highest RMSE 193
Table 25. RMSE between measure and calculated nominal power during the first 300 seconds of the CRW for CRP-5 participants and this study. Ranked from lowest to highest RMSE 196

LIST OF FIGURES

Figure 1. Illustration of two-phase composite moderator [37] 17
Figure 2. The AVR [58] (left) and the MK1 PB-FHR (right) [66] 24
Figure 3. a) A typical TRISO particle b) the fuel form for the HTR-10 [77] c) the fuel form for the PB-FHR-Mk1 [78] 28
Figure 4. Considered designs in the HTGTR [89]. Red solid box for the selected launching point and the blue dashed line for the HTGTR design 36
Figure 5. Size reduction of launching point design. 37
Figure 6. Assembly and microreactor images of traditional Fort St. Vrain style fuel assembly and proposed micro fuel assembly 39
Figure 7. Image of micro assembly highlighted regions. (Blue circles for coolant pins, smaller green circles for fuel pins, and surrounding gray region for moderating material.) 40
Figure 8. Radial (left) and axial (right) groupings of assemblies. 48
Figure 9. Contour plots of cycle length in EFPY of graphite microreactor design fueled with UCO TRISO (left) and UN TRISO (right) for various TRISO packing fraction and lattice pitch 51
Figure 10. Contour plots of cycle length in EFPY of MgO BeO (60/40) microreactor design fueled with UCO TRISO (left) and UN TRISO (right) for various TRISO packing fraction and lattice pitch 52
Figure 11. Contour plots of cycle length in EFPY of MgO Be (60/40) microreactor design fueled with UCO TRISO (left) and UN TRISO (right) for various TRISO packing fraction and lattice pitch 53
Figure 12. Contour plots of cycle length in EFPY of MgO $YH_{x=1.9}$ (85/15) microreactor design fueled with UCO TRISO (left) and UN TRISO (right) for various TRISO packing fraction and lattice pitch 54
Figure 13. Contour plots of cycle length in EFPY of MgO $ZrH_{x=1.6}$ (85/15) microreactor design fueled with UCO TRISO (left) and UN TRISO (right) for various TRISO packing fraction and lattice pitch 55
Figure 14. Contour plots of discharge burnup in units of MWdays/kgU of graphite microreactor design fueled with UN TRISO for various TRISO packing fraction and lattice pitch 57
Figure 15. Contour plots of discharge burnup in units of MWdays/kgU of MgO BeO (60/40) (left) and MgO Be (60/40) (right) fueled with UN TRISO for various TRISO packing fraction and lattice pitch 58
Figure 16. Contour plots of discharge burnup in units of MWdays/kgU of MgO $YH_{x=1.9}$ (85/15) (left) MgO $ZrH_{x=1.6}$ (85/15) (right) fueled with UN TRISO for various TRISO packing fraction and lattice pitch 59
Figure 17. Contour plots of cycle length in EFPY for the graphite microreactor design fueled with UCO TRISO for various TRISO packing fraction and core power 61
Figure 18. Contour plots of cycle length in EFPY for the MgO BeO (60/40) (left) and MgO Be (60/40)(right) microreactor designs fueled with UN TRISO for various TRISO packing fraction and core power 62

Figure 19. Contour plots of cycle length in EFPY for the MgO $YH_{x=1.9}$ (85/15) (left) and MgO $ZrYH_{x=1.6}$ (60/40) (right) microreactor designs fueled with UN TRISO for various TRISO packing fraction and core power 63
Figure 20. Cycle length in EFPY for all considered microreactor designs at a core power of 6MW and UN TRISO packing fraction of 0.50 67
Figure 21. Natural resource utilization in t/GW-year for all considered microreactor designs at a core power of 6MW and UN TRISO packing fraction of 0.50..... 68
Figure 22. Calculated fuel cycle costs in millions of dollars per GW-year for all considered microreactor designs at a core power of 6MW and UN TRISO packing fraction of 0.50..... 72
Figure 23. Radial (left) and axial (right) groupings of assemblies. 76
Figure 24. Fractional power distribution for each ring at each axial level for the graphite moderated microreactor with a UN TRISO packing fraction of 0.50..... 78
Figure 25. Fractional power distribution for each ring at each axial level for the MgO BeO (60/40) (left) and MgO Be (60/40) (right) moderated microreactor with a UN TRISO packing fraction of 0.50..... 79
Figure 26. Fractional power distribution for each ring at each axial level for the MgO $YH_{x=1.9}$ (85/15) (left) and MgO $ZrH_{x=1.6}$ (85/15) (right) moderated microreactor with a UN TRISO packing fraction of 0.50. 80
Figure 27 Nodalization of the microreactor design. 81
Figure 28. Thermal conductivity (left) and volumetric heat capacity (right) of FCM TRISO with 0.5 TRISO packing fraction. 84
Figure 29. Thermal conductivity (left) and volumetric heat capacity (right) of moderating materials. 86
Figure 30. Calculated coolant temperature differential and coolant mass flow rate for a given power for the graphite moderated microreactor..... 92
Figure 31 Calculated coolant temperature differential and coolant mass flow rate for a given power for the MgO BeO (60/40) (top) and MgO Be (60/40) (bottom) moderated microreactors..... 93
Figure 32. Calculated coolant temperature differential and coolant mass flow rate for a given power for the MgO $YH_{x=1.9}$ (85/15) (top) and MgO $ZrH_{x=1.6}$ (85/15) (bottom) moderated microreactors..... 94
Figure 33. Steady state temperature distribution for the graphite moderated microreactor. 96
Figure 34. Steady state temperature distribution for the MgO BeO (60/40) (left) and MgO Be (60/40) (right) moderated microreactor. 97
Figure 35. Steady state temperature distribution for the MgO $YH_{x=1.9}$ (60/40) (left) and MgO $ZrH_{x=1.6}$ (60/40) (right) moderated microreactor. 98
Figure 36. MTC as a function of burnup for all considered cases with a 0.50 TRISO packing fraction displayed for the entire range of burnup (left) and for the first 10 MW-day/kgU (right). 101
Figure 37. FTC as a function of burnup for all considered cases with a 0.50 TRISO packing fraction displayed for the entire range of burnup (left) and for the first 10 MW-day/kgU (right). 102

Figure 38. Total activity in units of millicurie of key isotopes contributing to EPZ size. 106
Figure 39. Contour plot of EPZ size for the graphite moderated microreactor at $6MW_{th}$ core power and 0.5 UN TRISO packing fraction for various levels of Nobel Gas and iodine mitigation. 108
Figure 40. Contour plot of EPZ size for the MgO BeO (60/40) (left) and MgO Be (60/40) (right) moderated microreactor at 6 MW_{th} core power and 0.5 UN TRISO packing fraction for various levels of Nobel Gas and iodine mitigation. 109
Figure 41. Contour plot of EPZ size for the MgO $YH_{x=1.9}$ (85/15) (left) and MgO $ZrH_{x=1.6}$ (85/15) (right) moderated microreactor at $6MW_{th}$ core power and 0.5 UN TRISO packing fraction for various levels of Nobel Gas and iodine mitigation. 110
Figure 42. Peak fuel (left) and moderator (right) temperatures during DLOFC. 113
Figure 43. Methodology for performing transient analysis in a generic FHR benchmark model..... 121
Figure 44. Axial (left) and radial (right) view of the gFHR (reproduced from Satvat et al. (2021) [20])..... 123
Figure 45. Single FHR pebble with randomly distributed TRISO particles..... 126
Figure 46. gFHR Serpent model with discrete reactivity control mechanisms. (left) top-down view (right) radial view with control rods inserted into the critical position 127
Figure 47. gFHR Serpent model with grey curtain reactivity control mechanisms. (left) top-down view (right) radial view with control rods inserted into the critical position 128
Figure 48. Radial diagram of components within the KP-AGREE model and coolant flow path..... 134
Figure 49. Average radial power density between Serpent and KP-AGREE using a) 2 energy groups, b) 4 energy groups, and c) 7 energy groups. Fuel temperature set to 959 K and all other component temperatures set to 900 K..... 140
Figure 50. Average axial power density between Serpent and KP-AGREE using a) 2 energy groups, b) 4 energy groups, and c) 7 energy groups. Fuel temperature set to 959 K and all other component temperatures set to 900 K..... 141
Figure 51. Control rod worth calculation for discrete control rod Serpent model, uncalibrated Serpent grey curtain model, calibrated Serpent grey curtain model, and KP-AGREE with 7 energy group homogenized cross-sections from calibrated Serpent grey curtain model. Fuel temperature set to 959 K and all other component temperatures set to 900 K 145
Figure 52. Steady-state fuel kernel temperature prediction in KP-AGREE for all rods out (left) and control rods inserted to the critical position (right) (control rod depth indicated by dashed line) 147
Figure 53. Steady-state coolant temperature prediction in KP-AGREE for all rods out (left) and control rods inserted to the critical position (right) (control rod depth indicated by dashed line) 148
Figure 54. Steady-state power density prediction in KP-AGREE for all rods out (left) and control rods inserted to the critical position (right) (control rod depth indicated by dashed line) 149

Figure 55. The a) decay heat, b) inlet coolant temperature, and c) coolant mass flow rate during LOFA from Kile et al. (2022) used as boundary conditions in KP-AGREE [88] 154
Figure 56. MELCOR and KP-AGREE predicted maximum fuel temperature (left) and maximum coolant outlet temperature (right) during LOFA 155
Figure 57. Maximum fuel kernel (left) and average coolant temperature and total power (right) during overcooling transient 158
Figure 58. Peak fuel kernel and peak coolant outlet temperature (left) and total core power (right) during CRW transient 161
Figure 59. a) Fuel kernel temperature and b) power density at peak burnup location and c) fuel kernel temperature and d) power density at lowest burnup location for the overcooling and CRW transients. 165
Figure 60. Image of the HTR-10 [64] 169
Figure 61. Nodalization from the CRP-5 report conduction model (left) and convection model (right) [182] 172
Figure 62. Full nodalization of the HTR-10 model in MELCOR 178
Figure 63. COR package nodalization in MELCOR 180
Figure 64. Steady state temperatures for the a) fuel, b) coolant, and c) pebble surface and graphite reflector 184
Figure 65. Steady state temperatures within the reflector for z=4.04(m) (top) and z=3.10(m) (bottom) [182] 186
Figure 66. Decay heat curve [182] 189
Figure 67. Region for fuel reactivity temperature feedback (left) and moderator reactivity temperature feedback (right). 190
Figure 68. Normalized power during the PLOFC for short term (top) and long term (bottom) 192
Figure 69. Normalized power during the CRW for short term (top) and long term (bottom) 195

CHAPTER 1
INTRODUCTION

1.1 High Temperature Advanced Reactors

High Temperature Advanced Reactors (HTARs) are one of the most researched Generation IV type nuclear reactors due in part to their high performance, large potential application space, and technological maturity [1]. The High-Assay Low Enriched Uranium (HALEU) TRistructural-ISOtropic (TRISO) fuel used in the HTAR design can allow for longer refueling periods, lower discharged heavy metal and plutonium mass per unit energy generated, and a higher discharge burnup than large pressurized water reactors [2]. The HTAR has one of the highest thermal-to-electric efficiencies of any given reactor design, around 50%, due to the high coolant temperature [3], which also enables applications beyond power generation such as hydrogen generation [4] with the potential to reduce the carbon footprint of many industrial processes. The successful operational experience of the Fort St. Vrain and Peach Bottom Unit No. 1 High Temperature Gas-Cooled Reactor (HTGR) contributes to the technological readiness of the HTAR design and its potential to support a commercial demonstration in the near future [1].

The HTAR has attractive inherent safety features such as negative temperature feedback, high thermal inertia, and passive decay heat removal systems [5]. The TRISO particles are shown to be extremely reliable. The Advanced Gas Reactor Fuel Development and Qualification (AGR) program conducted an irradiation experiment with 300,000 TRISO particles to a peak burn of 19.6% Fissions per Initial Metal Atom

(FIMA), a peak fast-neutron fluence of 4.3e25(n/m^2), and a maximum time-averaged fuel temperature of about 1470K without a single particle failure [6]. Experiments at the 10MW HTGR test module (HTR-10) demonstrated the inherent safety features of HTGRs during an overpower and undercooling event without SCRAM, both of these transients maintained a fuel temperature below 1500K [7]. Experiments at the High Temperature engineering Test Reactor (HTTR) had similar conclusions to that of the HTR-10 undercooling transients [8]. Both of these reports attribute the passive shutdown of the core to the negative temperature feedback and maintaining fuel temperatures below safety limits to the large heat capacity of the moderators [7] [8].

These experimental measurements and demonstrations provide merit to the inherent and robust safety claims of the HTAR platform. This particular reactor platform has served as the basis for many innovative concepts over the past few decades which have the potential to further enhance the overall performance and safety of nuclear energy. In this dissertation, the main focus is on three unique HTAR concepts : 1) high temperature gas cooled microreactors, 2) fluoride high temperature salt cooled pebble bed reactors, and 3) high temperature gas cooled pebble bed reactors. The study on high temperature gas cooled microreactors was performed to demonstrate a design approach for a microreactor, which is a type of reactor that has received significant interest over the years, and to assess the potential of the concept when implementing alternative moderators. A set of transient simulations was performed on a generic pebble bed fluoride high temperature reactor to investigate inherent safety characteristics and accident response as well as to identify the most limiting condition concerning fuel integrity. The pebble bed high temperature gas cooled reactor study was performed to

verify and validate pebble bed steady state and transient modeling for the systems level thermal-hydraulics and accident progression tool, MELCOR. The underpinning theme for all of these studies is the use of multiphysics modeling for performance and safety assessment of HTARs in the pursuit of expanding the knowledge on promising technologies that have the potential to further the sustainability of nuclear energy. An additional theme of this dissertation is evaluating the current state-of-the-art modeling tools to assess their capabilities, identify areas of modeling development, and highlight areas of uncertainty in multiphysics modeling.

1.2 Motivation and Key Questions to Answer

Despite the enticing features and robust safety characteristics of HTARs, there are no commercially operating HTAR within the United States (US) to date. The US commercial nuclear fleet has been primarily centered on large Light Water Reactors (LWRs). Although technology is being developed to enhance their performance and safety, they are rapidly approaching their retirement and would require a substitution. It is likely that within the next 30 years, nearly all of these currently operating nuclear reactors will be decommissioned [9]. This presents an opportunity to implement recent advancements in nuclear technology that can outperform the current fleet, the focus of which is to expand the energy application, enhance economic competitiveness, and improve sustainability.

To evaluate the performance of these recent advancements in nuclear technology, multiphysics modeling and methods are used for rapid design iteration and optimization, assessment, and down selection of the most promising candidates. The role of computer

modeling is to minimize the need for costly large-scale experiments and to expedite the timeline for implementing such technology. The main technologies which have high-potential are moderators alternative to graphite for use in high temperature gas cooled microreactors, fluoride salt coolant in high temperature reactors, and pebble bed high temperature reactors.

Microreactors are intended to be economically competitive with technologies of a similar scale and application, such as diesel generators [10]. One of the primary beneficiaries of microreactor technology would be the military, who have historically considered a land-based nuclear reactor operating at a low thermal power [11]. This concept is being revisited through the Office of Secretary of Defense (OSD) / Strategic Capabilities Office (SCO) Pele Program, which aims to develop a mobile microreactor prototype to reduce challenges, dangers, and strategic planning constraints of forward operating bases that are currently using diesel generators for power supply [12]. The frequent convoy operations required to transport fuel and other supplies for diesel generators have accounted for over half the casualties of United States troops from 2001 to 2010 [13]. Additionally, technology developed within the military could energize the commercial sector and mitigate technological lethargy where applications overlap [14]. It has been recognized that by using a composite moderator in an HTGR platform, significant size reduction can be achieved [15]. These composite moderators would make them well suited for a microreactor and it would be expected that they would outperform graphite. However, an approach to generate a microreactor design that satisfies key technical constraints, incorporates novel nuclear technology for enhanced

performance, outlines an operational space, and predicts a passive safety response under limiting accidents is not readily available in the literature.

The concept of FHRs is a promising and relatively new design concept which implements attractive features of the HTGR as well as the Molten Salt Reactor (MSR) designs [16]. FHRs are accident conditions do not correspond to those of LWRs or HTGRs. Experts have identified a list of initiating events for FHRs [17] that would potentially result in failure of the fuel form. Analysis of some of these initiating events to ensure the concept meets safety design criteria has been performed [18] [19] [20] and predicted that no fuel failure is expected for a loss of flow accident. It has been recognized that the knowledge of TRISO fuel in FHRs under anticipated operational occurrences and design basis accidents must be extended . TRISO fuel performance envelopes have been calculated for the internationally benchmarked GA mHTGR-350 design [21] for reactivity-initiated accidents [22]. However, FHRs have over twice the power density of HTGRs and the method of heat removal under accident conditions differ [23] which would result in vastly different fuel responses under accident conditions

Fixed fuel reactors, such as the prismatic HTGR, have well defined fuel and coolant channels in a fuel assembly. For a PB-HTR, the fuel pebbles take a packed bed configuration which leads to a non-uniform porosity distribution [24] within the core. Coolant passes through this porous media to extract heat from the fuel elements and has a complex flow path due to the nature of the packed bed. Modeling heat transfer is further complicated by the fuel elements since conduction through a pebble, conduction to localized stagnant fluid, conduction from a contacting pebble or wall, and thermal radiation to a nearby pebble or wall all contribute to the overall heat transfer from a

pebble in addition to convection cooling. The necessity of modeling the complexity of the heat transfer of a PB-HTR is to accurately identify fuel hot spots that may challenge fuel integrity during the design and safety analysis of a PB-HTR concept. The challenge is that the pebble bed typically consists of hundreds of thousands of fuel elements making high resolution Computational Fluid Dynamic (CFD) simulations unrealistic given the current state of computational power.

Based on the scope of this work the following questions are proposed:

1. How can an existing HTGR design be modified to reduce its overall size and core power to qualify as a microreactor design and be optimized for reactor cycle length?
2. How do composite moderators compare in terms of reactor performance relative to a graphite moderated system?
3. What is the allowable operational design space for a microreactor and how does a graphite moderated design differ from a composite moderated design?
4. Would a microreactor designed to provide a long reactor cycle length have an acceptable safety performance?
5. What accidents would be considered for a pebble bed FHR?
6. Could any of the postulated accidents in a pebble bed FHR contest safety?
7. Can the systems level code, MELCOR, be verified and validated for a high temperature gas cooled pebble bed reactor?

The contributions of this work are highly relevant to the current state of nuclear energy. Industries have set aggressive timelines to demonstrate HTAR concepts, and many of their concepts overlap with the one presented here. Vendors such as X-energy and Kairos Power are perusing their respective PB-HTR prototype designs to provide a

demonstration within the decade. BWXT has been awarded the Project Pele contract to demonstrate a high temperature gas cooled microreactor within the next few years. The breadth of HTAR concepts and technologies discussed within this dissertation and the state-of-the-art modeling tools used suggest that these studies will be relevant and impactful for years to come.

1.3 Contributions and Outline

This work presents new knowledge on various technologies that are considered in HTARs. CHAPTER 2 is a detailed review of the literature for the relevant concepts/technologies and outlines some of the gaps in knowledge. Each of the concepts discussed in the literature review is unique but not mutually exclusive. An overview of some of the computational methods used across these studies is also presented, highlighting the current paradigm in multiphysics modeling. The novel contributions from this work are:

1. Demonstrating an approach to developing a microreactor concept starting from a research reactor point design, highlighting the necessary design considerations to take in order to maximize performance within a set of technical constraints.
2. Performing parametric reactor physics studies to describe the potential operation of a high temperature gas cooled microreactor concept, including various fuel options, core configurations, and limitations of the design.
3. Comparing the reactor performance of various potential moderators for a high temperature gas cooled microreactor in metrics for natural resource requirements and fuel cycle costs.

4. Outlining the envelope of thermal-hydraulic operational conditions based on thermophysical and operational constraints for the microreactor with various moderating concepts
5. Quantify the safety of the microreactor systems by calculating key safety characteristics, emergency planning zone size under a maximum hypothetical accident scenario with various levels of plume mitigation, and reactor response under a fuel temperature bounding accident condition.
6. Developed a coupled reactor physics and thermal-hydraulics model for a generic pebble bed fluoride salt cooled high temperature reactor and presented a set of definitions for unique accidents to be considered for the reactor concept
7. Performed code-to-code verification of the industry tool, KP-AGREE, against results from a Nuclear Regulatory Commission (NRC) code, MELCOR for a loss of forced coolant accident
8. Simulated an overcooling transient and total control rod withdrawal transient to assess the response of the pebble bed fluoride salt cooled high temperature reactor
9. Developed a model for the HTR-10 within MELCOR and compared steady state and transient results to verify and validate the code's capability for pebble bed HTGR modeling

These contributions are described thoroughly within CHAPTER 3 through CHAPTER 6. CHAPTER 3 presents the design process for the preconceptual microreactor designs, the technical constraints of the design, reactor physics parametric studies, and calculations for natural resource requirements and fuel cycle costs. CHAPTER 4 presents the thermal-hydraulic design space calculations of the

preconceptual microreactor designs, steady state power and temperature distributions, transient response under a bounding fuel temperature accident, and emergency planning zone calculations for a maximum hypothetical accident with various levels of mitigation. CHAPTER 5 describes the pebble bed fluoride salt cooled high temperature reactor study including the methodology on model development, verification of the tools used within the study, postulated accidents and definitions of the accidents, and reactor response calculations for each unique accident considered. CHAPTER 6 outlines the approach to modeling the HTR-10 within MELCOR, describes the process for verification and validation of the model, and concludes with a discussion on modeling needs. Finally, CHAPTER 7 summarizes all of the findings from this work, outlines the contributions, and concludes the dissertation.

CHAPTER 2
LITERATURE REVIEW

The relevant reactor concepts for this dissertation are reviewed in this section. The purpose of this chapter is to identify the current base of knowledge for various HTAR concepts and to highlight specifically the gaps within the literature. The work presented in the subsequent studies is built on the foundation of the current literature, including the present state of each relevant technology and the multiphysics methods used for evaluation. These concepts/technologies are categorized into four major parts of review 1) igh temperature gas cooled microreactors, 2) omposite moderators, 3) fluoride salt cooled high temperature reactors, and 4) pebble bed high temperature reactors. The relevant reactor physics tools and methodologies are also discussed at the end of this section.

2.1 High Temperature Gas Cooled Microreactors

The HTGR platform is centered on achieving no significant fuel failure from any foreseeable accident related to either an over-powered or under-cooled transient [5]. Thus, the HTGR design has a high degree of inherent safety in postulated accident scenarios. A Depressurized Loss of Forced Coolant (DLOFC) accident representing the bounding case for fuel temperature [21] was modeled using the internationally benchmarked General Atomics (GA) modular HTGR (GA mHTGR-350) design and predicted that the passive cooling features of the HTGR design could adequately cool the core during the accident scenario [25]. Lu & Brown (2019) also modeled Reactivity Initiated Accidents (RIAs) and illustrated that the strongly negative fuel temperature

coefficients can quickly turn around core power in an over-powered transient. The HTGR is a robust and well understood advanced reactor design with numerous applications. As a result, many developers are pursuing the novel concept of microreactors based on the HTGR platform [26].

Microreactors are intended to be economically competitive with technologies of a similar scale and application, such as diesel generators [10]. One of the primary beneficiaries of microreactor technology would be the military, who have historically considered a land-based nuclear reactor operating at a low thermal power [11]. This concept is being revisited through the Office of Secretary of Defense (OSD) / Strategic Capabilities Office (SCO) Pele Program, which aims to develop a mobile microreactor prototype to reduce challenges, dangers, and strategic planning constraints of forward operating bases that are currently using diesel generators for power supply [12]. The frequent convoy operations required to transport fuel and other supplies for diesel generators have accounted for over half the casualties of United States troops from 2001 to 2010 [13]. Additionally, technology developed within the military could energize the commercial sector and mitigate technological lethargy where applications overlap [14]. It has been recognized that by using a composite moderator in an HTGR platform, significant size reduction can be achieved [15]. These composite moderators would make them well suited for a microreactor and it would be expected that they would outperform graphite. However, an approach to generate a microreactor design that satisfies key technical constraints, incorporates novel nuclear technology for enhanced performance, outlines an operational space, and predicts a passive safety response under limiting accidents is not readily available in the literature.

There are currently many reactor developers pursuing microreactor designs and a few have chosen to center their design around an HTGR platform (GAIN, 2021). What these developers have in common with respect to their design goals is having a transportable, long operating, accident tolerant energy source that relies on existing HTGR technology, such as graphite moderating material. However, these developers target civilian and/or military applications which have different emphases on design criteria and as a result, the constraints between developers on designing a solution vary. The developers also identify different performance metrics to optimize which results in different solutions implementing different technology when applications are similar. The following subsections identify some of the developers pursuing microreactors in an HTGR platform, their intended application and design philosophy, and some performance metrics.

2.2.1 BWX Technologies, Incorporated

The design developed by BWX Technologies, Incorporated (BWXT), named BWXT Advanced Nuclear Reactor (BANR), is intended for industrial customers in remote locations or military applications. BANR is designed to produce $50MW_{th}$ for a 5-year period. BWXT was selected to participate in the Department of Energy's (DOE's) Advanced Reactor Demonstration Program (ARDP) risk reduction for future demonstration projects. The goal of risk reduction is to develop nuclear technology to develop safe and affordable reactor technology to be implemented in the near future. The focus of BWXT is to target risk reduction technology of lesser mature technologies under DOE's ARDP in order to enhance economics rather than retrofitting highly matured technology for microreactors which could be costly. One example of the BANR design

implementing cost reduction is the use of uranium nitride TRISO particles instead of the conventional uranium carbide TRISO. The higher uranium density associated with uranium nitride TRISO fuel is expected to reduce overall fuel costs because a lesser amount of fuel could be manufactured while still maintaining similar performance. BWXT has partnered with INL to perform experimental testing on uranium nitride TRISO particles to mature the technology. BWXT is one of two companies selected by the Pele Program to proceed to a final engineering design after which a final company will be selected to build and demonstrate a microreactor prototype. As a result, many aspects of the BANR design are unknown to the public [27].

2.2.2 X-energy, LLC

X-energy, LLC is the other company selected under the Pele Program to proceed to a final engineering design. The concept, Xe-Mobile, is focused on military applications but can be extended to the civilian space. Xe-Mobile focuses on military applications and requires the design to be able to be rapidly deployed and set up. The design must also be able to shut down, relocate, and redeploy. The design requires a high degree of mobility and must be compatible with rail, truck, and military transport aircraft. All components of the design must also be contained within a standard ISO container. The Xe-Mobile microreactor can operate with at least $1MW_{ele}$ power output for more than 3 years. As in the case of the BANR design, many design aspects of Xe-Mobile are unknown to the public. [28].

2.2.3 Ultra Safe Nuclear Corporation

Ultra Safe Nuclear Corporation's (USNC's) Micro Modular Reactor (MMR^{TM}) is intended as a flexible nuclear battery capable of power generation and industrial applications for remote areas. MMR is a helium cooled; graphite moderated design capable of producing 15MW$_{th}$ core power for a 20-year operating cycle. The MMR operates at a low power density and has a high heat capacity which would result in very slow temperature changes during accidents. This slow temperature change makes the MMR walk away safe as the heat generated by the reactor can passively dissipate into the environment. Some of the principles that the MMR design implements are simplicity, reliability, safety, and maintainability. These principles dictate a two-plant energy system in which a nuclear plant, which includes the MMR, is separated from a non-nuclear facility that harnesses heat for customer specific applications. By separating the energy system, the MMR can be placed below ground level which enhances safety during transient events and mitigates irradiation to reactor components and the environment. A novel safety feature of the MMR is the use of TRISO fuel particles encased within a silicon carbide matrix, also known as Fully Ceramic Microencapsulated (FCM^{TM}) fuel. Having the TRISO particle encased in silicon carbide, which is the same material primarily responsible for fission product retention in the TRISO particle, enhances safety during operating and accident conditions [29].

2.2.4 HolosGen, LLC

HolosGen, LLC has proposed a microreactor concept named Holos-Quad which is considered for civilian applications in remote locations. The Holos-Quad design has a

focus on transportability by reducing core weight and on economic performance by maximizing the operational time. The design utilizes four Subcritical Power Modules (SPMs) that are all contained within a single 40-foot ISO container. These SPMs each contain a closed-loop gas Brayton cycle and reactivity can be controlled by increasing or decreasing the spacing between SPMs. The helium cooled; graphite moderated design is capable of producing $22MW_{th.}$ Where reactor performance outweighs transportability, the design can operate for 8.3 years with a total core weight of approximately 27 tons. In addition to the 40-foot ISO container size constraint, safety constraints such as reactivity shutdown, reactivity feedback, peak pressure drop, peak fuel temperature, and sub-criticality during a flooding event were all considered during the design process. Documentation on Holos-Quad also goes on to provide preliminary results on shielding requirements for the turbomachinery equipment that would also be within the 40-foot ISO container size constraint. The Holos-Quad provides a wide range of extensive analyses publicly available to not only provide a potential solution for a microreactor concept but to also advance the understanding of microreactors [30].

2.2 Two-phase Composite Moderators

While the HTGR represents a promising design to be used in the next generation of commercial reactors, it is plagued by challenges deriving from the graphite moderator and its unfavorable properties under irradiation. Graphite experiences non-uniform shrinkage followed by volumetric expansion [31] as well as an increase in residual stress while irradiated, limiting the material's in-core residence time [32]. The limited lifetime of graphite requires it to be replaced during the operating lifetime of the reactor, resulting in significant annual operating costs and contributing to the amount of radioactive waste

generated by the reactor. The thermal conductivity of graphite also decreases with accumulated radiation dose, which would decrease the amount of heat that the moderator is able to transfer from the fuel to the helium coolant [33]. These challenges with graphite have motivated studies to explore two-phase composite moderators using beryllium and hydride containing moderating phases entrained within a stable ceramic matrix, and results to date have demonstrated significant potential to enhance the performance of HTGRs [15] [34] [35].

Moderators alternative to graphite have been considered historically for when size constraints or mass constraints were of utmost importance. Beryllium (Be, BeO, Be_2C) and hydride (ZrH_x and YH_x) moderators have previously been used as moderating materials in their monolithic form, such as in the Aircraft Reactor Experiment (ARE) [36] and the Heat Transfer Reactor Experiment No. 3 (HTRE3) [37], respectively. In these experimental reactors, the choice of moderator enabled a smaller core than conventional graphite-moderated HTGRs. These alternative moderators would outperform graphite in a microreactor design due to their enhanced moderating capabilities, allowing for a smaller critical size. The historically alternative moderators were monolithic materials and, in some instances, did not mitigate irradiation challenges at high neutron doses. Over the past few years, a new class of engineered composite moderators has been proposed that are comprised of two phases, an irradiation stable host matrix and an entrained highly moderating phase, shown in Figure 1 [35].

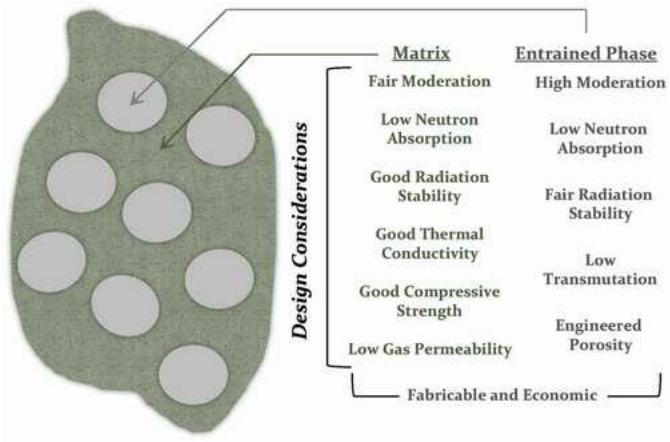

Figure 1. Illustration of two-phase composite moderator [35]

Snead et al. (2022) proposed a two-phase, ceramic matrix composite based on a magnesia (MgO) host matrix and either entrained beryllium-based or metal hydride-based moderating material. These two-phase composite moderators have been fabricated at the laboratory scale and preliminary reactor physics calculations in Snead et al. (2022) demonstrated the viability of these moderating materials. The implication of these results is that these alternative moderators could outperform graphite in the microreactor space while simultaneously mitigating irradiation challenges.

Composite moderators composed of a radiation and chemically stable magnesia (MgO) host matrix with an entrained beryllium [34] or hydride moderating phase [31] have been shown to be suitable replacements for graphite in an HTGR platform [15]. Assembly level calculations for the GA mHTGR-350 [21] for these proposed alternative moderators performed by Duchnowski et al, (2020) predicted a higher overall performance and reduced core size relative to a graphite moderated system. A follow up study on the safety assessment of beryllium-based two-phase composite moderators was performed to explore the safety response of these concepts under transient conditions [38]. Karriem et al. (2021) looked at a drop-in replacement with either 60%MgO 40%BeO or 60%MgO 40%Be composite moderators for graphite in the GA mHTGR-350. Reactor physics calculations predicted that the beryllium-based moderators would shift the power profile more towards the axial center of the reactor relative to graphite for an otherwise identical core configuration, which would reduce overall peak fuel and moderator temperatures within the core. Safety analyses performed by Karriem et al. (2021) also demonstrated a relatively similar response for either overpower or undercooling transient events between moderating materials. Cheng et al. (2022)

fabricated MgO BeO two-phase composite moderators and performed measurements on the thermophysical properties of the material. Cheng et al. (2022) also described the microreactor implications from a reactor physics and thermal-hydraulics perspective of the fabricated moderating material, concluding the potential for reduced fuel cycle costs and longer operating periods for the MgO BeO moderator relative to graphite. However, Duchnowski et al, (2020) stated that one of the most promising two-phase composite moderator concepts was a hydride-based material and none of the previously mentioned studies explored this option. Furthermore, these studies never fully assessed the design space of a high temperature gas cooled microreactor using two-phase composite moderators or investigated the response of the microreactor under accident conditions.

2.3 Fluoride Salt Cooled Reactors

The novelty of the FHR with respect to other conventional reactor concepts relies primarily on the selection of reactor coolant and fuel form, both of which have been developed separately under various programs [16]. Molten fluoride salt coolant has been researched under the aircraft reactor propulsion program and molten salt programs [39] [40] as the coated particle fuel form used within the FHR was initially developed for HTGRs [41]. These features not only allow for a high-performance system but also mitigate fission product release. The particle fuel form proposed for FHR designs, typically TRISO, is focused on retaining fission products at high temperatures. TRISO fuel consists of a uranium-based fuel kernel encased in a graphite buffer layer and coated with multiple pryocarbon and silicon carbide layers for fission product retention. This fuel particle is typically then embedded in a graphite matrix for use in a pebble or

prismatic fuel geometry, adding to the number of fission product boundaries. Experiments with TRISO particles for gas-cooled reactors have demonstrated the robust fission product retention capabilities of the fuel form even at high temperatures and high burnup [42].

Coolant candidates must have acceptable characteristics such as low neutron absorption, low melting temperature, high boiling temperature, compatibility with reactor core materials, and high heat transfer. The leading coolant candidate is Li_2BeF_4, denoted as FLiBe, with enriched Li-7 to mitigate neutron absorption. The binary FLiBe salt has a melting temperature of 732 K, lower than single component salts, and a high boiling temperature of 1703 K, higher than that of sodium coolant. FLiBe was researched under the molten-salt breeder reactor program and significant operational experience exists for this particular coolant [16]. The FLiBe coolant also has the added safety measure of retaining radionuclides that may escape from the fuel [43] and this added measure of safety provided by FLiBe may also allow for reducing containment redundancies, improving the economics of the design [44]. The FLiBe coolant also retains safety characteristics that mitigate potential consequences during accident conditions. The large thermal conductivity and volumetric heat capacity of FLiBe, and in turn, the large thermal inertia, provide a slow rate of temperature change under accident conditions [45]. Unlike the HTGR, the FHR operates at nearly atmospheric pressure and does not have a high risk of coolant leaking from the primary loop [45]. Added measures of controlling heat generation through intrinsic core temperature feedback are granted by the strongly negative coolant void and temperature reactivity feedback [46], mitigating power and fuel temperature increases in reactivity-initiated accidents.

FHRs accident conditions do not correspond to those of LWRs or HTGRs. The low-pressure FLiBe coolant immersing the fuel pebble in the case of a pebble bed FHR design as well as the lack of large quantities of water within the reactor building effectively eliminate significant temperature increase in the event of an accident and water/air ingress events that are postulated events in HTGRs [23]. However, given the similarity of FHRs to HTGRs many of the initiating events for postulated failure modes are similar [47] [48]. Experts have identified a list of seven categories of initiating events for FHRs [17] which also overlap with HTGRs initiating events that would potentially result in failure: 1) Increase in heat removal by the secondary system 2) Decrease in heat removal by the secondary system 3) Decrease in reactor coolant system flow rate 4) Reactivity and power distribution anomalies 5) Increase in reactor coolant inventory 6) Decrease in reactor coolant inventory 7) Radioactive release from a subsystem or component. These initiating events are considered during the design process and must follow safety design criteria to maintain control of radionuclides, control heat generation and removal, maintain coolant inventory, and maintain core and reactor building integrity [49].

Although FHRs have never been built to date, analysis of these initiating events to ensure the concept meets safety design criteria has been performed. For initiating event 3) Decrease in reactor coolant system flow rate, it was shown a pebble bed design with pool reactor auxiliary cooling heat exchangers coupled to the direct reactor auxiliary cooling system would result in negligible peak fuel temperature increase when SCRAM occurs and no greater than a 100K temperature increase when SCRAM does not occur [18]. For a preconceptual FHR engineering demonstration reactor based on prismatic

fuel forms rather than pebbles, calculations of a similar loss of forced coolant flow with SCRAM demonstrated the passive safety features of an FHR [19]. A sensitivity study performed on a publicly available generic FHR specification [20] predicted that no fuel failure is expected for a loss of flow accident with SCRAM but coolant outlet temperatures may challenge vessel temperature limits.

Although the design of the FHR has similar or in some cases enhanced safety characteristics of other more extensively researched advanced reactor designs such as the High-Temperature Gas-cooled Reactor (HTGR), the differences between reactor physics, operation, and selection of components require a more exhaustive investigation on FHRs safety. The FHR has a high coolant operating temperature and power density, which were considered as potentially limiting criteria [50] [51]. Moreover, pebble bed FHR platforms achieve a much higher discharge burnup than fixed fuel designs, which may potentially lead to fuel failure [52]. It has been recognized that the knowledge of the TRISO fuel form in FHRs under anticipated operational occurrences and design basis accidents must be extended [53], demonstrating that TRISO fuel integrity is not predicted to be compromised under transient events is necessary.

2.3 Pebble Bed High Temperature Reactors

Pebble Bed High Temperature Reactors (PB-HTRs) are a type of advanced nuclear reactor that is designed to enhance efficiency, safety, and the economics of nuclear energy relative to the current Light Water Reactor (LWR) nuclear fleet. The design features of the gas-cooled PB-HTR have been recognized as one of the most promising reactor concepts to be used in the next generation of commercial reactors [1]. The history

of the high temperature pebble bed reactor began with the initial criticality of the German Arbeitsgemeinschaft Versuchs Reaktor (AVR) in 1967 [54], Figure 2a. The AVR proved the feasibility of the high temperature gas cooled pebble bed reactor and the larger scale Thorium Hochtemperatur Reaktor (THTR) [55] concept soon followed. More recent pebble bed reactor designs leveraged the lessons learned in the aircraft nuclear propulsion program [56] and molten salt reactor program [57] to develop the concept of a molten salt cooled pebble bed reactor known as the Pebble Bed Advanced High Temperature Reactor (PB-AHTR) [16] [58], eventually leading to the University of California, Berkeley (UCB) Mark-1 Pebble Bed Fluoride-salt-cooled High-temperature Reactor (MK1 PB-FHR) concept, Figure 2b. Currently, the only operating PB-HTRs are the Chinese HTR-10 [59] and HTR-PM [60]. However, vendors such as X-energy and Kairos Power are perusing their respective PB-HTR prototype designs to provide a demonstration within the decade. Listed in Table 1 are some PB-HTR concepts with accompanying design features and intended purpose.

The selection of a coolant other than water, which is not unique to PB-HTRs but is a defining characteristic of advanced reactors [1], allows for higher achievable coolant outlet temperatures. Higher coolant outlet temperatures improve thermal-to-electric efficiencies and extend the application of the nuclear power plant beyond electricity production [1].

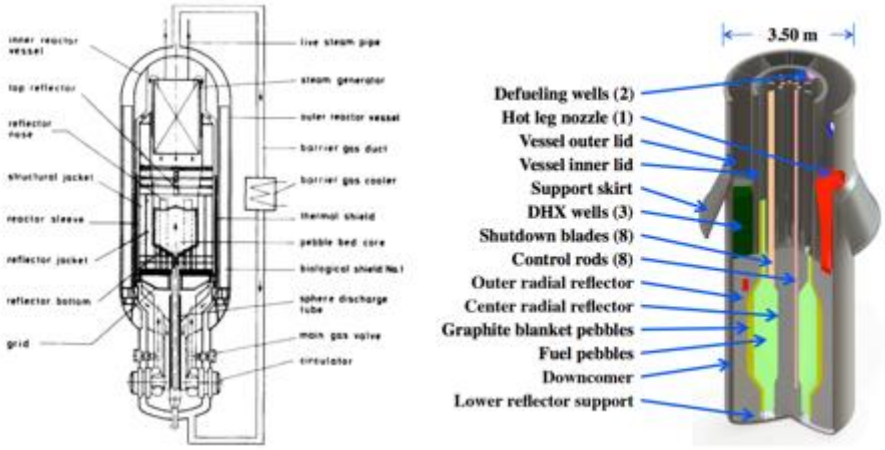

Figure 2. The AVR [54] (left) and the MK1 PB-FHR (right) [61]

Table 1. High temperature pebble bed reactor concepts

Concept	Coolant	Inlet / Outlet Temperature [ºC]	Thermal Power [MW_{th}]	Defined Purpose	Reference
PBMR-400	Helium	500 / 900	400	Ultra safe and economically competitive energy source	[62]
AVR	Helium	275 / 950	46	Demonstration of pebble bed concept	[54] [63]
THTR	Helium	250 / 750	750	Demonstration of large-scale power production with thorium cycle	[55]
HTR-10	Helium	250 / 700	10	Acquire knowledge, perform experiments demonstrate safety	[59]
HTR-PM	Helium	250/750	2x250	Demonstrate economic competitiveness and safety	[64]
Mk1 PB-FHR	FLiBe	600 / 700	236	Provide new value proposition for nuclear power	[61]
PB-AHTR	FLiBe	600 / 704	900	Outline a development plan for high temperature reactors	[58]
HTR-Modul	Helium	250 / 700	200	Simple and safe design for electricity or heat production	[65]
TMSR-SF	FLiBe	600 / 700	395	Realize development, maintenance, physical behavior, and safety of thorium based molten salt reactor for future commercialization	[66]
KP-FHR	FLiBe	550 / 650	320	Pebble bed FHR commercial reactor	[67]
Hermes	FLiBe	550 / 620	35	Low-power test reactor for support of KP-FHR	[68]
Xe-100	Helium	260/750	200	Generating energy, providing high quality heat, or cogeneration applications	[69]

Moreover, the coolant selection in the PB-HTR allows for a lower core pressure relative to LWRs [70] which significantly reduces the risk of accident scenarios. The two primarily considered coolant options in PB-HTRs are helium and FLiBe. Helium is a good coolant candidate because of its thermo-physical properties, chemical compatibility with core components, and unrestrictive temperature limits. In gas cooled PB-HTRs, helium typically flows from the upper inlet plenum, through the packed bed, and exits through the bottom plenum. This coolant direction avoids pebble levitation as both the coolant flow and gravitational forces are in the same direction. FLiBe is an excellent coolant candidate for PB-HTRs because of superior thermo-physical properties relative to helium, comparable compatibility with core components, and an option for near-atmospheric pressure operation. The low pressure associated with FLiBe cooled PB-HTRs is an attractive feature from a safety perspective but the coolant concept is not to the same level of technological maturity as helium. In FLiBe cooled PB-HTRs, the coolant flows from bottom to top in line with the direction of buoyant forces. In both concepts, the coolant passes through the packed bed to remove heat from the fuel and deposit heat through the primary heat exchanger during nominal operation.

The spherical fuel element that contains the embedded TRISO fuel is the defining characteristic of the PB-HTR. Thousands of fueled graphite pebbles form a packed bed configuration within a graphite walled core. These fuel pebbles are continuously circulated through the core region, allowing them to take multiple passes through the core until a desired discharge burnup is reached at which point, the batch of fuel pebbles are discarded and replaced with a fresh batch of fuel pebbles. In gas-cooled PB-HTRs, the pebbles are introduced from the top of the core and exit out the bottom. In FLiBe cooled

PB-HTRs the direction of pebble movement is opposite. The fuel elements in a FLiBe cooled PB-HTR are less dense than the coolant and buoyant within the pebble bed. These fuel pebbles enter from the bottom of the core and exit out the top. Continuously cycled fuel schemes commonly operate with many more batches than fixed fuel reactor designs and can achieve a higher discharge burnup and fuel utilization which has beneficial economic outcomes. Figure 3 shows the typical fuel form for a gas cooled and FLiBe cooled pebble bed reactor. In a comparative study between prismatic High Temperature Gas-cooled Reactors (HTGRs) and gas-cooled PB-HTRs, a fuel cycle cost savings of 5-fold is expected for the pebble bed designed when average over 30 years [71].

2.4 Computational Simulating Tools for High Temperature Advanced Reactors

Several state-of-the-art computational tools were used for the multiphysics modeling of advanced high temperature reactors. The continuous-energy Monte Carlo reactor physics burnup code Serpent was used for depletion calculations, power tallying, temperature feedback calculations, and group cross section generation within this dissertation [72]. Serpent is a probabilistic three-dimensional neutron transport code that accounts for neutron energy dependency correctly by utilizing a continuous cross section library which mitigates inaccuracy due to multi-group approximation at the expense of computational time.

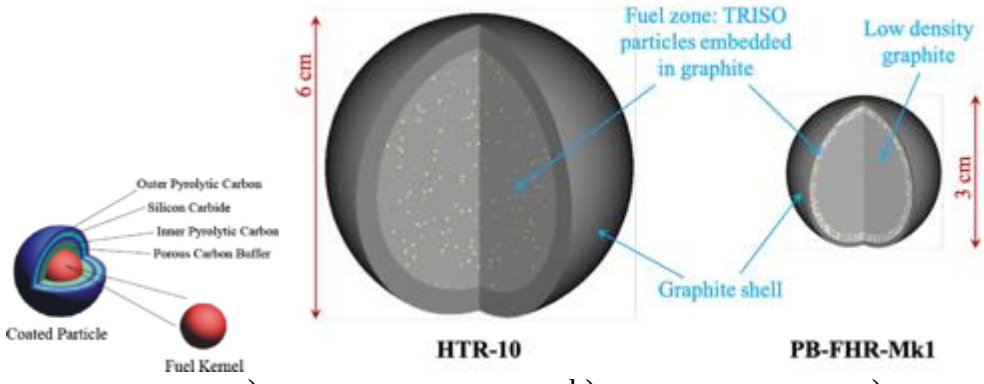

a) b) c)

Figure 3. a) A typical TRISO particle b) the fuel form for the HTR-10 [73] c) the fuel form for the PB-FHR-Mk1 [74]

s

This neutron transport code is capable of generating complex geometries which lends itself to be capable of modeling nearly any type of reactor design.

Idaho National Laboratory's (INL's) Reactor Excursion and Leak Analysis Program 3D (RELAP-3D) was initially designed to model LWR components and transients [75] but has been extended and validated to model prismatic high temperature gas cooled designs [76] [77]. The deterministic finite differencing method that RELAP employs allows for rapid and accurate simulation of reactor components. Moreover, the multi-dimensional neutron kinetics module contained in RELAP allows for temperature feedback effects to be accounted for during transient simulations [78].

The Kairos Power Advanced Reactor Evaluator (KP-AGREE) is a thermo-fluids code to solve the steady state and time dependent mass, momentum, and energy equations in three- dimensions for HTGR analyses specifically for pebble bed type designs [79]. KP-AGREE is a reduced order model capable of modeling the complexity of a pebble bed FHR during control rod withdrawal, loss of forced cooling, and loss of heat sink transients. The model implements the nodal diffusion neutronics method with a thermal-hydraulics two-temperature field porous media method to allow for direct neutronic and thermal-hydraulic coupling. The nodal diffusion method requires homogenized multi-group cross sections and can account for multiple reactor component temperature branches, both of which can be provided by Serpent. The code has been validated for simulating the PBMR-400 [79] and the full set of SANA experiments, which is an electrically heated pebble bed test facility [80] [67]. The primary use of KP-AGREE to-date is for the rapid iteration of the KP-FHR design [20].

The integrated systems-level thermal-hydraulics, accident progression, and source term code, MELCOR, has been built for the US NRC since the early 1980s by Sandia National Laboratories (SNL) [81]. The initial purpose of the code was for LWR modeling but non-LWR modeling capabilities have been developed over the recent years. Of particular interest, MELCOR has been developed to be able to simulate steady state and transient conditions for high temperature gas cooled and fluoride salt cooled pebble bed reactors [82] [81]. MELCOR is organized into packages which are grouping of regions or code functionalities. These packages serve as the building blocks for modeling a nuclear system. The modeling approach in MELCOR is similar to that of INL's RELAP-3D, were hydrodynamic control volumes and coolant flow path connections describe the circulation of coolant within the core. The unique feature of MELCOR is the ability to perform integrated calculations of radionuclide release, transport, and deposition. The tool has been verified against the PBMR 400 OECD benchmark study [83].

CHAPTER 3
TWO-PHASE COMPOSITE MODERATOR HIGH TEMPERATURE GAS COOLED MICROREACTOR: DESIGN AND NEUTRONICS PERFORMANCE

A version of this chapter was originally published by Edward M. Duchnowski et al.:

Duchnowski E.M. et al. "Pre-conceptual high temperature gas-cooled microreactor design utilizing two-phase composite moderators. Part I: Microreactor design and reactor performance." *Progress in Nuclear Energy* 149 (2022) 104257.

In the original publication, I led the formal analysis, investigation, developed the computational models, and wrote the original draft. Robert F. Kile assisted some of the early computational model development along with Kenny Bott. Robert F. Kile also reviewed and edited the original draft. Jason R. Trelewicz, Lance L. Snead, and Nicholas R. Brown are credited with the conceptualization and funding acquisition as well as reviewing and editing the original draft.

3.1 Motivation for Microreactors

Microreactors are intended for applications where compact size and the ability to transport a power station takes precedence over large electrical power output. They are intended to be economically competitive with technologies of a similar scale and application, such as diesel generators [10]. One of the primary beneficiaries of microreactor technology would be the military, who have historically considered a land-based nuclear reactor operating at a low thermal power [11]. This concept is being revisited through the Office of Secretary of Defense (OSD) / Strategic Capabilities Office (SCO) Pele Program, which aims to develop a mobile microreactor prototype to reduce challenges, dangers, and strategic planning constraints of forward operating bases that are currently using diesel generators for power supply [12]. The frequent convoy operations required to transport fuel and other supplies for diesel generators have accounted for over half the casualties of United States troops from 2001 to 2010 [13]. Additionally,

technology developed within the military could energize the commercial sector and mitigate technological lethargy where applications overlap [14]. However, an approach to generate a microreactor design that satisfies key technical constraints, incorporates novel nuclear technology for enhanced performance, outlines an operational space, and predicts a passive safety response under limiting accidents is not readily available within the literature.

Here, an approach for generating a pre-conceptual microreactor based on a HTGR platform is demonstrated and employed in a comparative study between the performance characteristics of a composite moderated design relative to a reference graphite moderated case. The starting point of this pre-conceptual design comes from INL's High Temperature Gas-Cooled Test Reactor (HTGTR), which inherits many of the design features of the GA mHTGR 350 but designed to provide a versatile, multi-purpose, high flux facility for fuel and material irradiations [83]. Coarse design changes to the overall power and size of the reactor are made to satisfy technical constraints inspired by the Pele Program [84]. Various moderating material, fuel types, and design configurations are compared to provide insight into reactor performance and maximize reactor cycle length. This design is intended to be operated as a long-lasting, single-batch cycle. Cycle length was chosen as the metric to maximize as to reduce the frequency of replacing the reactor with parameters such as core configuration and fuel type down selected throughout this study as a result. Additional metrics were calculated, such as natural resource utilization and fuel cycle cost, to enlarge the envelope of expected performance enabled by the novel composite moderator materials. Overall, the aim of this study is to generate a pre-conceptual microreactor design and compare key metrics of reactor performance between

a traditionally graphite moderated system against proposed composite moderators that are hypothesized to be better suited for microreactor designs**.**

3.2 Design Constraints, Launching Point, and Coarse Changes

The starting point of the pre-conceptual microreactor design was to identify technical constraints governed by the intended application of microreactors, such as operation time, power output, size, safety, and fuel type, as summarized in Table 2. Inspired by the Pele Program, a set of constraints was implemented within an HTGR platform, though it should be noted that this work is not intended to design a military microreactor as part of the Pele Program. HTGRs are designed with HALEU TRISO fuel, and experiments at HTR-10 and the HTTR have demonstrated the inherent safety of the design for a loss of coolant accident [7] [85]. Moreover, it has been demonstrated that a microreactor based on the HTGR platform that has a compact size and reasonable thermal power output would not expect a compromise on safety for an undercooling or overpower transient [86]. Consequently, a microreactor using composite two-phase beryllium- and hydride-based moderators could potentially satisfy the design constraints of the Pele Program, and the purpose here is to demonstrate the benefits of designing a gas-cooled microreactor around the composite two-phase moderators rather than a graphite moderator.

The pre-conceptual microreactor design leverages concepts of other HTGRs within the open literature to meet technical requirements. The INL HTGTR point design [83] was selected as the initial design launching point to generate a state-of-the-art compact HTGR based on operational information from the Fort St. Vrain Generating Station and experimental information from the successful Advanced Gas Reactor (AGR) Program [6].

Table 2. Constraints inspired by Project Pele [84]

Technical Requirement	Technical Objective
Operation Time	> 3 years of operation at 100% power without refueling
Power Generation	1 – 10 $MW_{electric}$
Size	All components fit within ISO 688 certified 20-foot CONEX box. (5.898m X 2.350m X 2.390m *Internal Dimensions) [87]
Safety	Semiautonomous shutdown under limiting loss of coolant accident
Fuel	HALEU TRISO fuel.

Sterbentz et al. (2016) considered various core configurations for the HTGTR design, shown Figure 4, to identify optimal test performance. The final selected design for the HTGTR is shown in the blue dashed box in Figure 4, and the red solid box is one of the considered HTGTR designs that was used as the launching point for this pre-conceptual microreactor. This selection for the launching point design is to provide the most fuel dense design (i.e., a design that is non-annular) to maximize the limited space and improve cycle performance.

The first objective after selecting the launching point was to satisfy the technical size constraint. The radial core size was limited to 90cm, which allows for an outer reflector, and the total reactor radius was 116.5cm allowing for a similar reactor pressure vessel and core barrel width in the HTGTR design while still satisfying the size constraint. The height of the core was limited to 395.5cm, allowing for three standard Fort St. Vrain fuel assemblies with upper and lower reflector assemblies of identical fuel assembly height. This height also provides adequate space for a modified heat exchanger intended for advanced nuclear reactors to also fit within the size constraint [88]. Figure 5 shows the radial changes made to the initial launching point design, including the removal of irradiation loops and control rod holes.

It was recognized that reducing the assembly size would enhance performance by allowing for higher initial fuel loading. A micro assembly design was conceived that reduced the number of fuel and coolant channels but maintained a similar geometry to the Fort St. Vrain style fuel block. Reducing the size of the assembly allows for some of the reflector region to be replaced with fueled assemblies, increasing fuel loading by ~56%.

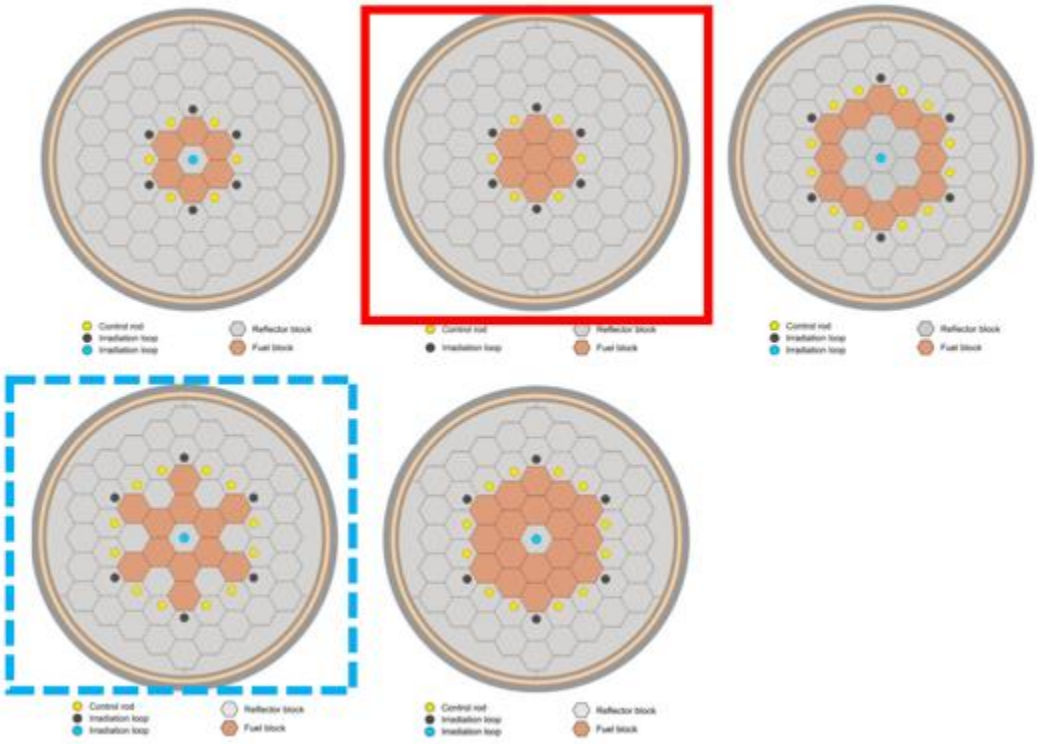

Figure 4. Considered designs in the HTGTR [83]. Red solid box for the selected launching point and the blue dashed line for the HTGTR design.

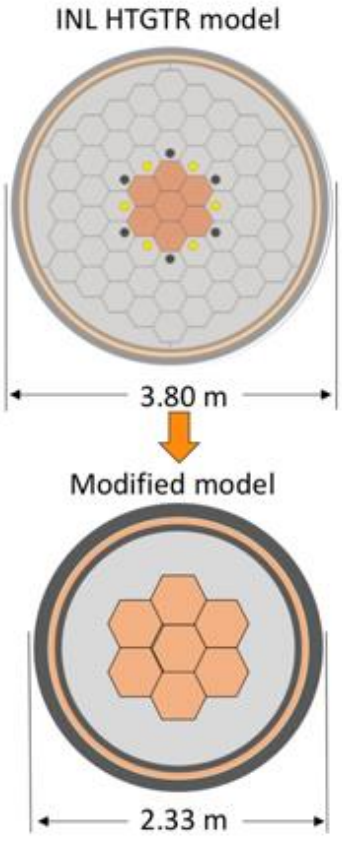

Figure 5. Size reduction of launching point design.

Figure 6 shows a comparison between the traditionally sized Fort St. Vrain style assembly and the micro assembly. The minimal size of the assembly was selected such that the outermost region could host fuel, coolant, and potently Lumped Burnable Poisons (LBP) for initial reactivity hold down. An image of the micro assembly containing outlined hexagonal rings is shown in Figure 7 with Table 3 summarizing the justification for minimal assembly size based on the hexagonal rings.

3.3 Neutronics Model

The continuous-energy Monte Carlo reactor physics burnup calculation code Serpent [72] was used to assess the reactor performance of the pre-conceptual microreactor designs. All materials were set to 900K and used the ENDF/B-VII.0 cross-section library. When available, the $S(\alpha,\beta)$ library was used for thermal neutron scattering. The simulation was modeled with the height of a single fuel element, 4.93cm, with periodic axial boundaries to represent an infinitely tall core. Power was scaled down from the expected full core to this 2D representation by the number of fuel assemblies (3) and number of fuel elements per assembly (15) based on the Fort St. Vrain assembly design [21]. The following sections describe the neutronics model starting from the fuel and stepping outward to the entire core.

3.3.1 Fuel Type

Two fuel types were initially considered in this study, AGR TRISO in a graphite compact with a uranium oxycarbide (UCO) fuel kernel and FCM TRISO in a Silicon Carbide (SiC) compact with a uranium nitride (UN) fuel kernel.

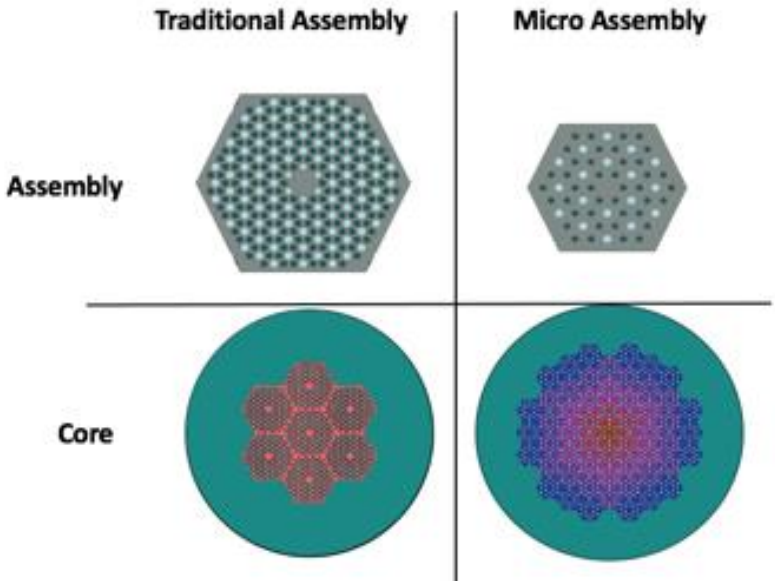

Figure 6. Assembly and microreactor images of traditional Fort St. Vrain style fuel assembly and proposed micro fuel assembly

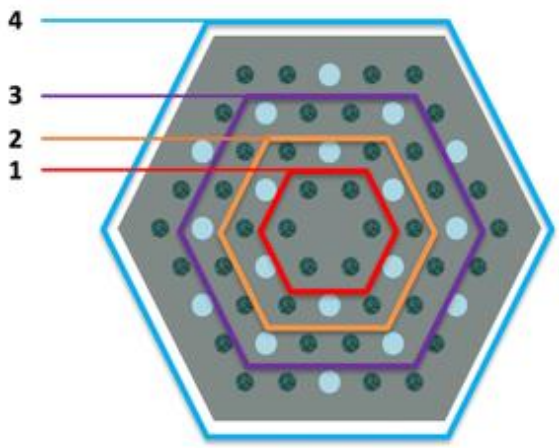

Figure 7. Image of micro assembly highlighted regions. (Blue circles for coolant pins, smaller green circles for fuel pins, and surrounding gray region for moderating material.)

Table 3. Justification of minimal micro assembly size based on Figure 7

Highlighted Perimeter #	Justification	Conclusion
1	Does not contain any coolant channels	Unacceptable
2	Region would be under-fueled if LBP were to be incorporated	Unacceptable
3	Region would be under-cooled if LBP were to be incorporated	Unacceptable
4	Fuel, coolant, and LBP could all be incorporated into outer edge, acceptable minimal size	Acceptable

UCO TRISO was used as the baseline fuel from the mHTGR-350 (Gougar H. et al, 2010) and the robust safety of the particle [6]. UN TRISO was used because of the higher kernel density in UN fuel as well as added measures of protection due to being embedded in a SiC compact [25]. Table 4 is a summary of the properties of UCO TRISO [25] and UN TRISO [89].

3.3.2 Moderators and Assembly

The beryllium- and hydride-based moderators were selected for the microreactor design from a comprehensive list of candidates in Snead et al. (2021) and further based on the analyses as described in Duchnowski et al. (2020) and Cheng et al. (2021). An additional yttrium hydride-based composite moderator candidate is considered in this study due to its similar performance to zirconium hydride but with improved thermal stability [90]. The thermal scattering libraries for zirconium and yttrium hydrides were assumed to be identical [91]. Consistent with prior descriptions, the moderators are modeled as two-phase composites with MgO as the host matrix for its irradiation performance and chemical stability [31] and the entrained moderating phase including beryllium- and hydride- based materials. Selection of these candidates follow their lower nuclei mass and similar scattering cross section to graphite, allowing for neutrons to thermalize over a much shorter distance [92].

The micro assembly incorporates many aspects of the Fort St. Vrain style fuel assembly. Coolant channel radius, fuel channel radius, and repeating pattern of coolant/fuel channels were left unchanged. This was expected to maintain a similar amount of coolant-to-fuel ratio of the Fort St. Vrain style fuel block, which showed acceptable safety performance under postulated accidents [93].

Table 4. Summary of AGR TRISO fuel, FCM TRISO fuel used for this study

Parameter		UCO TRISO [25]	UN TRISO [89]	Units
Kernel				
	Material	UCO ($UC_{0.5}O_{1.5}$)	UN	-
	Density	10.9	14.3	g/cm^3
	Outer radius	0.02125	0.0425	cm
Buffer Layer				
	Material	Porous graphite	Porous graphite	-
	Density	1.0	1.0	g/cm^3
	Outer radius	0.03125	0.0475	cm
Inner PyC Layer				
	Material	Carbon	Carbon	-
	Density	1.9	1.9	g/cm^3
	Outer radius	0.03525	0.0510	cm
SiC Layer				
	Material	Silicon carbide	Silicon carbide	-
	Density	3.2	3.2	g/cm^3
	Outer radius	0.03875	0.0545	cm
Outer PyC Layer				
	Material	Carbon	Carbon	-
	Density	1.9	1.9	g/cm^3
	Outer radius	0.04275	0.0580	cm
U-235 Enrichment		19.9	19.9	%
Matrix surrounding TRISO particles		Graphite	Silicon carbide	-

Volumetric fractions are chosen based on fabrication abilities and optimal ratios between host matrix and entrained phase, e.g., [94]. Shown in Table 5 is a list of the considered moderating materials along with host matrix and moderating phase volume fractions. These aspects were consistent across all designs and are summarized in

Table 6. The table does not specify assembly size because lattice pitch, a parameter varied in the design studies, impacts assembly size.

3.3.3 Reactor Core

As previously mentioned, the reactor core was modeled for the height of a single fuel compact with periodic boundary conditions, but power was scaled down from a full-sized design. The neutronics model only considers fuel assemblies and the outer reflector for calculations, neglecting the core barrel and pressure vessel as they are not expected to have an impact on performance.

Table 7 presents the unchanged parameters between microreactor designs. The design references "rings", which are radial groupings of assemblies needed for thermal-hydraulic calculations. Figure 8 is an image of the full core and how the groupings are defined.

3.4 Lattice Pitch Study

Scoping fuel-to-moderator studies for moderators alternative to graphite were performed during down selection of materials for the Transformational Challenge Reactor (TCR) which was intended as a demonstration high temperature gas cooled microreactor [95]. Bergeron A. et al. (2020) performed calculations comparing initial k_{eff} on a single hydride or beryllium moderator phase for a simple spherical geometry. The geometry considered TRISO packing fraction of 0.5 with various volumes of moderating material.

Table 5. Volume fraction of considered moderating materials

Cases hereinafter denoted as	Host material	Moderating Material
Graphite	-	Nuclear grade graphite (H-451) – 100% by volume
MgO BeO (60/40)	MgO – 60% by volume	BeO– 40% by volume
MgO Be (60/40)	MgO – 60% by volume	Be– 40% by volume
MgO $YH_{x=1.9}$ (85/15)	MgO – 85% by volume	$YH_{x=1.9}$ – 15% by volume
MgO $ZrH_{x=1.6}$ (85/15)	MgO – 85% by volume	$ZrH_{x=1.6}$ – 15% by volume

Table 6. Unchanged parameters of fuel assembly within this study [21]

Micro assembly parameter	Value	Unit
Fuel channel radius	0.794	cm
Number of fuel channels	42	-
Coolant channel radius	0.635	cm
Number of coolant channels	18	-

Table 7. Unchanged parameters of the reactor core within this study

Reactor Core parameter		**Value**	**Unit**
Number of assemblies:			
	Ring 1	1	-
	Ring 2	6	-
	Ring 3	12	-
	Ring 4	18	-
	Ring 5	18	-
	Total	55	-
Total core outer radius		90	cm

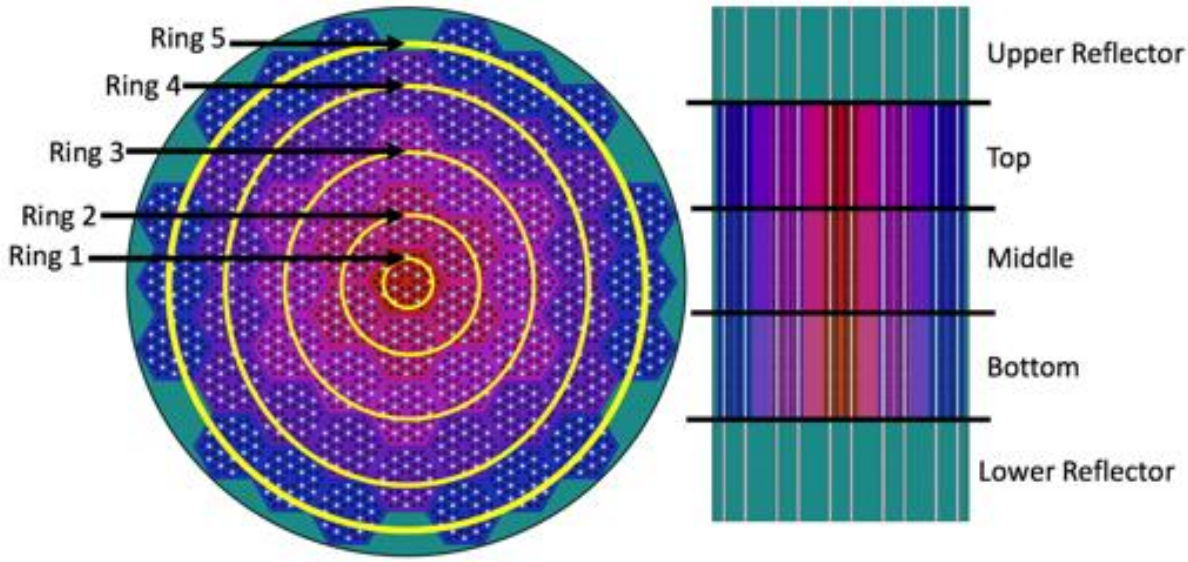

Figure 8. Radial (left) and axial (right) groupings of assemblies.

This work extends this scoping study of moderators alternative to graphite by performing a more comprehensive analysis including a more realistic geometry, various fuel and assembly configurations, assessing composite moderators instead of single phase moderators, and calculating additional metrics that are of high interest to microreactor developers, such as cycle length and fuel cycle costs.

A parametric study on TRISO packing fraction and fuel/coolant channel lattice pitch was conducted to explore the impact on reactor performance and gain insight on microreactor design characteristics. The parametric study considered both UCO and UN TRISO fuel for each moderating material. The most important difference between fuel types is that the UN TRISO fuel can have much more fissile uranium-235 mass than the UCO TRISO cases due to the higher density of UN as compared to UCO and because of a larger kernel-to-particle size ratio. This was expected to yield longer cycle lengths for UN designs relative to UCO as the same geometry would contain more fuel. Since the UCO TRISO particle has a higher achievable packing faction due to its smaller size, its packing fraction was varied from 0.1 up to 0.6 while UN TRISO packing fraction was only varied from 0.1 up to 0.5. Across all moderators and fuel type designs, the lattice pitch was varied from 1.5cm (smaller would lead to fuel/coolant channels beginning to overlap) to 2.5cm (larger would lead to the fuel assemblies exceeding the 90cm radial size limit). Both parameters were varied to identify the optimal configuration for maximizing the cycle length. The power was identical across all cases and scaled from the highest power considered in this study, $20MW_{th}$.

Contour plots for cycle length as a function of the lattice pitch and TRISO packing fraction are shown in Figures 5-9 for the graphite, MgO BeO (60/40), MgO Be (60/40),

MgO $YH_{1.9}$ (85/15), and MgO $ZrH_{1.6}$ (85/15) moderators with both fuel types, respectively. Here, the cycle length is plotted in units of Effective Full Power Years (EFPY). It should be noted that the color range for each of the mentioned figures is identical to allow the reader to easily compare plots, but the contour lines are not plotted in the same frequency because the hydride cases exhibit a much larger range. Regions of white are where the design could not achieve criticality. All microreactor designs have a longer cycle length with UN TRISO and for higher TRISO packing fractions.

These results are consistent with expectations as reactors with more fuel can generally run at the same power for more time than reactors with less fuel. The moderating power of each moderator positively corresponds to the reactor cycle performance. Graphite, having the lowest moderating power, shows the shortest cycle length, and MgO $ZrH_{1.6}$ (85/15), having the highest moderating power, shows the longest cycle length, with UN TRISO and MgO $ZrH_{1.6}$(85/15) running nearly 10 times longer than UN TRISO and graphite. However, for UCO TRISO at a low TRISO packing fraction moderated by hydrides, the pre-conceptual microreactor design cannot become critical because the design is over-moderated. Since the UN TRISO fuel has a much higher performance for all considered moderators, it is the only fuel type considered for the remainder of this study.

Other metrics were calculated to provide additional insight on the performance of the pre-conceptual microreactor design. Discharge burnup relates to many metrics that are key in assessing reactor performance, such as fuel cycle cost and natural resource requirement [96].

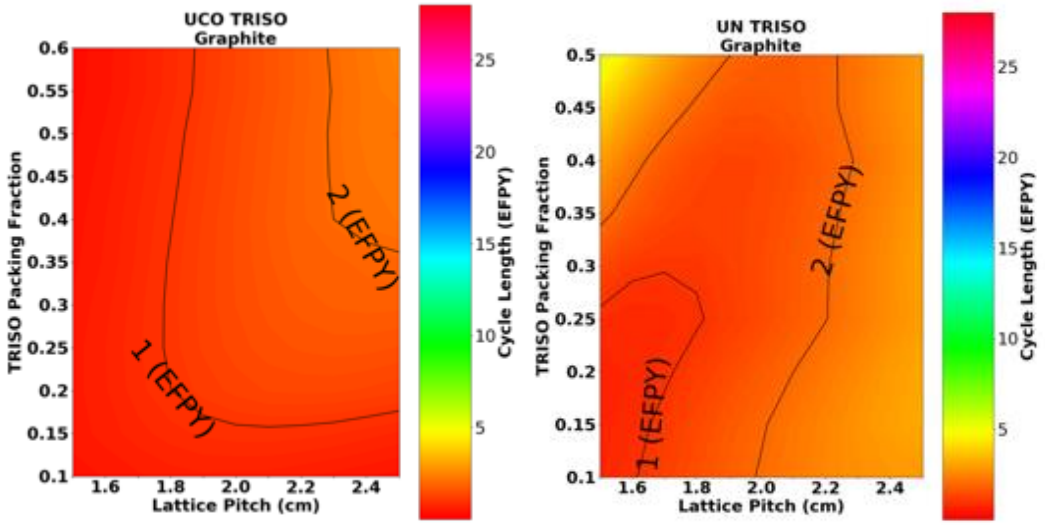

Figure 9. Contour plots of cycle length in EFPY of graphite microreactor design fueled with UCO TRISO (left) and UN TRISO (right) for various TRISO packing fraction and lattice pitch

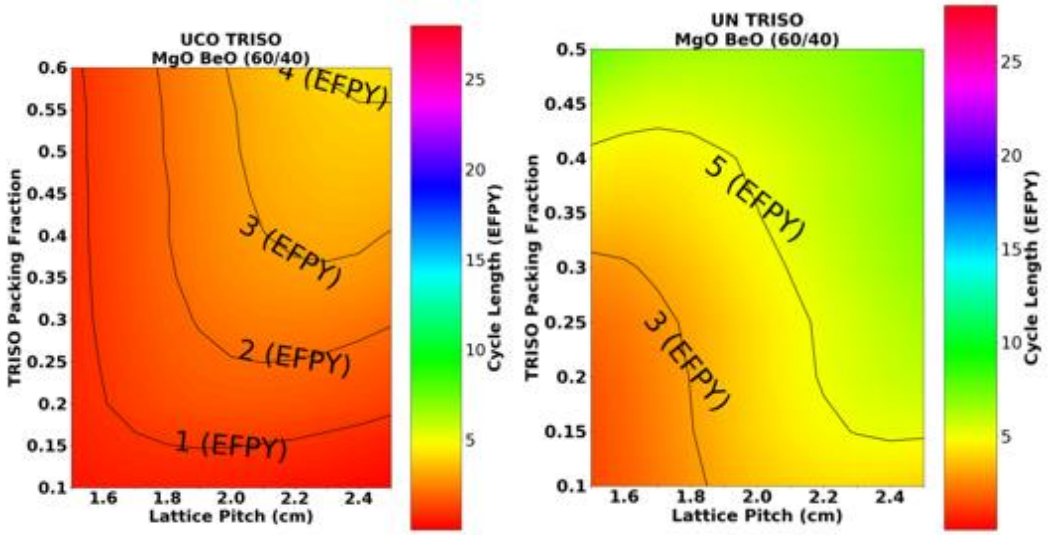

Figure 10. Contour plots of cycle length in EFPY of MgO BeO (60/40) microreactor design fueled with UCO TRISO (left) and UN TRISO (right) for various TRISO packing fraction and lattice pitch

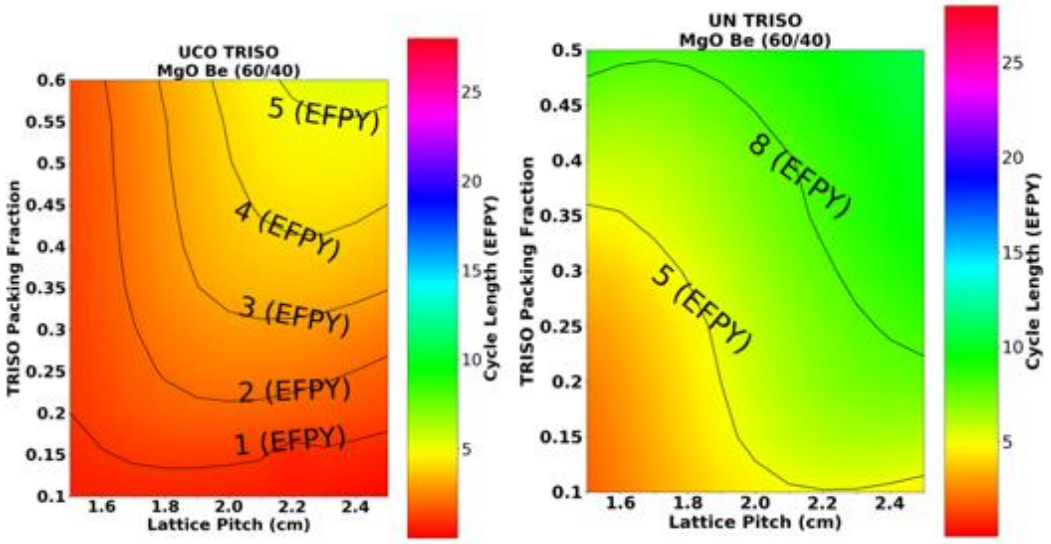

Figure 11. Contour plots of cycle length in EFPY of MgO Be (60/40) microreactor design fueled with UCO TRISO (left) and UN TRISO (right) for various TRISO packing fraction and lattice pitch

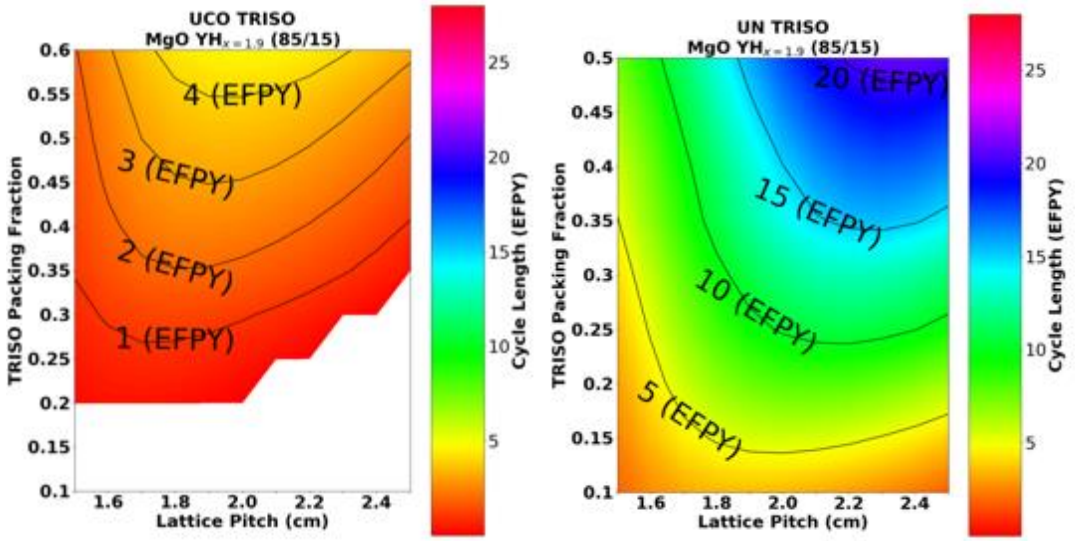

Figure 12. Contour plots of cycle length in EFPY of MgO $YH_{x=1.9}$ (85/15) microreactor design fueled with UCO TRISO (left) and UN TRISO (right) for various TRISO packing fraction and lattice pitch

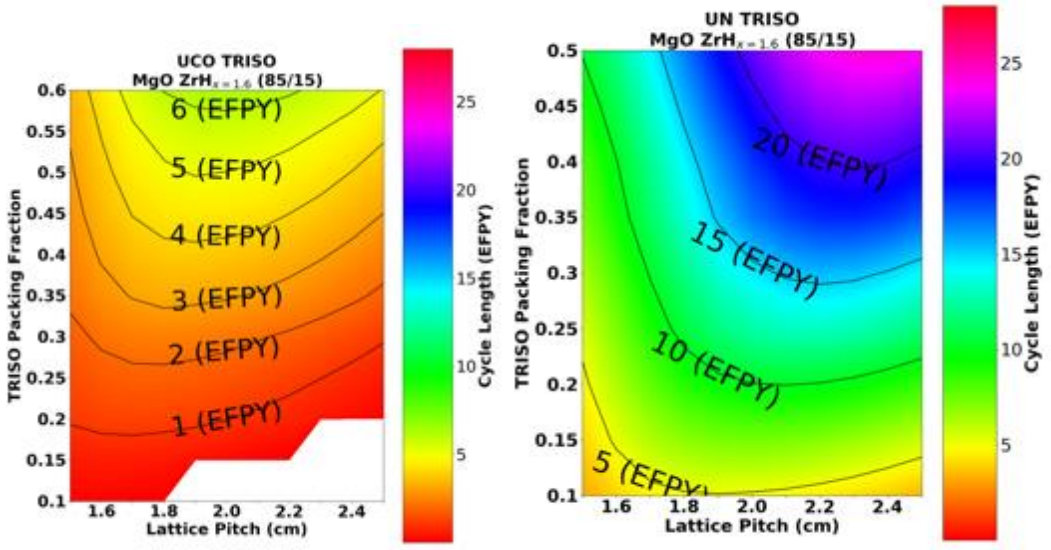

Figure 13. Contour plots of cycle length in EFPY of MgO ZrH$_{x=1.6}$ (85/15) microreactor design fueled with UCO TRISO (left) and UN TRISO (right) for various TRISO packing fraction and lattice pitch

Contour plots of discharge burnup are shown in Figures 10-12 for the graphite-, beryllium-, and hydride-based moderators with UN TRISO fuel, respectively. The images are plotted analogously to the contour plots of cycle length with the discharge burnup in units of MW-days / kgU.

The graphite moderated microreactor shows two distinct regions of improving performance, high packing fraction with minimal lattice pitch on the upper left of the plot and low packing fraction with the maximum lattice pitch on the lower right. The latter is due to the system approaching a more favorable fuel-to-moderator ratio as the moderating power of graphite is low and requires more moderating material to thermalize neutrons relative to the composite moderators. The former instead captures conditions where the design is operating in a much higher neutron energy region with significantly more uranium-238 fast fission occurring. The high rate of fast fissions is enough to compensate for the lack of thermal fission and improvements are realized when less moderator is present in the active core. While both sets of conditions produce comparable performance, the former was omitted as a possible design because operating with a higher dependence on fast fission decreases the influence of the moderating material, which is the focus of this study. Nonetheless, any considered configuration for the graphite moderated system still has a lower performance across every metric when compared to the composite moderators.

For all the designs, maximum discharge burnup occurs at a much lower TRISO packing fraction than for the maximum reactor cycle length. The fuel is being used more efficiently when the active core has less fuel and a more favorable fuel-to-moderator volume ratio.

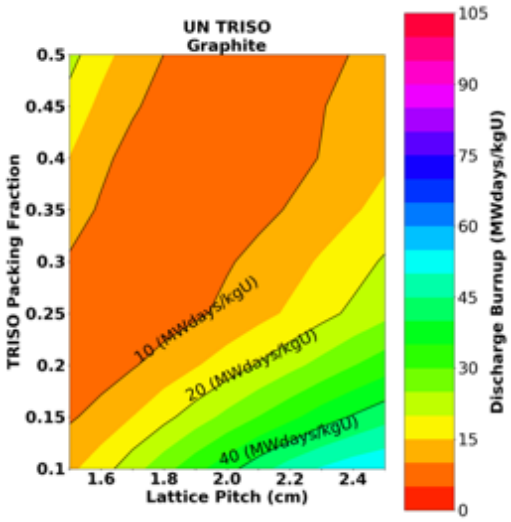

Figure 14. Contour plots of discharge burnup in units of MWdays/kgU of graphite microreactor design fueled with UN TRISO for various TRISO packing fraction and lattice pitch

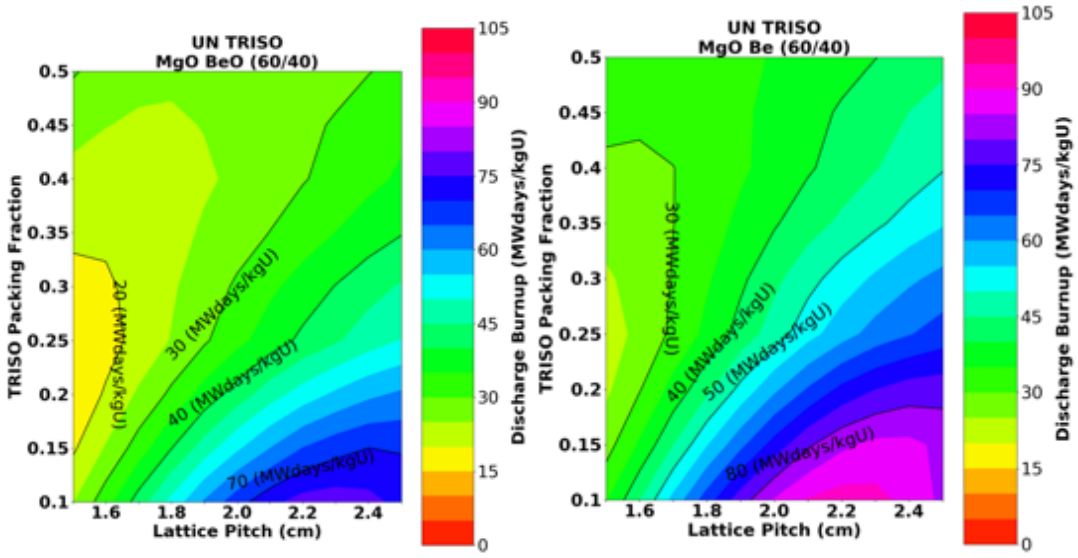

Figure 15. Contour plots of discharge burnup in units of MWdays/kgU of MgO BeO (60/40) (left) and MgO Be (60/40) (right) fueled with UN TRISO for various TRISO packing fraction and lattice pitch

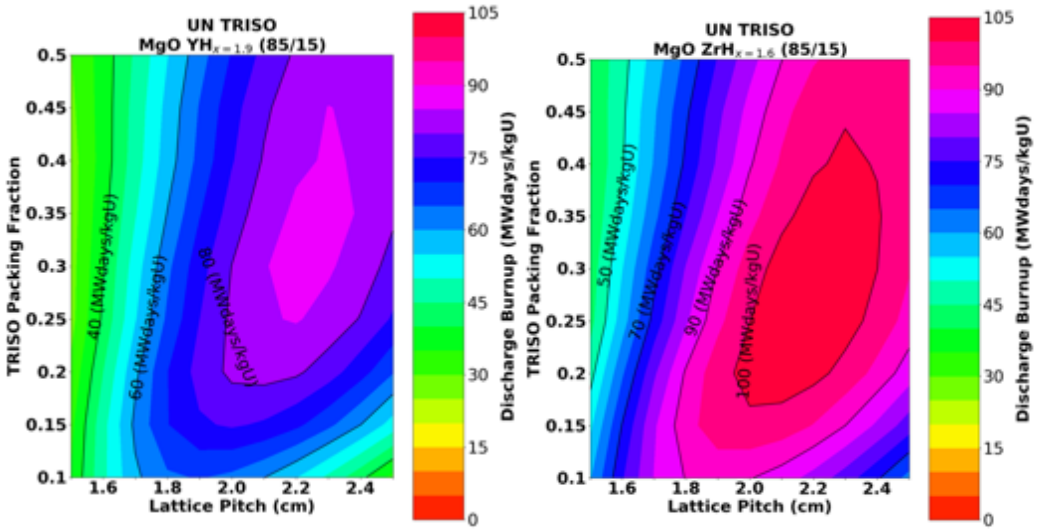

Figure 16. Contour plots of discharge burnup in units of MWdays/kgU of MgO $YH_{x=1.9}$ (85/15) (left) MgO $ZrH_{x=1.6}$ (85/15) (right) fueled with UN TRISO for various TRISO packing fraction and lattice pitch

In terms of fuel utilization, each design is operating in an under-moderated state when parameters have been selected to be maximized for cycle length. For these contour plots, a maximum discharge burnup zone can be clearly seen for the hydride-based moderators and could be inferred for the beryllium-based moderators. Graphite shows no indication of a maximum zone because the design is much more under-moderated than the two-phase moderator designs.

3.5 Power Study

A second parametric study was performed to determine the impact TRISO packing fraction and core power on cycle length. Power for the 2D neutronics model of the pre-conceptual microreactor design was varied from 2 to 20 MW_{th}. The purpose of this study was to gain insight on performance response and provide an expected cycle length for various core power and TRISO packing fractions. Contour plots of cycle length for the graphite-, beryllium-, and hydride-based designs are shown in Figures 13-15, respectively. The contour plots are similar to the previous plots with the exception of core power on the horizontal axis instead of lattice pitch.

As expected, lower core power and higher TRISO packing fractions result in longer cycle lengths for any design, and the beryllium and hydride moderated design can achieve much longer cycle lengths than graphite with the MgO $ZrH_{x=1.6}$ (85/15) case exhibiting the highest performance. Across all designs, a noticeable trend of non-linearity between cycle length and core power can be seen for any single TRISO packing fraction. This trend can be explained by the higher equilibrium concentration of xenon for higher core powers.

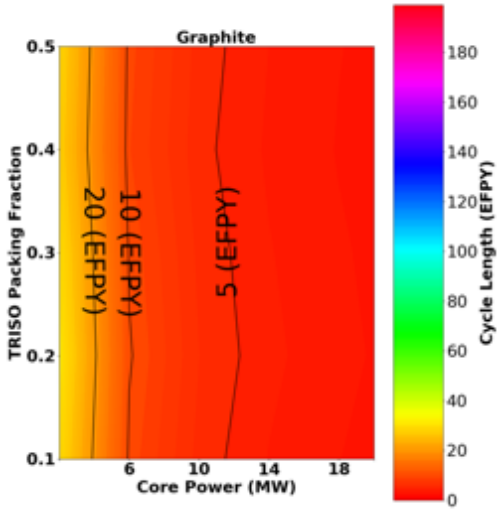

Figure 17. Contour plots of cycle length in EFPY for the graphite microreactor design fueled with UCO TRISO for various TRISO packing fraction and core power

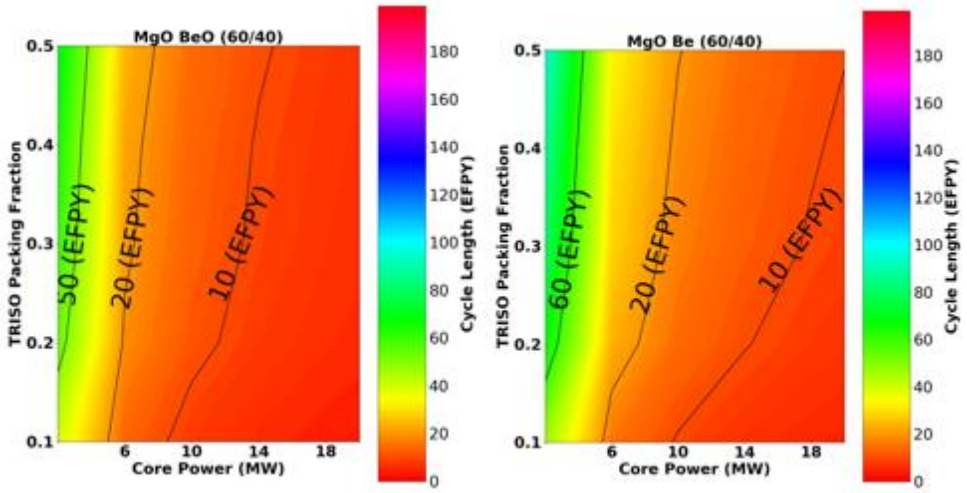

Figure 18. Contour plots of cycle length in EFPY for the MgO BeO (60/40) (left) and MgO Be (60/40)(right) microreactor designs fueled with UN TRISO for various TRISO packing fraction and core power

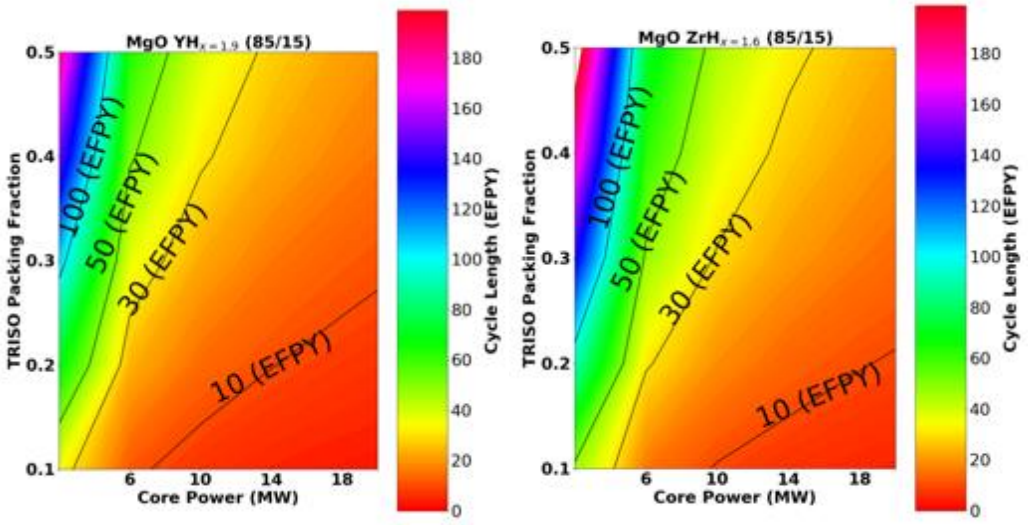

Figure 19. Contour plots of cycle length in EFPY for the MgO $YH_{x=1.9}$ (85/15) (left) and MgO $ZrYH_{x=1.6}$ (60/40) (right) microreactor designs fueled with UN TRISO for various TRISO packing fraction and core power

Near the BOC while the xenon concentration is approaching equilibrium, a large decrease in reactivity occurs because of the production of the highly neutron absorbing xenon-135 isotope. After the equilibrium concentration of xenon is reached, the reactivity letdown is fairly linear and corresponds to power fairly linearly as well. The compounding effects of a lower decrease in reactivity near the BOC and a smaller reactivity letdown for designs that have a lower power is the explanation for this non-linearity between cycle length and core power trend. This phenomenon was also shown for HTGTR scoping calculations in Sterbentz et al. (2016).

The graphite moderated system exhibited the shortest cycle length with very little improvement for high TRISO packing fractions. Graphite's low moderating power means the design can be easily overwhelmed with fuel. With increasing TRISO packing fraction, the graphite moderator has decreasing fuel efficiency. In Figure 17, the difference between cycle lengths for 0.1 and 0.5 TRISO packing fraction across all considered power never exceeds 3%. Realistically, such a marginal improvement would not justify the fivefold required increase in fuel, and a much lower TRISO packing fraction would be preferred from the perspective of fuel cycle cost. However, the only metric that was maximized was cycle length, and consequently, metrics such as fuel cycle cost did not influence decisions on the design. If additional metrics were to be considered, such as discharge burnup or fuel cycle cost, the beryllium and hydride moderators would still outperform graphite because of their higher moderating capabilities.

3.6 Natural Resource Utilization and Fuel Cycle Cost

Other parameters of interest were considered to better quantify the relative performance of these systems. Natural resource requirement and fuel cycle cost were calculated to assess how efficiently the fuel is being utilized. The methodology for determining the natural resource requirement is derived from U.S. Department of Energy (DOE) Evaluation and Screening (E&S) of fuel cycle options [3]. The assumptions made for these calculations were a 50% thermal-to-electric efficiency, a depleted uranium-235 enrichment of 0.25wt.% $(enr_{depleted})$, a natural uranium-235 enrichment of 0.711wt.% $(enr_{natural})$, and a fuel uranium-235 enrichment of 19.9wt.% (enr_{fuel}). Shown in Eq. 1 is the amount of fabricated fuel required ($\bar{M}_{charge}^{fuel}$) to achieve the desired discharge burnup (DB), where $P_{thermal}$ and $P_{electric}$ is the thermal and electric power, respectively. Eq. 2 is the required amount of natural feed uranium ($\bar{M}_{uranium}^{natural}$) from the amount of required fabricated fuel based on the enrichment assumptions. Calculations were performed for 0.5 TRISO packing fraction and 6MW$_{\text{thermal}}$ across all designs.

$$\bar{M}_{charge}^{fuel} = \frac{P_{thermal}}{P_{electric} * DB} \qquad (Eq.\ 3.1)$$

$$\bar{M}_{uranium}^{natural} = \bar{M}_{charge}^{fuel} * \frac{enr_{fuel} - enr_{depleted}}{enr_{natural} - enr_{depleted}} \qquad (Eq.\ 3.2)$$

A comparison of the cycle length for all designs utilizing a 0.5 TRISO packing fraction and 6MW core power in units of EFPY is shown in Figure 20 with enumerated values aligning with each respective bar. The increase in cycle length afforded by the composite moderators is conspicuously evident in Figure 16, where the beryllium-based moderators

offering a 2.5-4X increase in cycle length while the hydride-based moderators offer up to an 8X increase. These improvements will manifest in natural resource utilization, which is plotted in Figure 21 as the amount of natural feed uranium required per unit energy generated in units of metric tons per gigawatt year (t/GW-year). Here, the enumerated values shown along with each bar for the composite moderators is the percent difference relative to the calculated natural resource requirements for the graphite moderated case. The beryllium and hydride moderators are capable of utilizing the fuel more efficiently in a microreactor design, and as a result, produce power for longer than the graphite moderated system.

Comparing the zirconium hydride moderator to graphite, an expected 87% reduced amount of fuel is required when normalized to the total amount of power generated by the reactor. The fuel cycle cost was selected to show fuel efficiency from an economic perspective. The study provides a scoping calculation for the expected fuel costs and does not include the offset of potential reactor cost savings for large-scale manufacturing of the beryllium and hydride composite moderators. Furthermore, additional challenges and associated costs of having high TRISO packing fractions, which would likely need advanced manufacturing techniques in order to be achieved, are not considered here. The fuel cycle costs for mining, milling, conversion, enrichment, depleted uranium disposal, and fuel fabrication are taken from screening studies for modular HTGR [97] fuel and are shown in listed in Table 8.

The costs were applied to the various stages in the front-end fuel cycle. Mining, milling and conversion costs were applied to the amount of natural feed uranium ($\bar{M}_{uranium}^{natural}$) required.

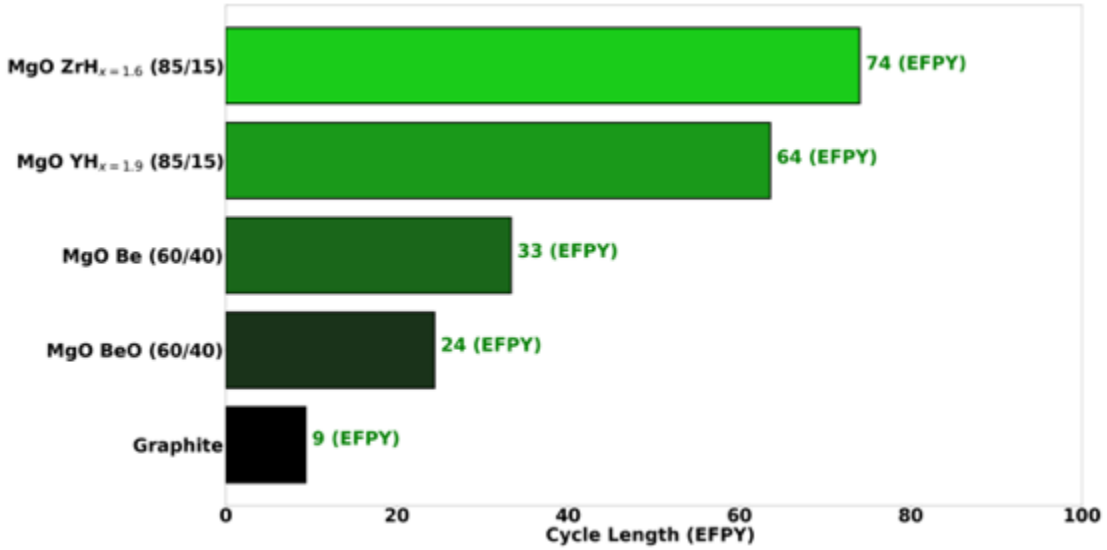

Figure 20. Cycle length in EFPY for all considered microreactor designs at a core power of 6MW and UN TRISO packing fraction of 0.50

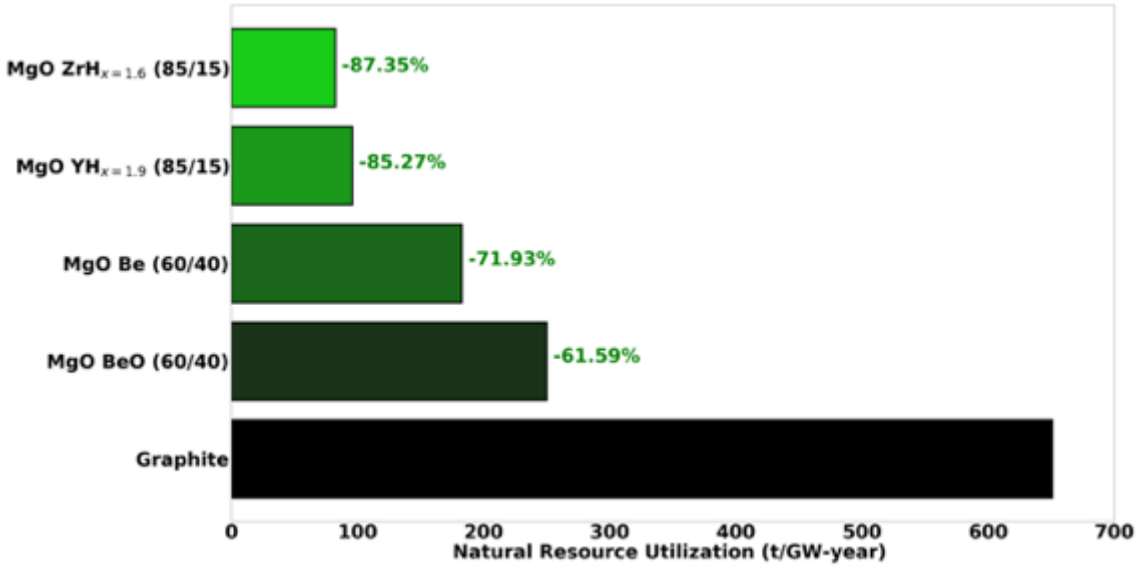

Figure 21. Natural resource utilization in t/GW-year for all considered microreactor designs at a core power of 6MW and UN TRISO packing fraction of 0.50

Table 8. Costs associated with TRISO fuel fabrications [97]

Category	Cost
Mining/milling	110 (Dollars/kgNatU)
Conversion	12 (Dollars/kgNatU)
Enrichment	100 (Dollars/kgNatU)
Depleted uranium disposal	4 (Dollars/kgDU)
Fuel fabrication	10000 (Dollars/kgLEU)

Enrichment costs were applied to Separative Work Unit (SWU), which captures the difference of enrichment from the fuel and de-enrichment of the depleted uranium to the natural enrichment of uranium. .The SWU uses the value function $\left(V(enr)\right)$ to scale the efforts of enrichment appropriately to their respective fuel front-end process. Depleted uranium disposal costs are applied to $\bar{M}_{charge}^{depleated}$, which is the difference between the natural feed uranium required and the amount of fabricated fuel used within the reactor. Fuel fabrication costs are applied to $\bar{M}_{charge}^{fuel}$, the amount of fuel initially loaded into the microreactor core.

$$V(enr) = (1 - 2 * enr) * \ln\left(\frac{1 - enr}{enr}\right) \qquad (Eq.\ 3.3)$$

$$\bar{M}_{charge}^{depleated} = \bar{M}_{uranium}^{natural} - \bar{M}_{charge}^{fuel} \quad (Eq.\ 3.4)$$

$$SWU = \bar{M}_{charge}^{fuel} * V\left(enr_{fuel}\right) + \bar{M}_{charge}^{depleated} * V\left(enr_{depleated}\right) - \bar{M}_{uranium}^{natural} * V(enr_{natural}) \qquad (Eq. 3.5)$$

The calculated fuel cycle cost in millions of dollars per gigawatt-year (M$/GW-year) for all designs is shown in Figure 22 is with the enumerated percent difference from graphite at the edge of each bar. Although each design is loaded with an identical amount of fuel with the same core power, the composite moderators produce power for longer periods of time. These increased cycle lengths of the composite moderated microreactors would possibly allow for capital costs to be distributed across the duration

of the reactors operational time, providing some economic incentive. If instead a set thermal power and cycle length is desired, then an ideal TRISO packing fraction could be found from Section Figure 23, which showed that the composite moderators would require less fuel than graphite. Overall, these results demonstrate that the higher fuel efficiency for microreactors utilizing composite moderators has the potential to considerably reduce fuel cycle costs.

3.7 Discussion

This pre-conceptual microreactor design required scaling down overall core size, assembly size, and core power from the selected initial HTGTR design but increasing fuel density to satisfy cycle requirements. HALEU fuel, UN TRISO fuel, and high TRISO packing fractions were all considered in this study for their ability to increase the overall fuel density of the microreactor design. It is likely that future microreactors that are based on a HTGR platform will incorporate UN TRISO fuel as the technology matures in the ARDP risk reduction project [98].

It was illustrated in this work that higher fuel density equates to longer cycle lengths but lower fuel efficiency for most cases. A noteworthy exception is the hydride moderated design that exhibited an improvement in discharge burnup from 0.1 to 0.25 UN TRISO packing fraction because of the high moderating capability. Although the UCO TRISO was not considered for much of this study, results from the parametric studies provide insights on the improve performance of the beryllium- and hydride-based moderated designs.

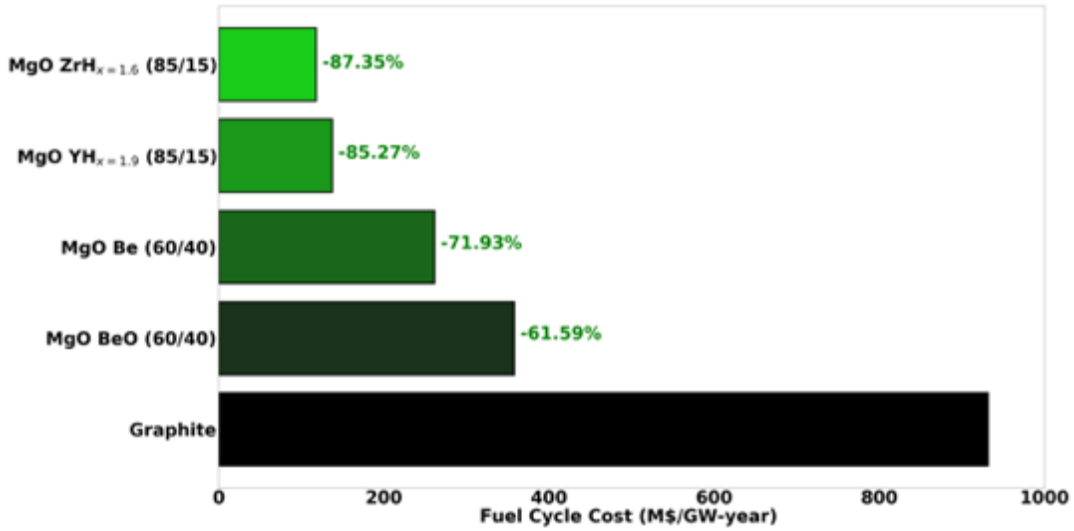

Figure 22. Calculated fuel cycle costs in millions of dollars per GW-year for all considered microreactor designs at a core power of 6MW and UN TRISO packing fraction of 0.50

The lattice pitch study for UCO TRISO fuel revealed that the beryllium- and hydride-based moderators have an optimal lattice pitch for cycle length within the considered range for a given TRISO packing fraction. The shorter mean free path and higher moderating power of the beryllium- and hydride-based moderators can result in under-moderation if lattice pitch is too small or over-moderation if lattice pitch is too large. For graphite, no optimal lattice pitch can be identified due to its much lower moderating power and larger mean free path. The graphite system is thus limited by the technical size constraint, and it can be concluded that the graphite moderated design is significantly under-moderated even for the least fueled UCO TRISO design. Further increasing the fuel loading by implementing UN TRISO exacerbates under-moderation in the graphite-based design.

Other microreactor design concepts also considered using higher fuel density by incorporating HALEU fuel to compensate for the higher neutron leakage from smaller core sizes [10], which has a strong impact on fuel cycle performance [99]. Microreactor designs would therefore have much higher fuel-to-moderator volume ratios as compared with larger reactor designs and would benefit from moderators that have enhanced performance for a higher ratio. Duchnowski et al. (2020) showed that beryllium and hydride moderated designs have a higher performance for higher fuel-to-moderator volume ratios relative to a graphite moderated design. High fuel density and high neutron leakage associated with a microreactor design requires a high performing moderator that can thermalize neutrons over a short distance, a condition that can be achieved by all the evaluated composite moderators.

CHAPTER 4
TWO-PHASE COMPOSITE MODERATOR HIGH TEMPERATURE GAS COOLED MICROREACTOR: SAFETY CHARACTERISTICS AND THERMAL-HYDRAULIC DESIGN SPACE

A version of this chapter was originally published by Edward M. Duchnowski et al.:

Duchnowski E.M. et al. "Pre-conceptual high temperature gas-cooled microreactor design utilizing two-phase composite moderators. Part I: Design space and safety characteristics." *Progress in Nuclear Energy* 149 (2022) 104258.

In the original publication, I led the formal analysis, investigation, developed the thermal-hydraulic models, and wrote the original draft. Veronica Karriem assisted in the development of the thermal-hydraulic models along with reviewing and editing the original draft. Jacob P. Gorton assisted in the early development of the thermal-hydraulic models and also reviewed and edited the original draft. Khian Skidmore developed the health physics models in collaboration with myself. Khian Skidmore also reviewed and edit the original draft. Jason R. Trelewicz, Lance L. Snead, and Nicholas R. Brown are credited with the conceptualization and funding acquisition as well as reviewing and editing the original draft.

4.1 Motivation for Design Space and Safety Analysis

The International Atomic Energy Agency (IAEA) has reported on HTGR design features that satisfy fundamental safety objectives and requirements. The design features implemented across all HTGR designs for safety performance are high performance coated fuel particles, single phase coolant, low power density, large heat capacity, high thermal conductivity, large thermal margins to failure, and negative fuel and moderator temperature coefficients [100]. Sterbentz et al. (2016) performed transient calculations for the HTGTR point design and showed no expected compromise of the fuel but that it was necessary to examine the performance of the pre-conceptual microreactor design under the bounding case for fuel temperature, a DLOFC transient.

Research on the preconceptual microreactor design is extended to compare the operable design space, safety characteristics, and transient response of the microreactor designs from CHAPTER 3 of this dissertation. Reactor physics calculations of steady

state power profile, Moderator Temperature Coefficient (MTC), and Fuel Temperature Coefficient (FTC) are in support of the thermal-hydraulic steady state and/or DLOFC transient calculations. An operable steady state design space is identified for each microreactor design that did not exceed global or design specific constraints. A set of steady state operation conditions is then selected and applied to all designs as the initial conditions for the DLOFC transient. An additional accident that considers levels of mitigation for key radioactive isotopes contributing to Emergency Planning Zone (EPZ) size is performed for all designs to illustrate that a reduced EPZ size is appropriate for a microreactor with comparisons across the designs. The overall aim of this work is to perform additional calculations related to safety parameters instead of reactor physics performance and compare graphite and beryllium/hydride-based composite moderated designs optimized for cycle length.

4.2 Thermal-Hydraulic Model

The pre-conceptual microreactor design descended from the HTGTR point design [83] with major changes to transform the design into a microreactor. Parametric studies in CHAPTER 3 informed further decisions aimed at maximizing the target metric of cycle length. All the designs implemented the changes but with different moderating materials. Figure 23 is a schematic of the pre-conceptual microreactor core with definitions of radial and axial groupings.

The continuous-energy Monte Carlo physics burnup calculation code Serpent [72] was used to model the pre-conceptual microreactor design. Calculation of power profiles were performed at the Beginning of Cycle (BOC) for each design to be implemented as initial conditions within the thermal-hydraulics model.

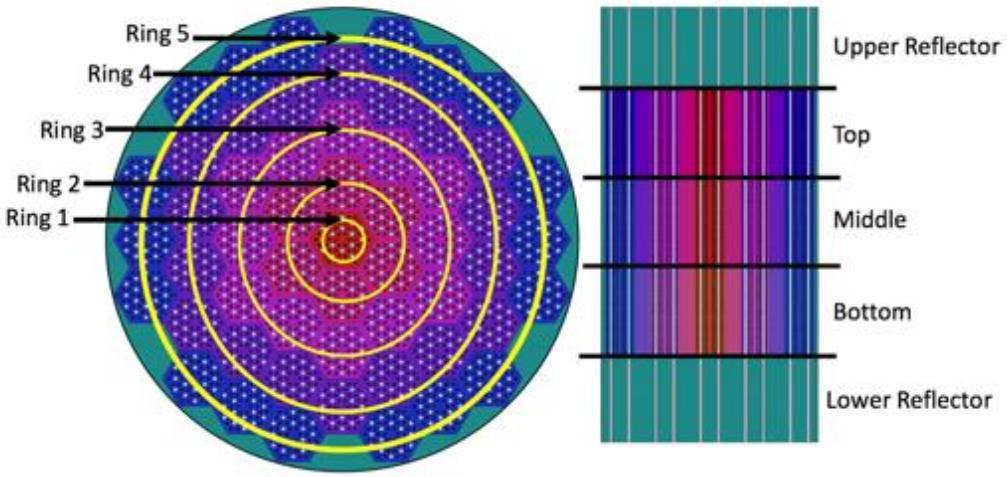

Figure 23. Radial (left) and axial (right) groupings of assemblies.

The calculated power of each assembly level per ring is shown in Figure 24-Figure 26 for the graphite-, beryllium-based, and hydride-based moderated designs. The power fraction is much greater in rings 3 and 4 due to the larger number of fuel assemblies while peak power density occurs in ring 1. The short mean free path associated with the beryllium and hydride containing moderators results in more power being produced towards the center of the core, in the middle layer. The thermal-hydraulics calculation for the pre-conceptual microreactor was modeled with INL's RELAP-3D [75]. The methodology employed here is similar to the INL HTGTR study as well as the internationally benchmarked GA mHTGR-350 [77]. Strydom et al., (2012) provides an excellent example of how the ring model is applied along with a unit cell configuration and RELAP5-3D nodalization diagram.

For the thermal-hydraulics study, control rods were not modeled as the transient calculation considered no active intervention such as the insertion of control rods. This would also provide the model with a higher power density and thus expected to be more conservative. Figure 27 is a nodalization diagram of the thermal-hydraulics microreactor model along with descriptions of the component numbers in Table 9 listed in order from coolant inlet outlet. The model incorporates 0.2mm coolant gas gaps between the fuel channels and the surrounding moderator as well as a 2mm radial gas gap between each assembly ring. The orange regions in the nodalization diagram are the heat structures that represent the fuel assemblies.

The thermal conductivity of the fuel compacts used in the thermal-hydraulics model combined the TRISO and surrounding matrix thermal conductivity values based on the Maxwell-Eucken equations for heterogeneous solids [101].

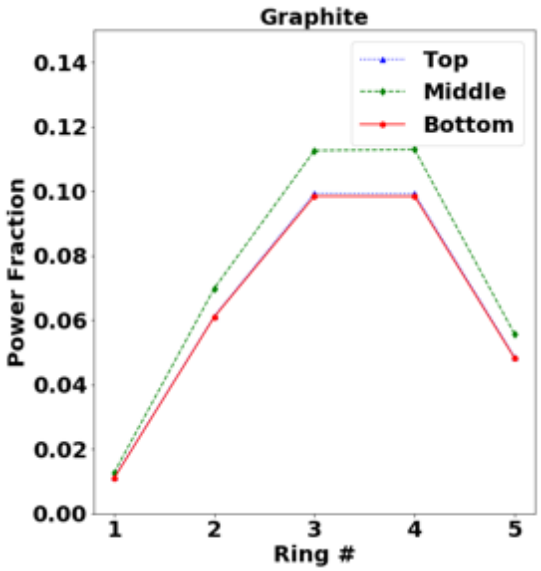

Figure 24. Fractional power distribution for each ring at each axial level for the graphite moderated microreactor with a UN TRISO packing fraction of 0.50.

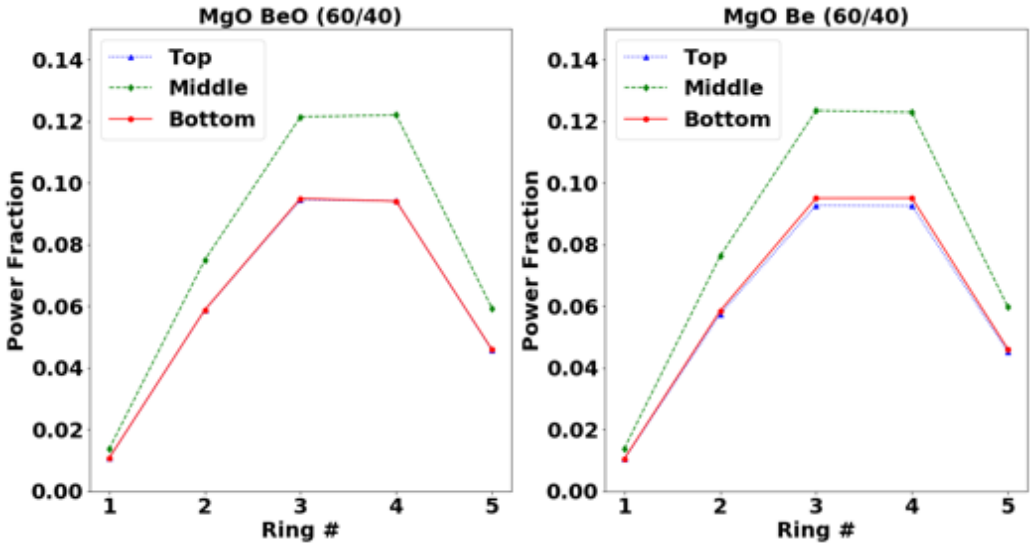

Figure 25. Fractional power distribution for each ring at each axial level for the MgO BeO (60/40) (left) and MgO Be (60/40) (right) moderated microreactor with a UN TRISO packing fraction of 0.50.

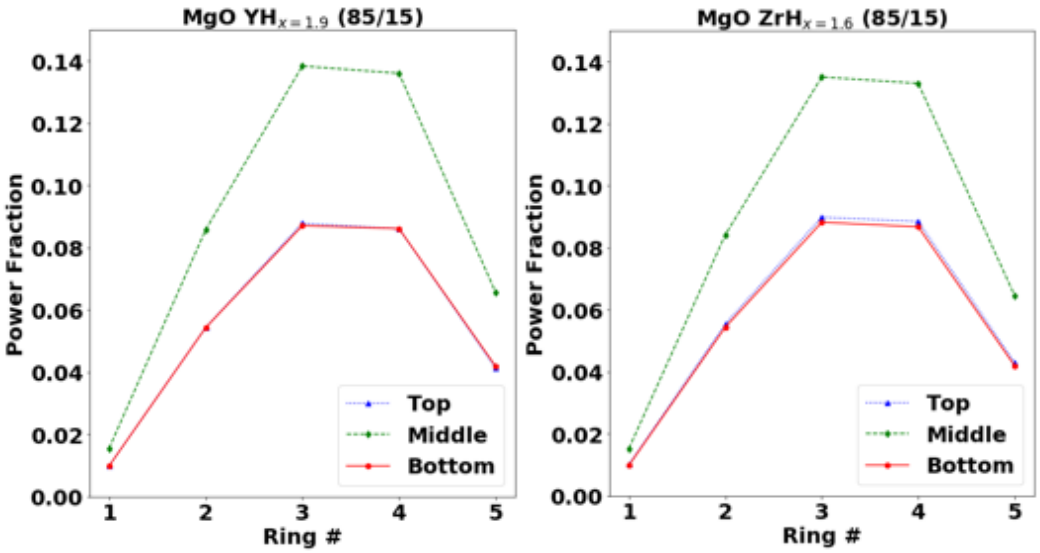

Figure 26. Fractional power distribution for each ring at each axial level for the MgO $YH_{x=1.9}$ (85/15) (left) and MgO $ZrH_{x=1.6}$ (85/15) (right) moderated microreactor with a UN TRISO packing fraction of 0.50.

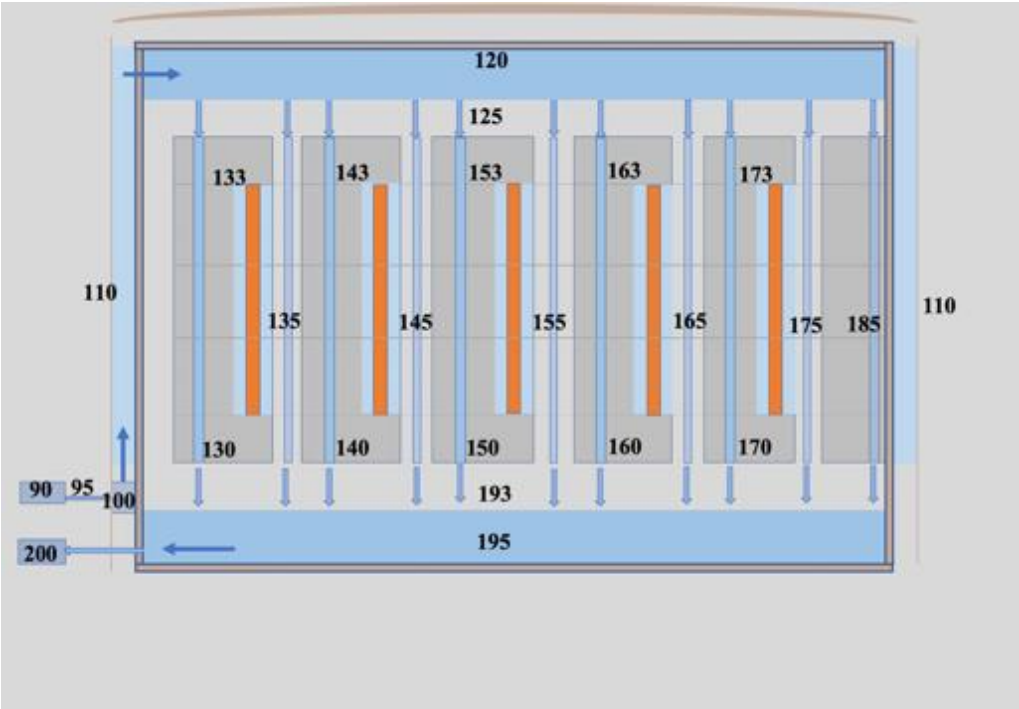

Figure 27 Nodalization of the microreactor design.

Table 9. List of components for the nodalization diagram.

Component number	Component type and description
90	Time dependent volume: Coolant Inlet
95	Time dependent junction: Inlet mass flow rate adjustment
100	Branch: Vessel inlet
110	Pipe: Coolant upcomer
120	Branch: Inlet plenum
125	Multiple junction: core inlet junction
133, 143, 153, 163, 173	Pipe: Fuel gas gap for ring 1, ring 2, ring 3, ring 4, and ring 5 respectively
135, 145, 155, 165, 175, 185	Pipe: Assembly gas gap for ring 1, ring 2, ring 3, ring 4, ring 5, and reflector respectively
130, 140, 150, 160, 170	Pipe: Coolant channels for ring 1, ring 2, ring 3, ring 4, and ring 5 respectively
193	Time dependent junction: flow outlet
195	Branch: Outlet plenum
200	Time dependent volume: Coolant Outlet

The equation for calculating the thermal conductivity of the fuel compact is shown in Eq. 4.1,

$$\frac{k_{compact}}{k_{matrix}} = \frac{1 + 2 * \beta * f}{1 - \beta * f}, \quad \beta = \frac{\frac{k_{TRISO}}{k_{matrix}} - 1}{\frac{k_{TRISO}}{k_{matrix}} + 2} \qquad (Eq. 4.1)$$

where $k_{compact}$ is the thermal conductivity of the fuel compact, k_{matrix} is the thermal conductivity of the matrix surrounding the TRISO particle, and f is the TRISO packing fraction within the fuel compact. With a lack of experimental data on the thermal conductivity of TRISO particles, the value of 12.01W/mK from Lee H.G. et al. (2017) was used in this study. Unirradiated SiC made through Nano-Infiltration and Transient Eutectic-phase (NITE) processing route was used for the thermal conductivity of the Fully Ceramic Microencapsulated (FCM) matrix [102]. The volumetric heat capacity of the fuel compacts was the volume-weighted heat capacity of each material inside the compact. The heat capacity of UN was based on Oetting et al., (1972) and the heat capacity of the SiC matrix was from Snead. et al. (2007) [103] [104]. Figure 28 is the volumetric heat capacity of UN TRISO fuel within a SiC matrix at a 0.5 packing fraction and the corresponding thermal conductivity.

The volumetric heat capacity and thermal conductivity of the four composite moderators are shown in Figure 29 relative to the graphite baseline. Parallel experimental measurement of thermophysical properties by Stony Brook University [94] demonstrated the values employed here are consistent with the measured thermal conductivity and heat capacity for the beryllium-containing composites; unpublished results confirm the same for the hydride-based moderators.

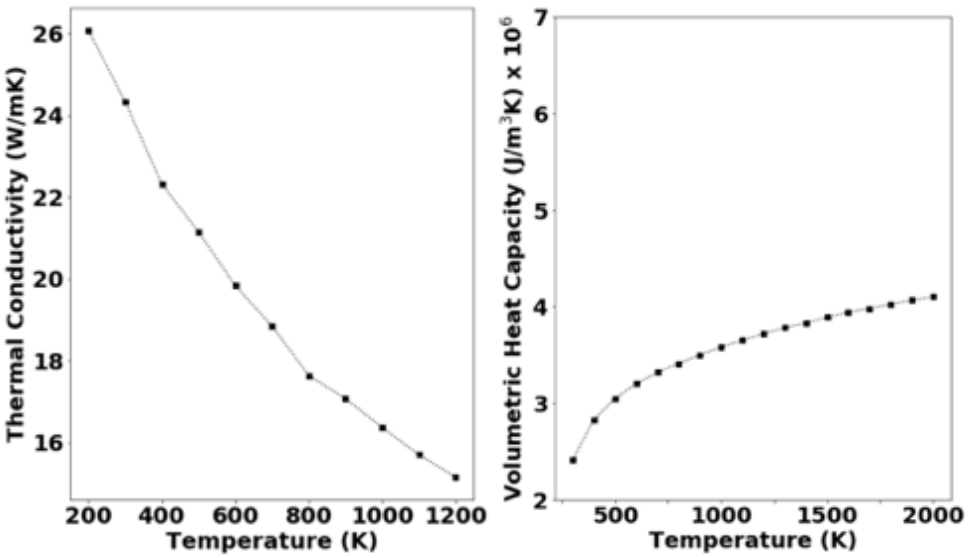

Figure 28. Thermal conductivity (left) and volumetric heat capacity (right) of FCM TRISO with 0.5 TRISO packing fraction.

Where direct measurements of the thermophysical properties were unavailable for the two-phase composite moderators (e.g., MgO-Be), the volumetric weighted average of the matrix MgO and specific moderating phase was employed using literature data cataloged in Table 10. For the case of $ZrH_{1.6}$, the values from the experimental results went up to a maximum temperature measurement of 700K as the thermophysical properties of zirconium hydrides are unavailable at elevated temperatures. Beyond this temperature, the values of $ZrH_{1.6}$ were assumed to remain unchanged even though values for temperatures of up to 1400K were utilized. This assumption was made to allow for convergence of the thermal-hydraulics model, and constraints on maximum moderator temperature were applied after the simulation converged during the design space study.

4.3 Design Space

To identify the operable design space of each microreactor, the Risk Analysis and Virtual Environment (RAVEN) [105] tool was used along with RELAP. RAVEN was used to perform a parametric sweep on the inlet coolant temperature, outlet coolant temperature, and total core power for each design. The upper and lower bounds of the input parameters are shown in Table 11. Core power was varied under the same range as CHAPTER 3. The ranges for inlet and outlet temperature are selected not as definite constraints but are intended to illustrate a general trend in the microreactor operating space. Constraints on allowable operating temperatures for the moderator/fuel and the coolant pressure drop limit are summarized in Table 12, and the composite moderators, represent a conservative approach to the upper bound.

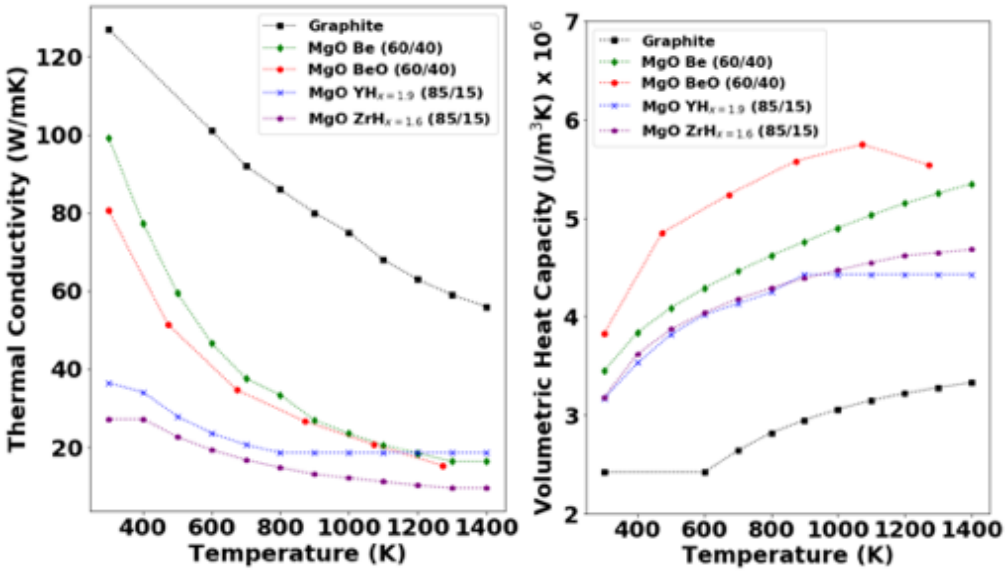

Figure 29. Thermal conductivity (left) and volumetric heat capacity (right) of moderating materials.

Table 10. Sources for thermophysical properties of the moderators.

Material	Source for volumetric heat capacity	Source for thermal conductivity
Graphite	[76]	[76]
MgO BeO (60/40)	[94].	[94].
MgO	[106]	[107]
Be	[108]	[108]
$YH_{1.9}$	[109]	[109]
$ZrH_{1.6}$	[110]	[110]

Table 11. Upper and lower bounds of parameters used for identifying the design space.

Parameter	Lower bound	Upper bound	Unit
Inlet temperature	523.15	673.15	K
Outlet temperature	675.15	1023.15	K
Core power	2	20	MW_{th}

Table 12. Constraints applied to the design space.

Constraints		Value	Unit
Maximum moderator temperature			
	Graphite	3000 [111]	K
	MgO Be	1273	K
	MgO BeO	1273 [94]	K
	MgO $YH_{1.6}$	1373 [112]	K
	MgO $ZrH_{1.9}$	1273	K
Maximum fuel temperature		1723 [52]	K
Maximum pressure drop		0.2 [83]	MPa

For example, the stability of the fully ceramic MgO-BeO composite certainly exceeds 1273K, but this limit is employed to be consistent with the MgO-Be moderator and aligns with prior thermophysical property measurements [94]. Steady state conditions that produced temperatures outside of these constraints were rejected as possible designs, though we note that future demonstrations of improved stability relative to these conservative estimates will expand the design envelope.

For the graphite and yttrium hydride, temperature limits were found within the literature while the beryllium-based and zirconium hydride limits were derived from experimental insights. During the fabrication of the MgO Be (60/40) composites, the entrained Be moderator reacted with the MgO host matrix forming a layer of BeO surrounding the entrained Be. This shell of BeO is assumed to limit additional reactions of Be with MgO under normal operating conditions and the same 1273K temperature limit is assumed. Thermophysical properties of the MgO BeO (60/40) were measured up to 1273K without compromising the integrity of the material and thus selected to be the conservative moderator temperature limit for this material [94]. At low temperatures (~700K), hydrogen in zirconium hydride powder begins to dissociate [113], which early experiments have demonstrated can be mitigated by entraining the zirconium hydride into the MgO matrix with no hydrogen desorption up to 1273K, hence the selected upper limit of 1273K.

A parametric study was performed by simulating steady state reactor operating conditions for unique combinations of power, inlet coolant temperature, and outlet coolant temperature. In addition to each microreactor design having constraints outlining the allowable operating space, simulation constraints were applied. The thermal-

hydraulics model uses a control variable to solve for the coolant mass flow rate under the unique set of inputs. Certain combinations of inputs (e.g. the minimum power and maximized coolant ΔT), caused the model to either fail to converge or calculate an oscillating negative-to-positive coolant mass flow rate. Any cases that predicted negative, oscillating, or unconverged coolant mass flow rates were rejected.

Figure 30, Figure 31, and Figure 32 are images of the coolant mass flow rate and temperature differential as a function of core thermal power for the graphite-, beryllium-, and hydride-based microreactor designs, respectively. The graphite moderated design exhibits the largest design window due to the high thermal conductivity and temperature limit of graphite, allowing the graphite moderated design to have more operating space at lower core thermal powers (~2MW_{th}) unlike the composite moderated designs. The lower core power would increase reactor cycle length but as concluded in CHAPTER 3 of this dissertation, both the beryllium- and hydride-based moderated designs would still have a longer cycle length than graphite.

The composite moderators' design spaces are limited primarily by the thermal conductivity and the moderator temperature limit. Either design cannot match the large design space associated with the graphite moderator due particularly to the moderator temperature limits, though as discussed above, are overly conservative and being expanded as additional stability data is acquired on each system. The hydride moderated designs have a slightly larger design space than the beryllium-based moderated designs despite having a lower thermal conductivity.

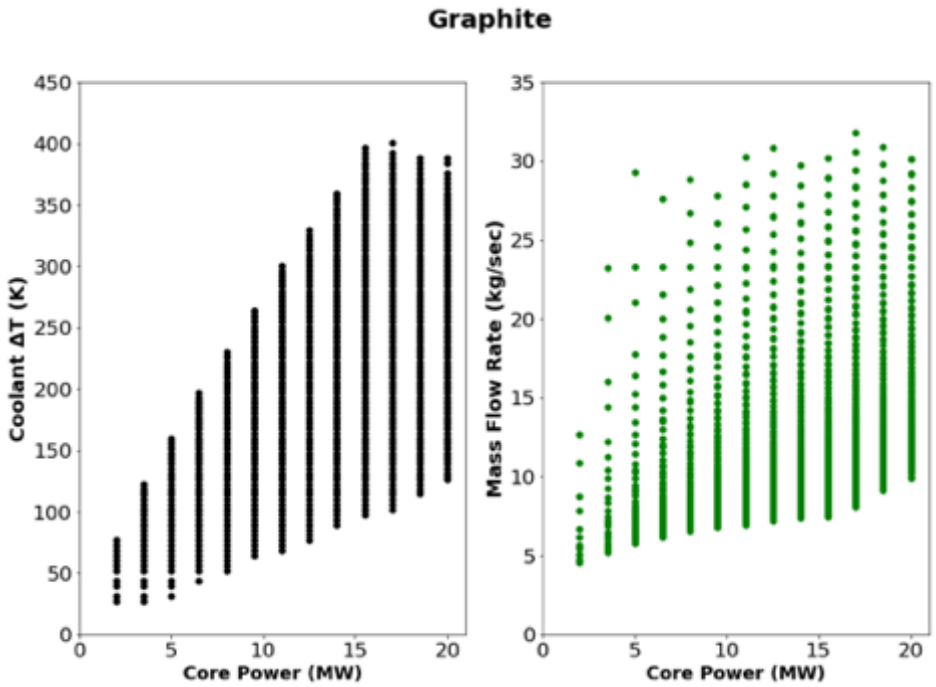

Figure 30. Calculated coolant temperature differential and coolant mass flow rate for a given power for the graphite moderated microreactor.

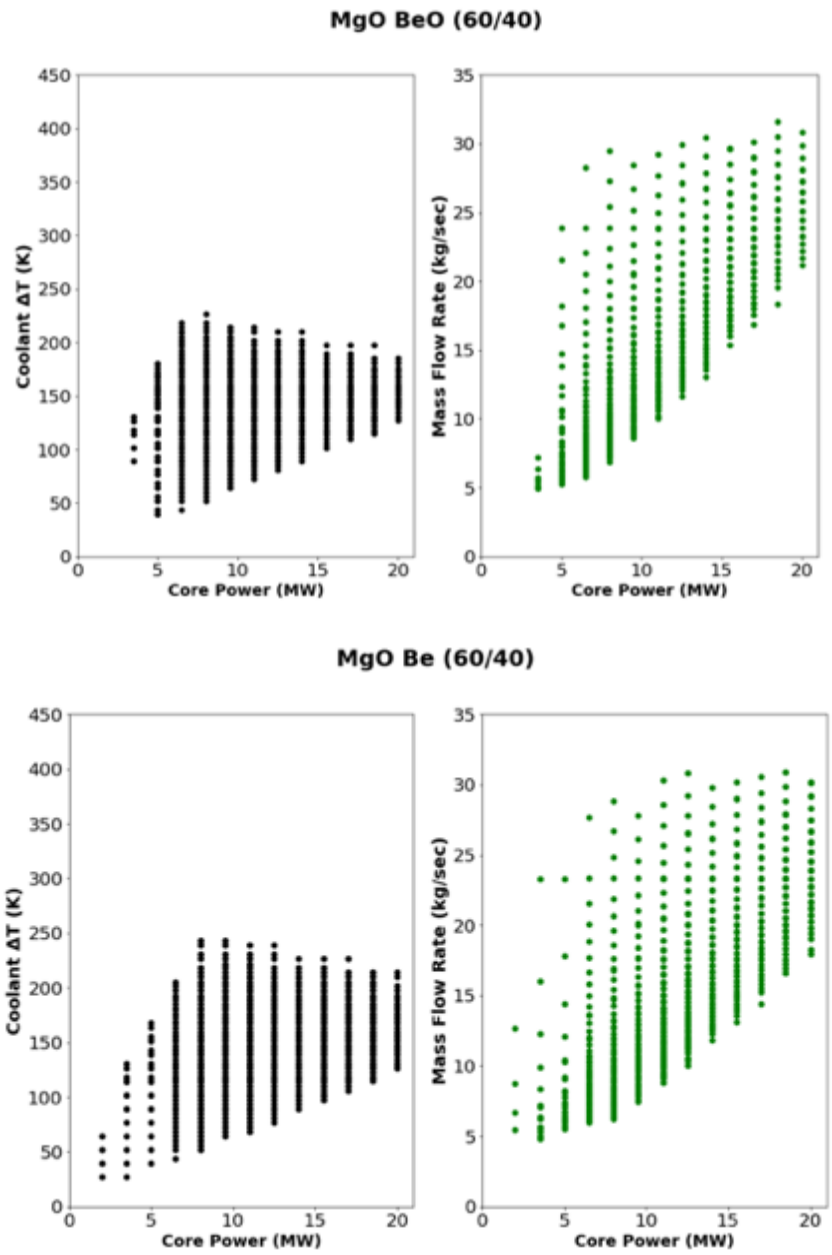

Figure 31 Calculated coolant temperature differential and coolant mass flow rate for a given power for the MgO BeO (60/40) (top) and MgO Be (60/40) (bottom) moderated microreactors.

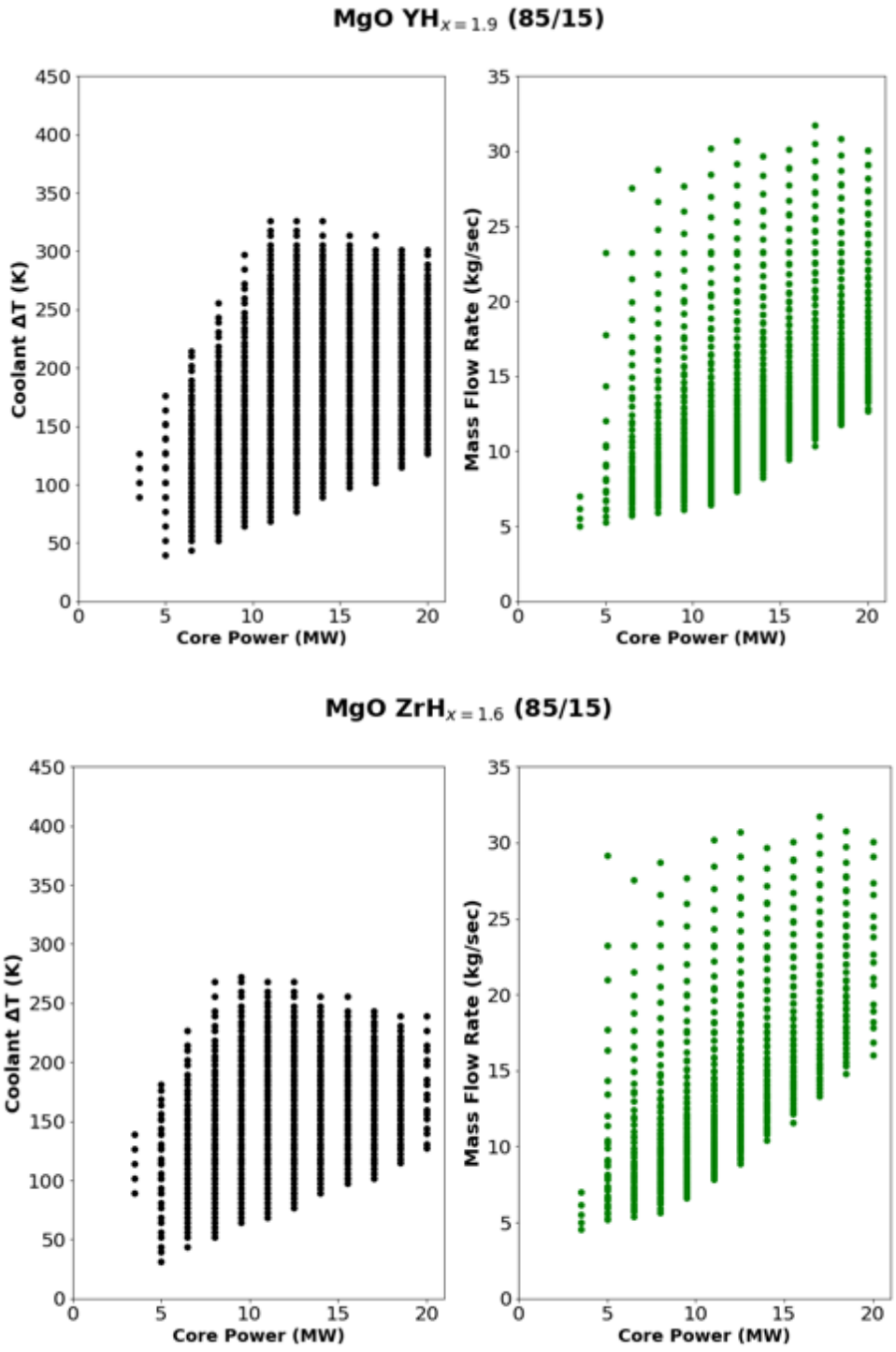

Figure 32. Calculated coolant temperature differential and coolant mass flow rate for a given power for the MgO $YH_{x=1.9}$ (85/15) (top) and MgO $ZrH_{x=1.6}$ (85/15) (bottom) moderated microreactors.

The improved design space is attributed to the hydride moderated designs having a larger fraction of power being generated in ring 3 and ring 4, which make up the majority of the active core with a larger amount of the coolant passing through these rings. Having more coolant exposed to higher power fractions allows for more heat to be transferred away from the moderator block, which seemingly is the most limiting factor in this study. Under the assumed temperature limits for each moderator, the yttrium hydride moderators produce the largest operating design space of the proposed composite moderators.

From the design space study, a set of parameters was identified that would be acceptable within all microreactor configurations: thermal power of 6 MW_{th}, inlet coolant temperature of 550K, and outlet coolant temperature of 700K. These conditions were selected to provide a constant comparison of steady state operating conditions solely on the thermophysical and neutronic properties of the moderating materials. These values are not intended to represent any final decision on parameters but rather used as an example case. Figure 33, Figure 34, and Figure 35 are the steady state moderator and fuel temperatures for the graphite-, beryllium-, and hydride- based microreactor designs under these boundary conditions.

All designs exhibited similar moderator and fuel temperature trends with slight differences attributed to their power profile and thermal conductivity. Regions near the coolant inlet or coolant outlet have similar temperatures for all designs because of the set boundary conditions at these locations and show differences at locations further away from the boundary.

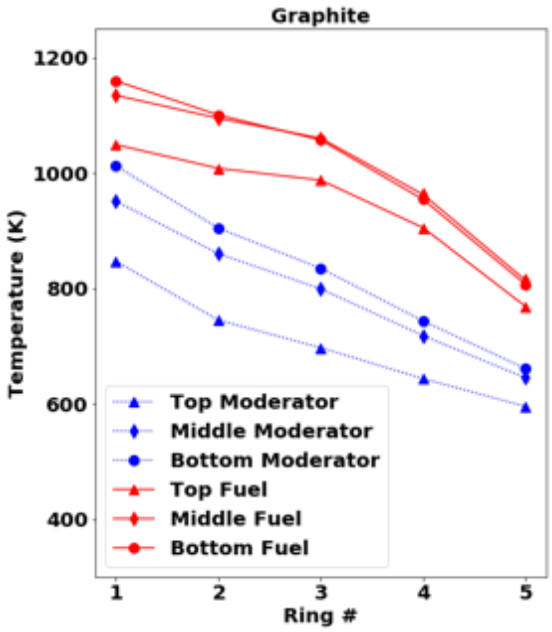

Figure 33. Steady state temperature distribution for the graphite moderated microreactor.

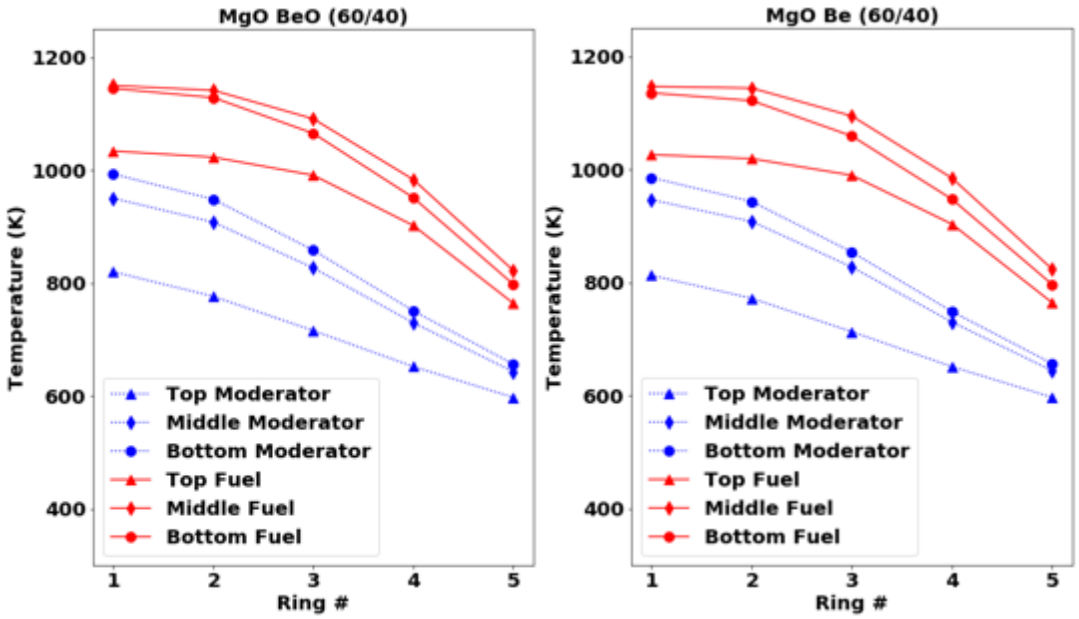

Figure 34. Steady state temperature distribution for the MgO BeO (60/40) (left) and MgO Be (60/40) (right) moderated microreactor.

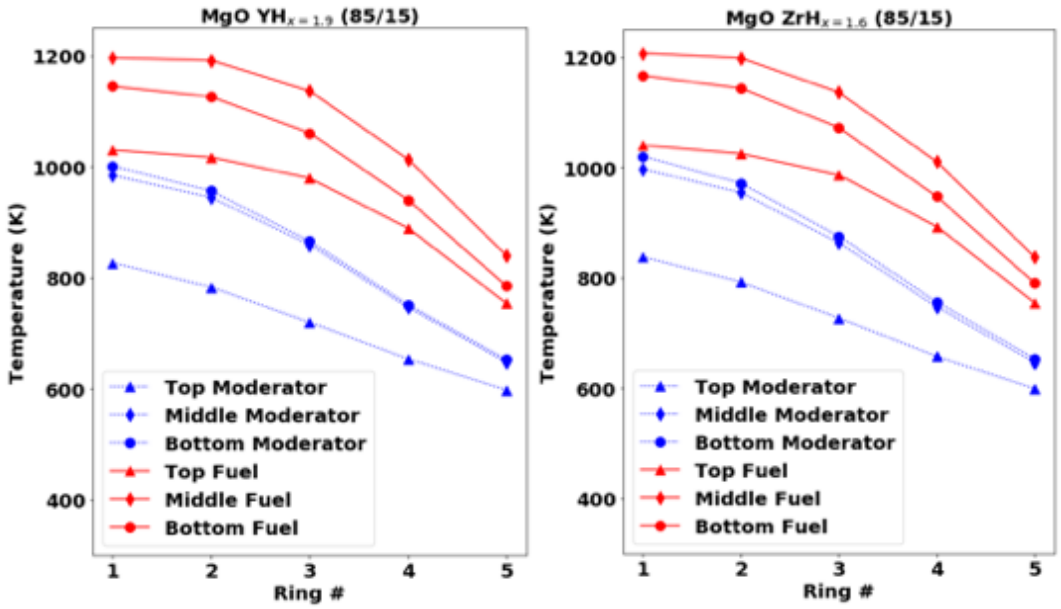

Figure 35. Steady state temperature distribution for the MgO $YH_{x=1.9}$ (60/40) (left) and MgO $ZrH_{x=1.6}$ (60/40) (right) moderated microreactor.

The hydride-based moderators in particular have a much higher middle axial level temperature compared to the other designs, which is attributed to greater power being produced at this level due to the shorter mean free path.

4.4 Reactivity Temperature Coefficient

Reactivity Temperature Coefficients (RTC) are key to a reactor design being inherently safe. For an HTGR, the Moderator Temperature Coefficient (MTC) and Fuel Temperature Coefficient (FTC) provide the intrinsic reactivity response as a function of temperature. The FTC and MTC were calculated by performing branch cases at selected burnup steps where moderator or fuel was individually perturbed from the nominal 900K to 600K with the reactivity difference, dk_{eff}, being recorded. The equation for calculating the temperature coefficients, α_T, with associated uncertainty, $\delta\alpha_T$, is shown in Eq. 2 and Eq. 3, respectively.

$$\alpha_T = \frac{1}{k_{eff}^2}\frac{dk_{eff}}{dT} \qquad (Eq.\,4.2)$$

$$\frac{\delta\alpha_T}{|\alpha_T|} = \left(\frac{\delta k_{eff,900K}^2 + \delta k_{eff,600K}^2}{\left(k_{eff,900K}^2 - k_{eff,600K}^2\right)^2} + \frac{\delta k_{eff,600K}^2}{k_{eff,600K}^2}\right) \qquad (Eq.\,4.3)$$

Here, $\delta k_{eff,Temperature}$ is the uncertainty in the calculation for a given temperature, k_{eff} is the multiplication factor, and dT is the change in temperature.

Figure 36 is the MTC as a function of burnup for each of the considered microreactor designs with the left image having burnup extend to 100MW-days/kgU and the right only to 10MW-days/kgU to magnify the trends at BOC. The hydride moderated systems have less negative values than other reactor designs, and at higher burnups, even maintain

positive MTC as shown in the yttrium hydride moderated design. The values for MTC are overall less negative than previous studies that investigated some of the same moderating material [15] due to the reduced the moderator-to-fuel volume ratio. This reduction suggests that the moderator would have less of an impact on controlling reactivity in the microreactor designs than in larger core sizes.

Figure 37 is the calculated FTC for each of the microreactor designs lotted in the same manner as the MTC figures with the calculations terminated before the end of each reactors respective cycle length. All FTC values are strongly negative with absolute values that exceed that of the MTC, which would give the microreactor design an overall negative isothermal temperature coefficient. The FTC value of hydride-based moderators is less negative than for any other case while the beryllium-based moderators are less negative albeit closer to the graphite case. This is attributed to a more thermal neutron spectra for the composite moderators that would have less neutrons over energy ranges where the FTC phenomena occurs. For all figures, the calculated uncertainties were too small to be shown in the figure (the largest uncertainty was < 0.01pcm/K).

4.5 Emergency Planning Zone

The Emergency Planning Zone (EPZ) surrounding a nuclear reactor is an important component of nuclear safety as it determines the area surrounding the reactor with a planned response for an accident that results in the release of radioactive material to ensure minimal harm to the general public. For this work, only the EPZ associated with the plume exposure pathway was considered.

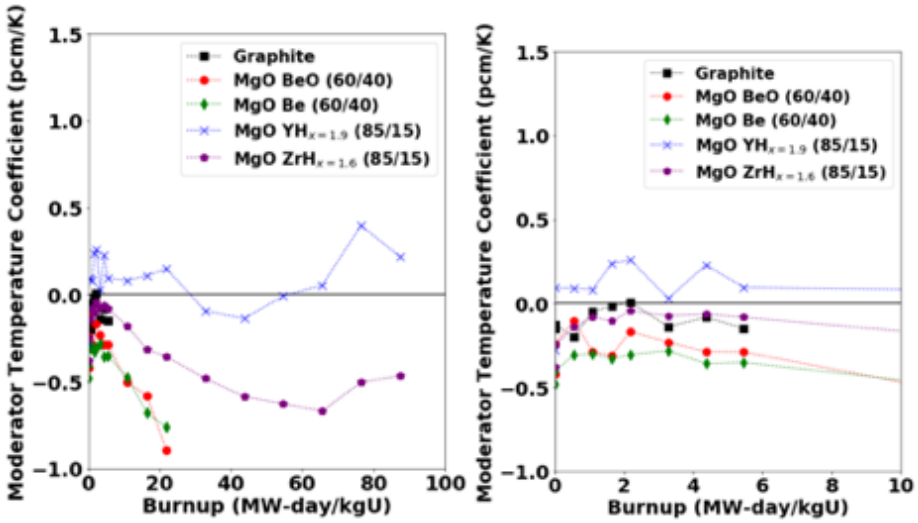

Figure 36. MTC as a function of burnup for all considered cases with a 0.50 TRISO packing fraction displayed for the entire range of burnup (left) and for the first 10 MW-day/kgU (right).

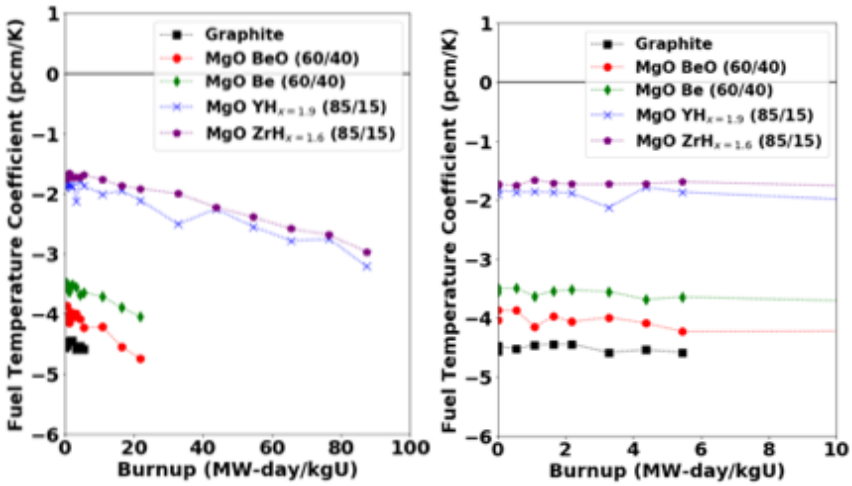

Figure 37. FTC as a function of burnup for all considered cases with a 0.50 TRISO packing fraction displayed for the entire range of burnup (left) and for the first 10 MW-day/kgU (right).

The Nuclear Regulatory Commission (NRC) determined the EPZ surrounding traditional light water reactors (LWRs) to be within a 10-mile radius based on recommendations from the Environmental Protection Agency (EPA) protective action guides [114]. The NRC has recognized that for gas cooled reactors or reactors with power levels less than $250MW_{th}$, the 10-mile radius based on LWRs may be excessive and a smaller EPZ size would be more appropriate [115]. The implications of a reduced EPZ size were explored in a study by Moe W. L. et al. (2014), which concluded that scaling down the EPZ from the current 10-mile radius to a 2-mile radius would reduce capital costs by ~75% and annual operating and maintenance costs of ~96% [116].

The approach for calculating the EPZ size follows the methodology presented in the National Bureau of Standards Reactor (NBSR) 14 Safety Analysis Report [117] and uses the Serpent burnup calculation code as isotopic input for the health and physics code HotSpot. This code provides estimations of radiation effects associated with atmospheric release of radioactive materials and has been evaluated against the Department of Energy (DOE) Safety Software Quality Assurance requirements with subsequent inclusion in the code toolbox of the Central Registry [118]. User specified initial concentrations of radionuclides and atmospheric conditions are provided to HotSpot to calculate a total effective dose equivalent as a function of distance from the source. The code uses the radiation dosimetry methodologies recommended by the International Commission on Radiological Protection (ICRP) to provide a library of dose coefficients for radionuclides. A plume exposure pathway is calculated by a set of Gaussian model equations to determine the time-integrated atmospheric concentration of a gas [119].

For the maximum hypothetical accident scenario to determine minimal EPZ size, a single coolant channel located in the highest burnup region of the microreactor was selected to be blocked, which would cause the six surrounding fuel channels from the top to the bottom of the active core to be compromised and result in a radioactive plume. Key isotopes that would contribute to EPZ size, such as iodine and noble gas fission products, were calculated by Serpent at the end of each design's respective reactor cycle length for the centermost core region (i.e., ring 1) where the highest concentration of these isotopes would be expected. Atmospheric conditions were set to be conservative by having a release height at ground level containing a relatively flat terrain, 1 m/s wind speed, and occurring at night. These assumptions reduced the amount of dispersion of the radioactive plume, which would result in a larger EPZ calculation. The dose limit was also set to 1rem to be conservative as this limit is where protective action is initiated [120]. Shown in Table 13 are the key isotopes from the Serpent calculations that contribute to EPZ size and are used for the HotSpot calculations.

Serpent calculations of key radionuclide concentrations that contribute to EPZ size were provided to HotSpot. The Serpent calculations used similar initial conditions as the steady state thermal-hydraulics calculations: 0.50 TRISO packing fraction and a core power of $6MW_{th}$. Shown in Figure 38 is the summation of activity for all key radionuclides mentioned in Table 13 for each microreactor design. The activity is taken at the end of each reactor's respective cycle length, which was assumed to have the highest concentration of these isotopes. Figure 38 also has the relative difference from the graphite moderated design enumerated at the end of each bar.

Table 13. Key isotopes contributing to EPZ size.

Key Isotopes of Iodine	Key Isotopes of Noble Gases
Iodine-128	Krypton-83m
Iodine-130	Krypton-85
Iodine-130m	Krypton-85m
Iodine-131	Krypton-87
Iodine-132	Krypton-88
Iodine-132m	Krypton-89
Iodine-133	Xenon-131m
Iodine-134	Xenon-133
Iodine-134m	Xenon-133m
Iodine-135	Xenon-135
	Xenon-135m
	Xenon-137
	Xenon-138

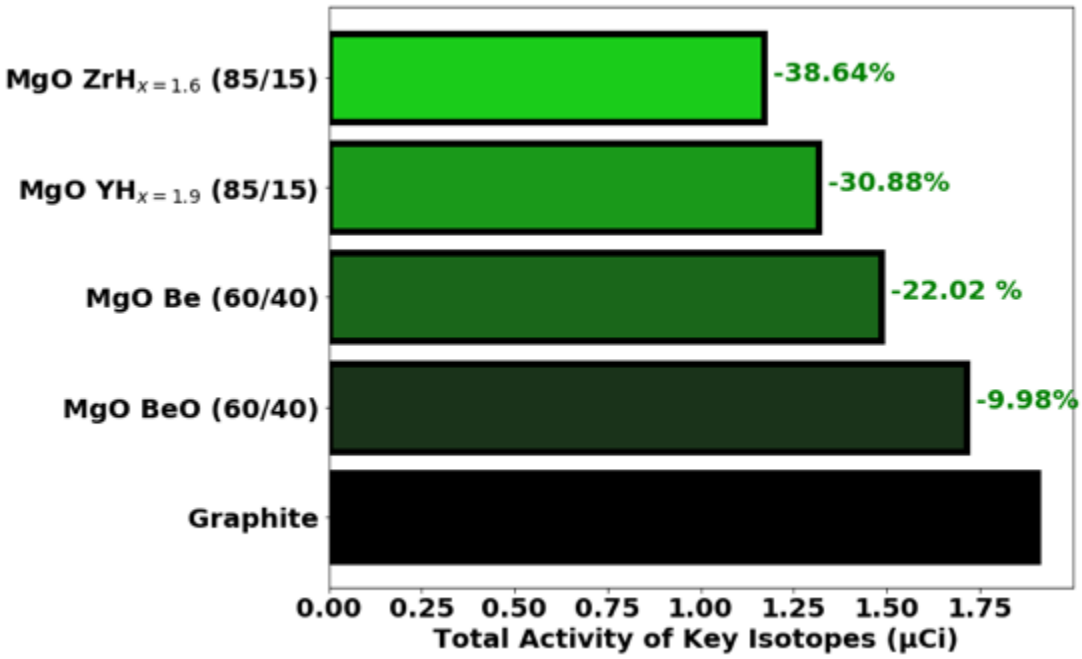

Figure 38. Total activity in units of millicurie of key isotopes contributing to EPZ size.

The beryllium- and hydride-based designs have a lower activity than graphite because of having the softer neutron spectrum [15], which in turn causes more isotopic destruction.

The key isotopes were separated into two groups, radioiodine and noble gas, with various levels of mitigation applied. The levels of mitigation ranged from radioactive release completely mitigated (0.0 fraction released) to no mitigation (1.0 fraction released) for both groups. Figure 39, Figure 40, and Figure 41 are contour plots of EPZ size determined under various levels of mitigation of both isotopic groups for the graphite-, beryllium-, and hydride-based microreactors, respectively. Separating isotopes into groups allowed for a visualization of the sensitivity of EPZ size for levels of mitigation based on a single group, and these two groupings were chosen as they are commonly referenced under discussions of airborne exposure [120].

The ranking of EPZ size for each microreactor design corresponds well to the EOC total activity of key isotope calculations. Radioiodine mitigation is shown to have a significant impact on the EPZ size as noble gas mitigation has a marginal impact. Even under the extremely conservative assumption that there is no mitigation, the EPZ of any design is still less than 2 miles. The small EPZ size associated with these microreactor designs is attributed to the small source term due to the limited core size and low thermal power, which reduces key isotopic concentrations compared to a higher thermal power.

4.6 Depressurized Loss of Forced Coolant

TCR is a bulk hydride moderated microreactor design based on the HTGR platform and is intended to demonstrate the applicability of additive manufacturing technologies in a design process. Calculations of a Pressurized Loss Of Forced Coolant (PLOFC) with SCRAM transient for TCR anticipated no fuel particle failure during the event [86].

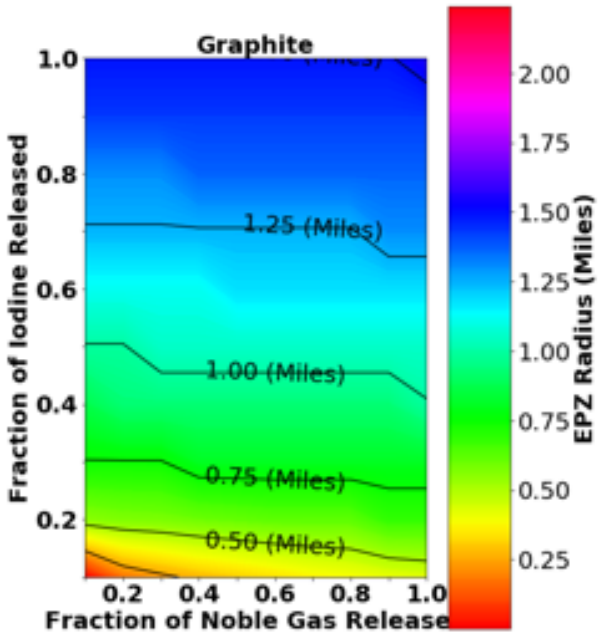

Figure 39. Contour plot of EPZ size for the graphite moderated microreactor at 6MW$_{th}$ core power and 0.5 UN TRISO packing fraction for various levels of Nobel Gas and iodine mitigation.

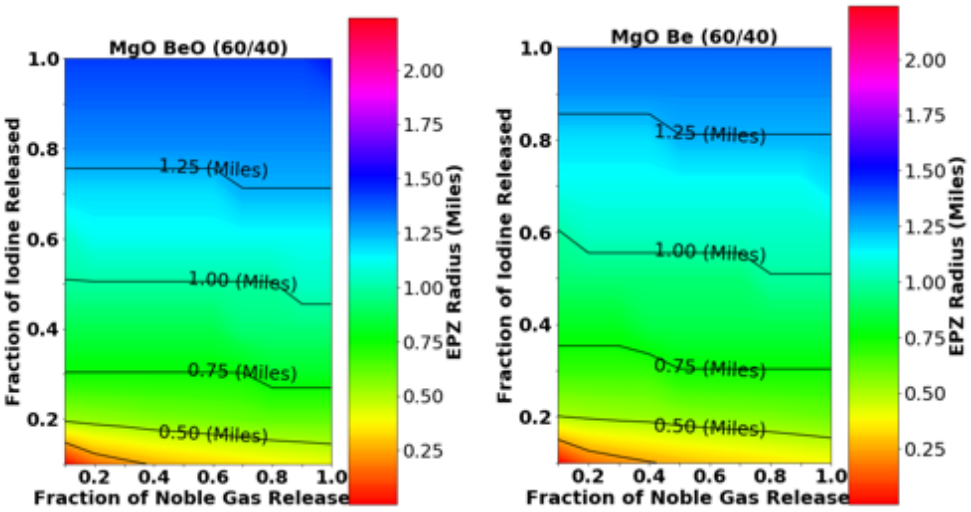

Figure 40. Contour plot of EPZ size for the MgO BeO (60/40) (left) and MgO Be (60/40) (right) moderated microreactor at 6 MW_{th} core power and 0.5 UN TRISO packing fraction for various levels of Nobel Gas and iodine mitigation.

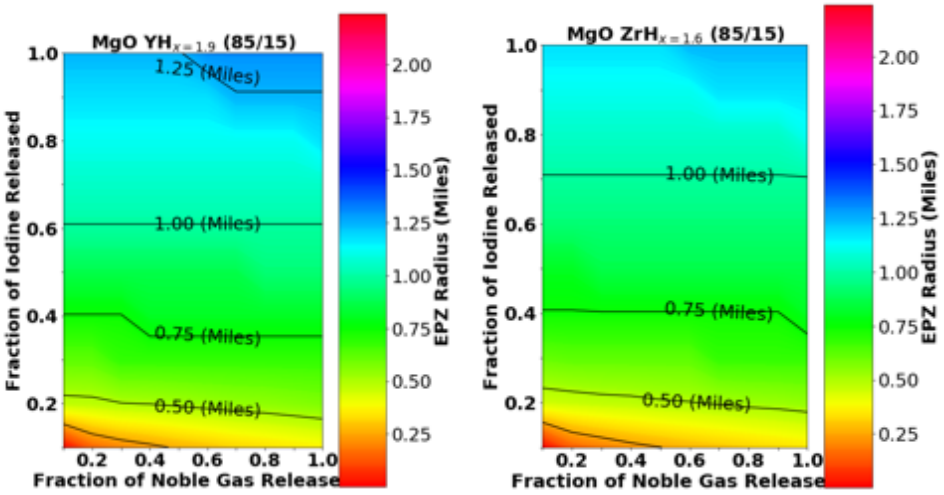

Figure 41. Contour plot of EPZ size for the MgO $YH_{x=1.9}$ (85/15) (left) and MgO $ZrH_{x=1.6}$ (85/15) (right) moderated microreactor at 6MW_{th} core power and 0.5 UN TRISO packing fraction for various levels of Nobel Gas and iodine mitigation.

However, TCR is intended as a demonstration reactor using a bulk hydride moderating material only intended to operate for less than 24hr [121].

The preconceptual design focuses on achieving a much longer operating cycle and considers multiple composite moderators along with graphite for the purpose of performance and safety comparison. Kile et al. (2021) predicted that enhanced heat transfer due to wavy coolant channels in TCR is the most important factor in removing heat from the fuel during a PLOFC with SCRAM, followed by when SCRAM occurs during the first ten seconds of the transient. In this preconceptual design, wavy coolant channels were not considered because the overall design was focused on conventional manufacturing techniques which would be economically unsuitable for wavy coolant channel geometry. Thus, to demonstrate that this preconceptual design is still capable of maintaining fuel integrity under postulated accidents when using composite moderators, designed for a long operating cycle, and does not use wavy coolant channels, a similar but more limiting loss of forced coolant accident was simulated.

The DLOFC without SCRAM was simulated for each microreactor design and followed the specifications of the internationally benchmarked GA mHTGR 350 design. This transient is considered to be the bounding case for fuel temperature in the GA mHTGR 350 [21]. A simulated pressure boundary rupture of the coolant system resulted in a five second blowdown of the system with the coolant mass flow rate coasting down to zero and the core pressure reaching atmospheric pressures of 0.101MPa. The transient occurs over 36 hours in which no active intervention is taken, such as SCRAM, to reduce core power or cool the core. BOC properties were considered as irradiation data on the two-phase composite moderators are unavailable.

The initial boundary conditions for all designs were: inlet coolant temperature set to 550K, outlet coolant temperature set to 700K, and core power set to $6MW_{th}$. These conditions were informed by the design space calculations and allowed all designs to operate at steady state. The much higher thermal conductivity of the graphite moderator would allow for a more favorable higher coolant ΔT. However, the purpose of the transient comparison was to illustrate the response of a loss of forced coolant primarily based on thermophysical and neutronic properties and less so on initial conditions.

A DLOFC is simulated for all microreactor designs with each design employing the same initial boundary conditions and differences limited to only the power profile, thermophysical properties, and neutronic properties. The simulation does not SCRAM or have any other means of active intervention to reduce core power/temperature. Microreactor safety performance is entirely dependent on the inherent design safety features. Figure 42 shows the peak fuel and moderator temperatures of each microreactor design during the transient.

Within the first three hours, all microreactor designs experience a fuel and moderator temperature rise due to the lack of adequate cooling. The temperatures then begin to drop due to the strongly negative FTC reducing core power, which results in the reduced amount of heat being generated within the core being adequately removed by means of thermal conduction. The reduced moderator and fuel temperatures allow for a slight increase in core power resulting in a temperature rise during the final hours of the simulated transient. These series of events occur in quicker succession for materials with higher thermal conductivity as they are able to dissipate heat more effectively.

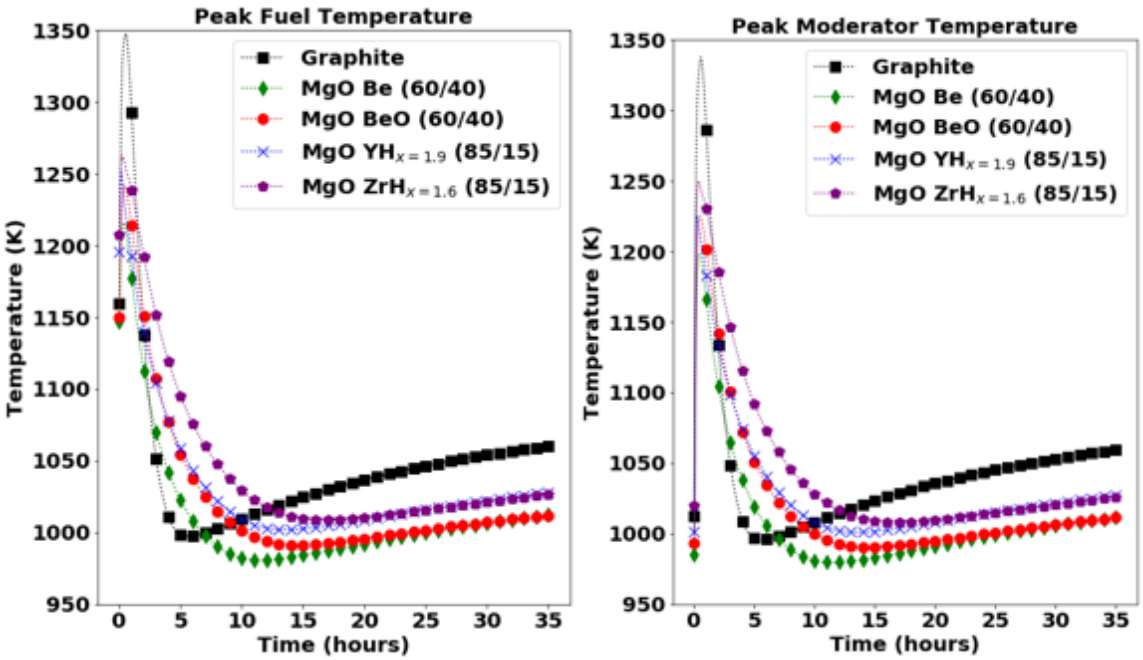

Figure 42. Peak fuel (left) and moderator (right) temperatures during DLOFC.

The fuel and moderator temperatures of the composite moderated designs are slower to decrease relative to graphite after the initial high temperature excursion due to their lower thermal conductivity; however, their higher volumetric heat capacity results in a smaller temperature increase during the final hours of the transient.

4.7 Discussion

In general, the differences in the design windows enabled by the various moderators were mainly a result of the moderating material's effective thermal conductivity, temperature limit, and power profile. Graphite had the largest design space for two reasons: a high moderator temperature limit and a high thermal conductivity. Of these, the graphite's increased temperature limit allowed for higher coolant outlet temperatures while its greater thermal conductivity enhanced heat transfer from the fuel to the coolant, mitigating challenges with fuel temperature limits. The higher thermal conductivity of graphite allows for low thermal power operation where the composite moderators cannot operate. The improved heat transfer of a graphite moderated design, relative to a composite moderated design, enables the coolant to increase to its necessary outlet temperature even when operating at low thermal power.

Steady state conditions were selected to be identical for all cases to provide a consistent comparison during the transient simulation. The selected range of temperatures was only meant to provide insight on expected trends of operating space but other temperatures could be acceptable. The notable drawback of the beryllium and hydride moderated designs is the trend of their lower coolant operating temperature relative to graphite. This would limit their feasibility for industrial heat applications and would be better suited for long lasting electrical power applications. However, further

refinement of the design space methodology as well as less conservative and experimentally relevant values for the temperature limits of the composite moderators could provide a better outline of the operating space. We note that the intent here was to provide a comparison between expected reactor operation for the composite moderators relative to graphite, from which we have identified the key assumptions that need to be revisited such as the upper temperature limits of the materials.

Calculations showed that the beryllium and hydride moderated microreactor designs have a smaller minimal EPZ size than a graphite moderated microreactor design. The higher moderating power of these composites provided a higher thermal neutron economy in the core. The isotopes that contribute to EPZ size have higher neutron absorption at thermal neutron energies and thus a lower concentration due to increased rates of isotopic destruction. Each design had an identical power of $6MW_{th}$ but the graphite moderated design could operate at a lower core power, which would significantly reduce the key isotopic inventory because of a smaller production rate of fission products. Nevertheless, the calculations showed that even for an accident that considered no barrier to the release of key radioactive isotopes by either the TRISO particle, silicon carbide fuel compact, moderating material, primary coolant loop, reactor pressure vessel/container, and reactor building, all designs predicted an EPZ radius of less than 2 miles.

DLOFC calculations revealed that the intrinsic safety of HTGR designs is dictated by the strongly negative isothermal coefficients. The microreactor design was able to passively cool down even without having favorable accident design features such as an annular core [38] or wavy coolant channels [86]. For the selected operating conditions,

none of the microreactor design are expected to exhibit failure of either the fuel or moderator. The graphite-moderated microreactor had the highest peak fuel and moderator temperature, but with the largest margin to failure based on the greater high moderator temperature limit of graphite given the conservative limits for the composite moderator materials. The higher fuel and moderator temperature in the graphite moderated case was attributed to the lower volumetric heat capacity of graphite. However, its higher thermal conductivity allows for the fuel and moderator temperature to respond much more quickly during the transient than either the beryllium or hydride moderated designs. Graphite had the most negative isothermal coefficient, which allowed for the most rapid reduction of fuel and moderator temperature due to the reduced core power relative to the other designs. Operating at core power levels and coolant temperatures lower than traditional HTGR designs enabled an operating condition that would not be expected to challenge moderator or fuel integrity under a loss of coolant accident.

CHAPTER 5
NEUTRONIC AND THERMAL-HYDRAULIC CALCULATIONS UNDER STEADY STATE AND TRANSIENT CONDITIONS FOR A GENERIC PBBLE BED FLUORIDE SALT COOLED HIGH TEMPERATURE REACTOR

A version of this chapter was originally published by Edward M. Duchnowski et al.:

Duchnowski E.M. et al. "Neutronic and thermal-hydraulic calculations under steady state and transient conditions for a generic pebble bed fluoride salt cooled high-temperature reactor" *Nuclear Engineering and Design* 414 (2023): 112520.

In the original publication, I led the formal analysis, investigation, developed the computational models, and wrote the original draft. Nader Satvat assisted in the development of the methodology and reviewed and edited the original draft. Nicholas R. Brown is credited with the conceptualization and funding acquisition as well as reviewing and editing the original draft.

5.1 Background

Recently, a considerable effort has been made to develop multiphysics tools and benchmark designs for FHRs and perform analyses to better understand reactor performance under nominal and transient conditions. The Mark-1 Pebble Bed FHR (Mk1 PB-FHR) is a pre-conceptual design developed by The University of California, Berkeley (UCB) with the intended application of providing a highly flexible power output for grid support services, enabling a new value proposition for nuclear energy [122]. The complex geometry of the reactor core and fuel form required developing modeling tools to accurately represent the Mk1 PB-FHR, including computational tools for solving for the equilibrium core of an arbitrary continuously refueled pebble bed reactor and coupled neutronics and thermal-hydraulics full core models [123] [124]. Kairos Power has leveraged the lesson learned under the development of the Mk1 PB-FHR to become one of the leading entities in designing and licensing the FHR concept [67]. To encourage collaboration between industry, academia, and national laboratories and to build

confidence in modeling and simulating tools and methods, Kairos Power has developed a generic pebble bed FHR (gFHR) benchmark, which is a non-proprietary model that retains vital neutronic and thermal-hydraulic characteristics of their advanced reactor concept, KP-FHR [20]. The gFHR has been used for demonstrating an uncertainty analysis framework based on nuclear data uncertainties, manufacturing tolerances, and operational uncertainties [44].

Transient modeling capabilities have also been developed specifically for pebble bed FHR accident analysis [125]. Wang (2018) developed a methodology for the numerical modeling of FHRs and developed models with different spatial and energy resolution levels. Wang (2018) exercised their methodology by exploring unprotected overcooling and reactivity-initiated accidents for the Mk1 PB-FHR and TMSR Solid Fuel-1 (SF-1). These transients were selected for code demonstration and insight into FHR safety response. The Control Rod Ejection (CRE) transients Wang (2018) considered were beyond the design basis. They would be regarded as an unrealistic scenario because the transient definitions defined a fast insertion of reactivity which is not a credible scenario in FHRs because of the nature of the design [19]. However, the CRE considered by Wang (2018) could provide a bounding case for safety analysis [125]. The transient results from Wang (2018) showed the extreme resilience of the designs under transient conditions, even under the severe case of CRE.

System-level transient analyses have been performed for the Mk1 PB-FHR by adapting existing light water reactor transient tools [126] or adapting current non-light water reactor tools [127] [128] [129]. Liu et al. (2017) implemented liquid and vapor thermophysical properties and transport properties of fluoride salt into the RELAP MOD

3.2 source code. They simulated unprotected loss of coolant flow transients and overpowered transients. Liu et al. (2017) predicted that in either a single coolant pump failure or the insertion of 450 pcm of reactivity, the coolant outlet temperature and maximum fuel temperature maintain an acceptable safety margin. O'Grady et al. (2022) reported on the enhancements to SAM for FHR modeling, including a novel coolant freezing model and transient safety analysis for a reference FHR based on the Mk1 PB-FHR concept. O'Grady et al. (2022) demonstrated the new features within their report and predicted that all transients eventually reach a stable state within a few hours after the initiating event. The gFHR has been used with the multipurpose radiation transport and reactor physics code system, SCALE, and the severe accident code, MELCOR, for the application of FHR steady-state and transient analysis [82]. Kile et al. (2022) performed a loss of flow sensitivity study and identified that coolant inlet temperature, graphite thermal conductivity, SCRAM time, and friction multipliers were the most important factors that impacted peak coolant outlet and peak fuel temperatures. These mentioned analyses on FHR transient primarily focus on demonstrating methodology and exploring a few accident conditions. We expand on this knowledge by presenting a new methodology for FHR model development, exploring a range of transients, and comparing safety characteristics and transient results to published results.

5.2 Model Development

To perform transient modeling of pebble bed FHRs, an appropriate selection of a benchmark model is needed along with capable multiphysics computational tools. The benchmark selected for this study is the gFHR which is a simplistic model that retains vital neutronic and thermal-hydraulic characteristics of pebble bed FHRs. Design

specifications and steady-state calculations are publicly available for the gFHR [20]. This benchmark model has been used for demonstrating an uncertainty analysis framework [44] and for the assessment of the multipurpose radiation transport and reactor physics code system, SCALE, and the severe accident code, MELCOR [82]. The coupled neutronics/thermal-hydraulics transient code, KP-AGREE, is used as the transient modeling tool. We implement a two-step approach for developing the KP-AGREE model by first generating homogenized multigroup cross-sections in the continuous energy Monte Carlo neutron transport code Serpent [130] version 2.1.31 for the fine mesh finite difference neutronics module in KP-AGREE. A description of the overall methodology of performing transient analysis in the gFHR is shown in Figure 43.

5.2.1 The generic FHR

The gFHR was selected because of its non-proprietary simplistic design and available literature on key neutronic and thermal-hydraulic design parameters. Much of the design details of the gFHR can be better described in the literature [20], but some high-level aspects of the design are described in Table 14 and an image of the gFHR reproduced from the benchmark paper is shown in Figure 44. The gFHR is based on a pebble bed reactor platform with TRISO particles embedded in a fuel layer within the pebble. The use of pebble fuel allows for continuous refueling/defueling of the reactor during operation and discharge after a specified core residence period. For the gFHR, the pebbles are cycled through the core eight times, having an average residence period of 522 days before achieving an average discharge burnup of 17.6% FIMA (Fissions per Initial Metal Atoms) [20]. The fuel is contentiously cycled, entering from the bottom of the core and exiting out the top.

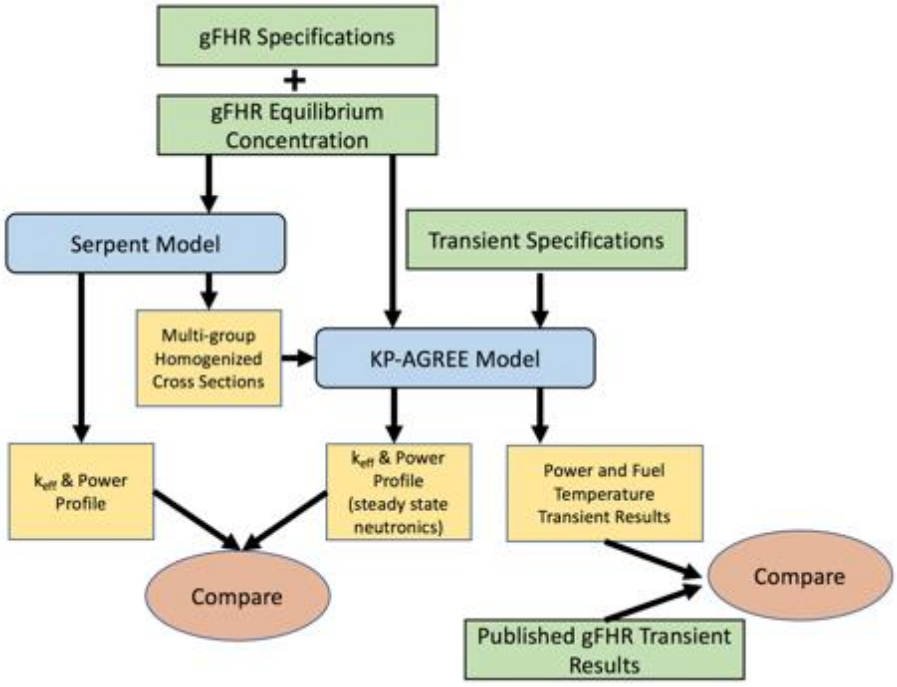

Figure 43. Methodology for performing transient analysis in a generic FHR benchmark model

Table 14. Key parameters of the gFHR used in generating the multiphysics models [18]

Parameters	Description	Units
Core Parameters		
Core Power	280	MW
Core Radius	120	cm
Core Height	309.47	cm
Reflector Thickness	60	cm
Core Barrel Thickness	2	cm
Downcomer Width	5	cm
Vessel Thickness	4	cm
Coolant Inlet Temperature	825	K
Coolant Outlet Temperature	923	K
Coolant Mass Flow Rate	1,173	kg/s
Coolant Density	2413.0 – 0.488*T(K)	kg/m^3
Peak Discharge Burnup	~20%	FIMA
FLiBe Enrichment	50	ppm Li-6
TRISO Parameters		
Kernel Radius	0.02125	cm
Graphite Buffer Thickness | Density	0.01 | 1.05	cm | g/cm^3
Inner PyC Thickness | Density	0.004 | 1.9	cm | g/cm^3
SiC Thickness | Density	0.0035 | 3.18	cm | g/cm^3
Outer PyC Thickness | Density	0.004 | 1.9	cm | g/cm^3
TRISO Packing fraction	0.22	-
Pebble Parameters		
Inner Shell Radius | Density	1.38 | 1.41	cm | g/cm^3
Fuel Layer Thickness | Density	0.42 | 1.74	cm | g/cm^3
Outer Shell Thickness | Density	0.2 | 1.74	cm | g/cm^3
Pebble Packing Fraction	0.60	-
Reactivity Control System		
Control Rod Material	B_4C	-
Control Rod Radius | Density	2.6 | 1 .76	cm | g/cm^3
Length of Control Rods	369.47	cm
Radial Distance from Core	7.9 (to center of rod)	cm
Control Rod B-10 Enrichment	100	%
Number of Control Rods	10	-

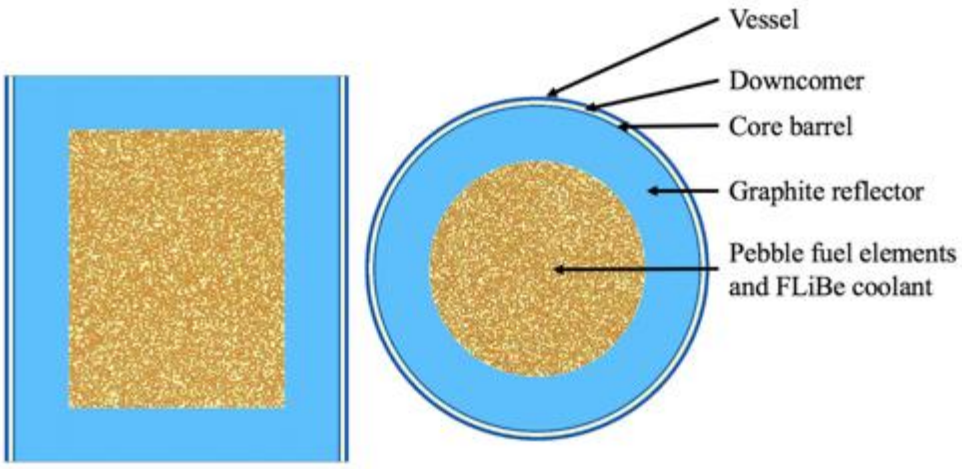

Figure 44. Axial (left) and radial (right) view of the gFHR (reproduced from Satvat et al. (2021) [20]**)**

This leads to a steady-state isotopic distribution in the core, also referred to as an equilibrium core condition. Isotopic distributions of the fuel for an equilibrium core have been made publicly available [131] and were used alongside design parameters to generate the necessary multiphysics models. Additional model parameters, such as the reactivity control mechanism for the gFHR, have recently become available but were not included in the gFHR benchmark [132]. The control rod mechanism consists of ten equally spaced control rods inserted into the outer reflector. For the LOFA transient, the control rods were set in the all rods out position and a point kinetic module was used to simulate SCRAM. This procedure was consistent with the gFHR LOFA reference results that we are using as a point of comparison [82].

5.2.2 Serpent Model

The Serpent model was generated using specifications from the gFHR benchmark [20]. The zone-wise fuel isotopic concentrations at core equilibrium used in this study came from additional documentation on the gFHR [131]. Serpent can explicitly model TRISO particle layers and locations within the fuel pebble and the explicit dimensions and locations of the fuel pebbles in the reactor core. The use of explicit TRISO and pebble modeling in full-core pebble-bed simulations is preferred as the randomness of locations of TRISO particles in pebbles and pebbles in the core is preserved while also avoiding clipping at surface boundaries, mitigating systematic errors [133]. The models used Serpent's automated dispersion routine to generate the TRISO and pebble locations. The gFHR is modeled in three-dimensions within Serpent and multigroup cross-sections are calculated as homogenized regions in two-dimensions, radial and axial. One of the main advantages of utilizing continuous energy Monte Carlo neutron transport for cross-

section generation is that the double heterogeneity of the fuel form, including the self-shielding effect of the fuel, is naturally preserved [134]. Shown in Figure 45 are the TRISO particles packed with a 0.22 packing fraction annularly in a graphite matrix within a single fuel pebble. The pebble consists of fuel free graphite outer shell, a fueled graphite matrix shell, and a low-density graphite center enabling the pebble to be buoyant in the FLiBe coolant. The fuel kernel compositions are mapped from the published zone-wise equilibrium core concentration [131].

Fuel pebbles are then packed with a 0.60 packing fraction in the reactor core and submerged in the FLiBe coolant. The FLiBe coolant is 99.995% Li-7 enriched to reduce the neutronic penalty associated with Li-6. A graphite reflector then surrounds the entire active core region. The coolant downcomer, reactor barrel, and reactor vessel are also included in this model based on the gFHR benchmark specifications. From the additional documentation on reactivity control mechanisms [132], ten control rods were molded within the side reflector that extended from the top of the upper reflector to the bottom of the active core, just above the bottom reflector, shown in Figure 46. The KP-AGREE model assumes azimuthal symmetry, and to correctly model reactivity control mechanisms, an additional Serpent model was created that eliminated the azimuthal dependence of the control rods by modeling the ten discrete control rods as a cylindrical skirt, also referred to as a grey curtain, shown in Figure 47.

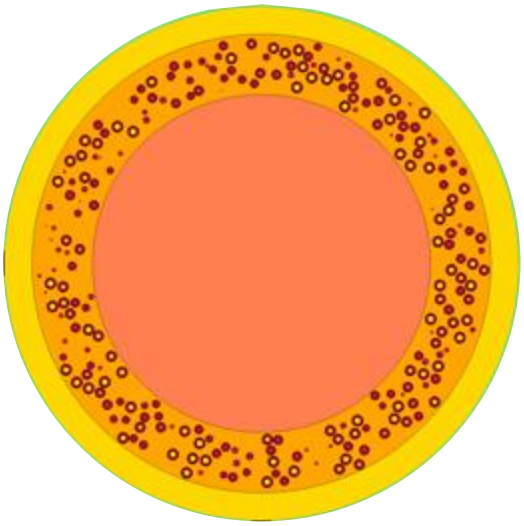

Figure 45. Single FHR pebble with randomly distributed TRISO particles

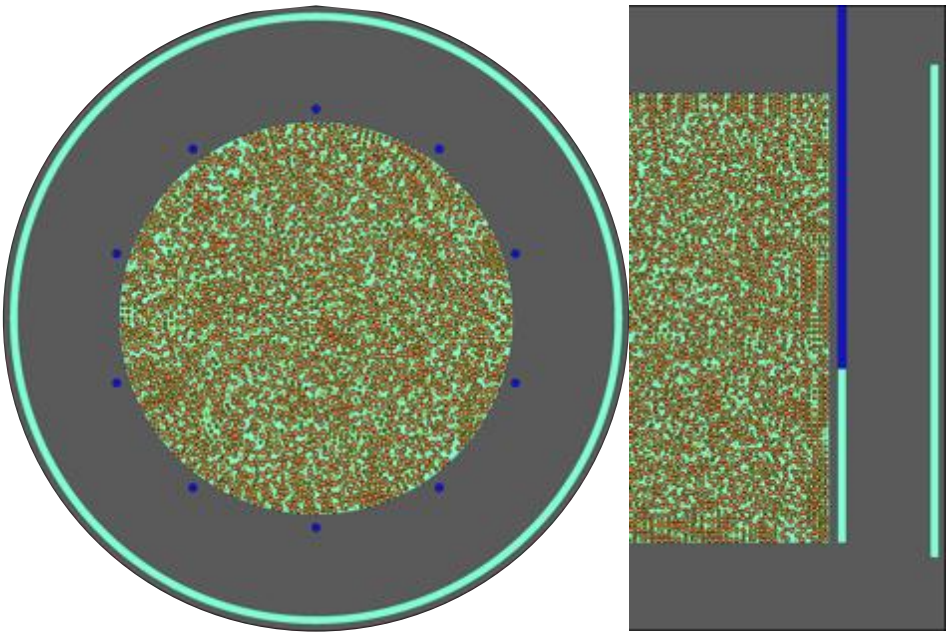

Figure 46. gFHR Serpent model with discrete reactivity control mechanisms. (left) top-down view (right) radial view with control rods inserted into the critical position

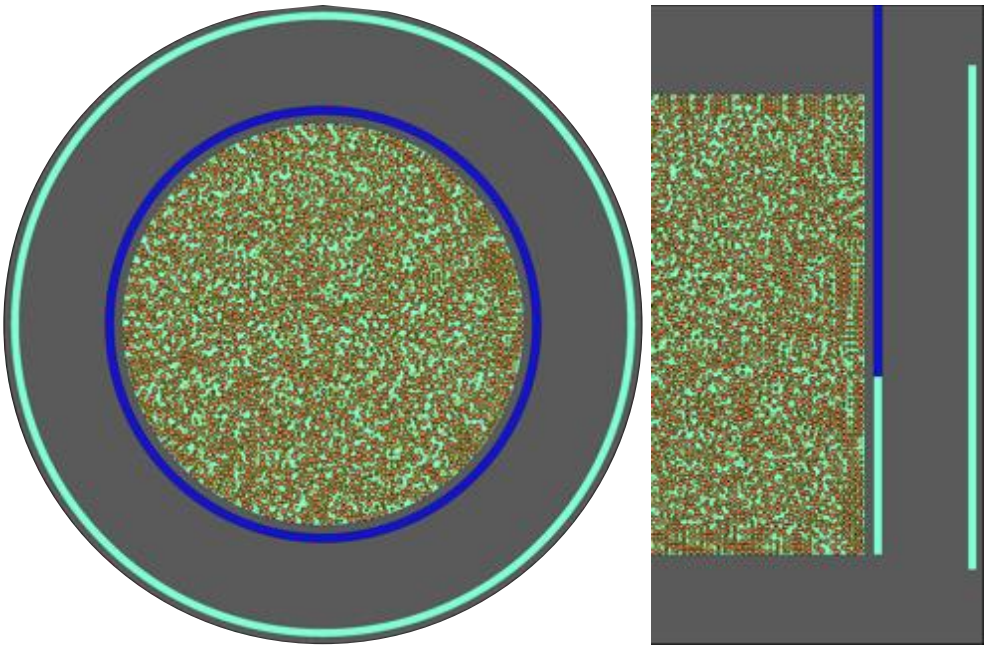

Figure 47. gFHR Serpent model with grey curtain reactivity control mechanisms. (left) top-down view (right) radial view with control rods inserted into the critical position

The diameter of the control rods is preserved as the thickness of the grey curtain and the distance from the core is also preserved. Initially, the material composition of the grey curtain region is the volume-weighted average composition along the azimuthal direction in the control rod region.

The grey curtain Serpent model is calibrated to the discrete control rod Serpent model by adjusting boron density in the grey curtain, further described in Section 5.1. The cross-sections generated from the calibrated Serpent grey curtain model are then directly provided to KP-AGREE with no additional modifications. The grey curtain approach in modeling reactivity control mechanisms has been used in other multigroup neutron diffusion codes for pebble bed reactor analysis [135] [136] [137]. Rod cusping treatment for the KP-AGREE model was unnecessary because of the relatively small axial node sizes within the control rod region. The Serpent model employed the ENDF/B-VIII.0 nuclear data library and used a neutron population of 100,000 with 100 inactive and 100 active cycles for all calculations. This gave a similar statistical uncertainty in the prediction of k_{eff} to that in the benchmark model and was considered sufficient for predicting core reference values and homogenized multigroup cross-sections.

5.2.3 KP-AGREE Model

KP-AGREE is the pebble bed-specific version of the Advanced Gas Reactor Evaluator (AGREE) code developed for the Nuclear Regulatory Commission (NRC) [138] [67]. KP-AGREE is a systems-level thermo-fluids code that solves the steady state and time-dependent porous media mass, momentum, and energy equations. The model uses an equation of state to describe the flow field model with resistance coefficients

based on the KTA rule [139]. More on the momentum solution implemented within KP-AGREE can be found in Seker (2007) [140]. The code relies on thermal-hydraulic boundary conditions as the current version used in this work does not model components such as heat exchangers or coolant pumps. The randomly packed pebbles in a pebble reactor result in complex coolant flow distributions that cannot be represented by unit-cell calculations or become computationally intensive when performing full core CFD calculations. To accurately describe the heat transfer in a pebble bed reactor with reasonable computational power, KP-AGREE uses the two-temperature porous media approach to describe the energy equation [140]. Other multiphysics codes such as Pronghorn [141] [142] [143], SAM [144] [145], and THPP [146] [147] also implement the two-temperature porous media approach. The time-dependent energy balance for the solid medium as described in Seker (2007) [140] is,

$$\frac{\delta}{\delta t}\left[(1-\epsilon)\rho_s c_{p_s} T_s\right] = \nabla(1-\epsilon)k_s \nabla T_s - \alpha_{s\,to\,f}\left(T_s - T_f\right) + Q \qquad (Eq.\,5.1)$$

where ϵ is the porosity, ρ is the density, k is the effective thermal conductivity, c_p is the specific heat capacity, T is the temperature, α is the solid-to-fluid heat transfer coefficient, and Q is the nuclear heat source. The subscripts s and f stand for solid and fluid, respectively. The heat transfer in the solid medium is influenced by thermal radiation and pebble contact. The effective thermal conductivity based on the Zehner-Schlunder model is used to capture this dependence. The time-dependent energy balance for the fluid medium is,

$$\frac{\delta}{\delta t}\left[\epsilon\rho_f c_{p_f} T_f\right] + \nabla\left(\rho_f c_{p_f} u T_f\right) = \nabla\epsilon k_f \nabla T_f - \alpha_{s\,to\,f}\left(T_f - T_s\right) \qquad (Eq.\,5.2)$$

where u is the velocity of the fluid. The energy equations for the solid medium and fluid medium are coupled by the second term on the right-hand side of Eq. 5.1 and Eq. 5.2, and the solid-to-fluid heat transfer coefficient, $\alpha_{s\ to\ f}$, is described as,

$$\alpha_{s\ to\ f} = 6\frac{1-\epsilon}{d_p} * \frac{k_f Nu}{d_p} \qquad (Eq. 5.3)$$

where d_p is the diameter of the pebble and Nu is the Nusselt number for pebble bed geometry which can be represented through the KTA Rule [148] as,

$$Nu = 1.27\frac{Pr^{\frac{1}{3}}}{\epsilon^{1.18}}Re^{0.36} + 0.033\frac{Pr^{\frac{1}{2}}}{\epsilon^{1.07}}Re^{0.86} \qquad (Eq. 5.4)$$

where Pr and Re are the Prandtl and Reynolds numbers, respectively. KP-AGREE has a feature to model the TRISO kernel temperature within the pebble fuel matrix. This feature becomes important when modeling fuel temperature feedback during fast reactivity insertions and is defined as,

$$T_{kernel} = \alpha_{PUEBH} * Q''' + T_{matrix} \qquad (Eq. 5.5)$$

where T_{kernel} is the TRISO kernel temperature in units of K, T_{matrix} is the matrix temperature of the fueled region in the pebble in units of K, Q''' is the local power density in units of W/cm^3 , and α_{PUEBH} is the factor for fuel kernel temperature in units of K/(W/cm^3). The factor for fuel kernel temperature can be determined by comparing predicted TRISO kernel temperatures to an explicit kernel model, as in the case of gas-cooled pebble bed designs [149] [150]. We found that a value of 2.903 for the factor for fuel kernel temperature gave a reasonable prediction when compared to explicit kernel modeling in the Mk1 PB-FHR through the multiscale thermal-hydraulics tool, Pronghorn [151], when a similar TRISO packing fraction as the gFHR fuel form is considered.

To provide the nuclear heat source term in Eq. 5.1, the time-dependent multigroup neutron diffusion equation is used to predict the neutron flux and power distribution within the core. The general form of the time-dependent neutron diffusion equation is,

$$\frac{1}{v_g}\frac{d\phi_g}{dt} = \frac{\chi_{p,g}}{k_{eff}}\sum_{g=1}^{G} v_{p,g}\Sigma_{f,g}\phi_g + \chi_{d,g}\sum_{k=1}^{K}\lambda_k C_k + \sum_{g'=1(g'\neq g)}^{G}\Sigma_{s,g'\to g}\phi_{g'} - \Sigma_{t,g}\phi_g + \nabla D_g \nabla\phi_g \qquad (Eq.\,5.6)$$

where ϕ is the neutron flux, v is the neutron speed, X is fission neutron energy distribution, k_{eff} is the multiplication factor, Σ_f is the macroscopic fission cross-section, λ is the delayed neutron precursor decay constant, C is the delayed neutron precursor concentration, Σ_s is the macroscopic scattering cross-section, Σ_t is the macroscopic total cross-section, and D is the neutron diffusion coefficient. The subscript g represents the neutron group out of G groups, k is the delayed neutron precursor group out of K groups, p stands for prompt neutrons, and d stands for delayed neutrons. The discretization in KP-AGREE allows for a finer refinement of the mesh for neutronics calculations to accurately predict the neutron flux and temperature-dependent cross-section tables. The coupled neutronics and thermal-hydraulics solution approach starts with user-defined initial core-wide temperatures. The code then converges on a solution to the porous media mass, momentum, and energy equations to update the user-defined core-wide temperatures. The neutron flux is then solved through the neutron diffusion equation, which accounts for temperature-dependent cross-sections generated from Serpent. The solution iterates between the two modules, updating the core-wide temperatures and neutron flux distribution until convergences are met. The transient solution in KP-AGREE begins by solving for the steady-state solution and follows a

similar approach with an added iteration at each user-defined timestep. This overall solution method in KP-AGREE allows for modeling control rod movement through spatial kinetics. The code also has a point kinetics module available for transient calculations that would not expect a considerable spatial variation of the power, such as in protected loss of flow accidents.

Shown in Figure 48 is a diagram of the gFHR components in KP-AGREE with arrows representing the coolant flow path. The side and bottom of Figure 48 describe the thermal-hydraulics meshing used in this model, represented by the number and size of nodes. For neutronics calculations in KP-AGREE, the first 15.0cm radial node in the side reflector adjacent to the pebble bed core is further discretized to model the reflector material between the core and grey curtain, the grey curtain, and reflector material surrounding the grey curtain with widths of 5.3cm, 5.2cm, and 4.5cm, respectively. The pebble bed region assumes a three-dimensional flow but with azimuthal symmetry, the outlet region and reflector region just below the active core take a two-dimensional flow, and the coolant inlet, downcomer, and the flow path connecting from the downcomer assume a one-dimensional flow. The cross-sections generated in Serpent had four temperature branches for the fuel, coolant, and moderator, which were 600K, 900K, 1200K, and 2500K. Additionally, the coolant density at these temperatures was varied according to the function listed in Table 14. We should note that although a 2500 K temperature branch for coolant was generated, it was not used in the transient simulation because FLiBe has a boiling temperature of approximately 1703K [152].

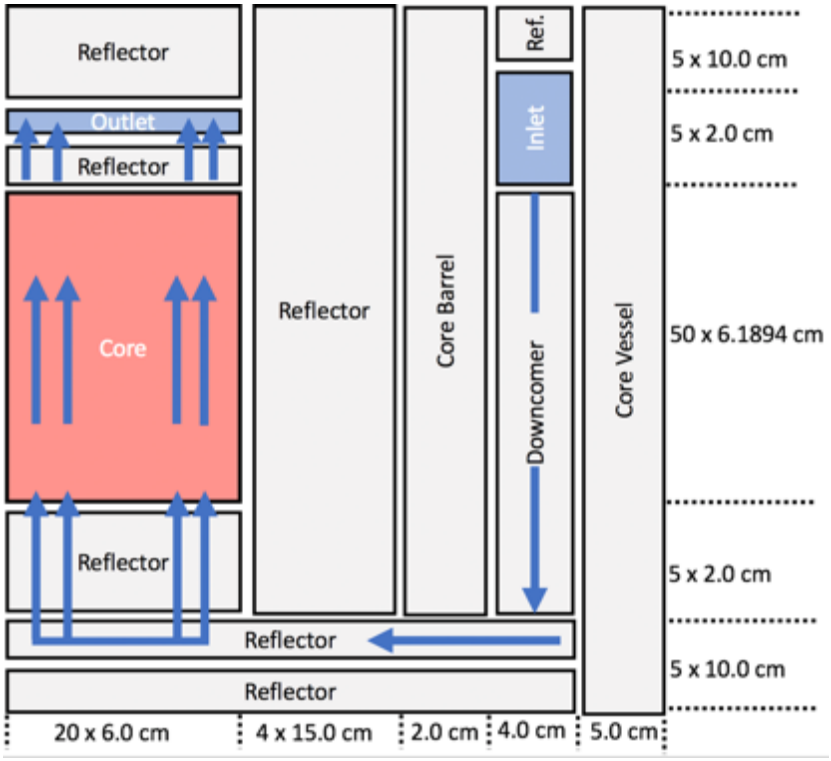

Figure 48. Radial diagram of components within the KP-AGREE model and coolant flow path

All other out-of-core materials had only two temperature branches, 600K and 1200K. The thermal physical properties of different reactor components used in the KP-AGREE model are described in Table 15.

5.3 Steady State Results

Simulations of the gFHR in the Serpent model and KP-AGREE model are presented and compared. The comparison between Serpent and KP-AGREE ensures that the transient modeling tool, KP-AGREE, has the appropriate initial conditions. Where applicable, the models are compared to reported values in the literature to build confidence in modeling. The gFHR benchmark calculation utilized 9,022 randomly packed TRISO particles dispersed within a single fuel pebble and 250,190 randomly distributed fuel pebbles within the core. At equilibrium with fuel temperature set to 959 K and all other material set to 900 K, the predicted k_{eff} within the core was 1.01230 ± 0.00068 using Serpent version 2.1.32 with ENDF/B-VII.I nuclear libraries [20]. For the Serpent models, the fuel temperature was set to 959 K and all other materials to 900 K. We used Serpent's dispersion function to generate 9,021 randomly packed TRISO particles dispersed within a single fuel pebble and 250,190 fuel pebbles randomly distributed within the core. We calculated a k_{eff} of 1.01467± 0.00091 in the all rods out configuration with ENDF/B-VIII.0 nuclear data libraries and Serpent version 2.1.31. The difference between the reference k_{eff} and the predicted value is an approximate 231 pcm difference. This discrepancy is considered to be relatively low and within good agreement for full reactor core models [74]. The discrepancy between values may be explained by the set of assumptions made in developing the Serpent models.

Table 15. Thermophysical properties used in the KP-AGREE model

Parameters	Description	Units	Justification
Thermal Conductivity of Inner Shell	0.355	W/cm K	Default MELCOR value [82] [153]
Volumetric Heat Capacity of Inner Shell	2.351	J/cm^3 K	Graphite at 900 K [153] with density from Table 14
Thermal Conductivity of Fuel Layer	0.15	W/cm K	Average pebble fuel effective conductivity [20] [153]
Volumetric Heat Capacity of Fuel Layer	2.901	J/cm^3 K	Graphite at 900 K [153] with density from Table 14
Thermal Conductivity of Outer Shell	0.355	W/cm K	Default MELCOR value [82] [153]
Volumetric Heat Capacity of Outer Shell	2.901	J/cm^3 K	Graphite at 900 K [153] with density from Table 14
Thermal Conductivity of Reflector	0.355	W/cm K	Default MELCOR value [82] [153]
Volumetric Heat Capacity of Reflector	2.901	J/cm^3 K	Graphite at 900 K [153] with density from Table 14 [80]
Thermal Conductivity of Core Barrel/Vessel	0.237	W/cm K	Default KP-AGREE value
Volumetric Heat Capacity of Core Barrel/Vessel	4.757	J/cm^3 K	Stainless Steel at 900 K [153] with density from Table 14

In the Serpent models, the graphite material in the reflector, pebbles, and TRISO particles are pure carbon-12. Nuclear-grade graphite has trace amounts of carbon-13 and small concentrations of boron impurities. The presence of the isotopes, especially boron impurities within the reflector, impacts eigenvalue calculations because of neutron absorption [154]. The gFHR benchmark [20] and the gFHR LOFA [82] studies do not report the quality of graphite used within their modes, and we assume this to be one of the reasons for the discrepancy in k_{eff}. Another potential source for discrepancy in k_{eff} is the fuel compositions used in these models. The zone-wise isotopic concentration at equilibrium comes from additional documentation on the gFHR [131]. This additional documentation is a truncated list of only the most impactful nuclides. The rejected list of nuclides contributes to less than a 100 pcm difference in k_{eff} [155]. Walton et al. (2022) reported a slight bias in k_{eff} between their gFHR model and the reported benchmark value when using this truncated list of nuclides and a different graphite-carbon evaluation from the benchmark [155]. For this work, Serpent was used primarily to generate homogenized cross-sections for the transient tool KP-AGREE. We conclude that the level of agreement between both the Serpent and KP-AGREE models is sufficient for performing transient analysis

5.3.1 Standalone Neutronics

Utilizing the two-step method of generating cross-sections in a continuous energy transport code for a neutron diffusion solver requires a sufficient number of energy groups. The reflector surrounding the active core in the gFHR thermalizes a large number of neutrons and results in a local power increase near the edges of the

core/reflector interface. When an insufficient number of energy groups are implemented for a neutron diffusion solver, a large discrepancy can occur in these regions, impacting the power profile and the core eigenvalue [79]. A study was performed on the necessary amount of energy group required to accurately model the gFHR in KP-AGREE. Shown in Table 16 are energy group cutoff values for 2, 4, and 7 energy groups. The selection of energy group structures comes from the analysis of other high-temperature reactors including pebble bed reactors [79] [156]**.** The average radial and axial power profiles predicted in KP-AGREE with control rods completely withdrawn for various energy group structures are shown in Figure 49 and Figure 50, respectively. The eigenvalue and power profile difference, Table 17, was selected as the metrics of comparison between Serpent and KP-AGREE. The Root Mean Square Error (RMSE) was used to compare the axial and radial power profile between Serpent and KP-AGREE and is defined as,

$$RMSE = \sqrt{\frac{\sum_{i=1}^{N}(x_i - \hat{x}_i)^2}{N}} \qquad (Eq. 5.7)$$

where N is the number of data points, x_i is the Serpent calculated power density at location i, and $\hat{x}_i$ is the KP-AGREE calculated power density at location i. The agreement between Serpent and KP-AGREE improves with increasing the number of energy groups used in KP-AGREE. For the remainder of this study, we implement the 7-group energy structure based on evaluation and recommendations from the literature [79] [156].

Table 16. 2, 4, and 7 energy group structures [79] [156]**.**

Energy Groups			
Energy Cutoffs (eV)	**2**	**4**	**7**
	3.059E+0	9.118E+3	5.000E+5
		8.5000E-1	9.118E+3
		1.000E-1	4.000E+0
			1.097E+0
			5.000E-1
			1.000E-1

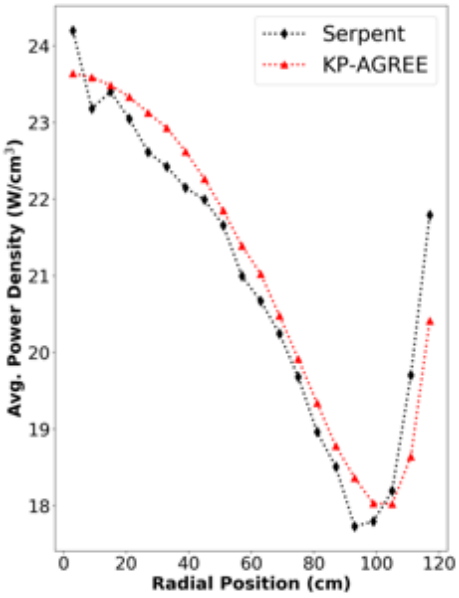

(a)

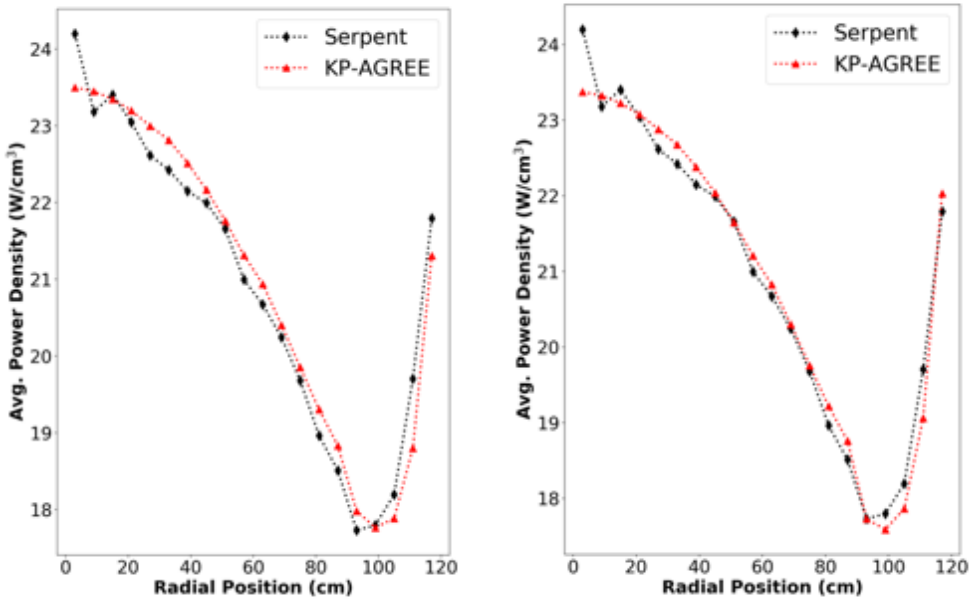

(b) (c)

Figure 49. Average radial power density between Serpent and KP-AGREE using a) 2 energy groups, b) 4 energy groups, and c) 7 energy groups. Fuel temperature set to 959 K and all other component temperatures set to 900 K

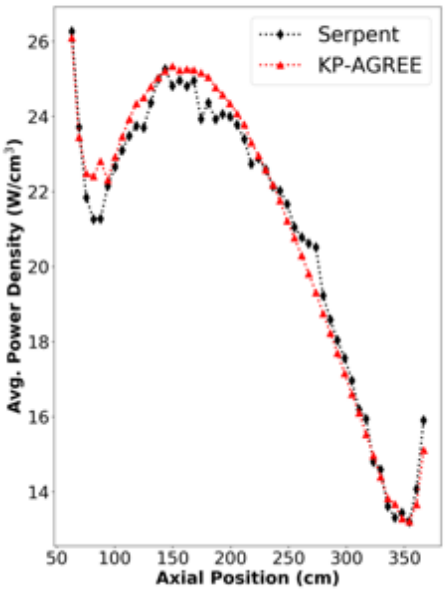

(a)

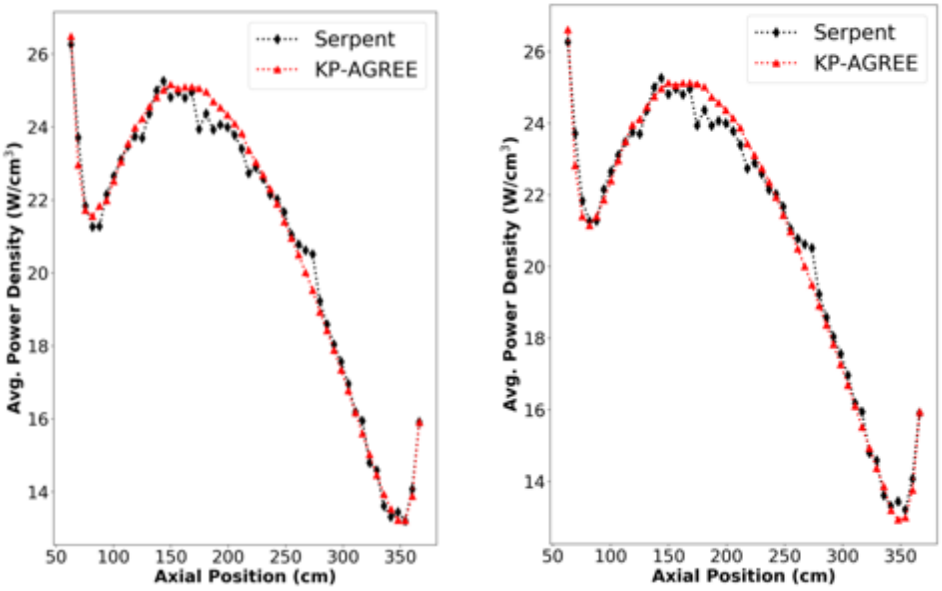

(b) (c)

Figure 50. Average axial power density between Serpent and KP-AGREE using a) 2 energy groups, b) 4 energy groups, and c) 7 energy groups. Fuel temperature set to 959 K and all other component temperatures set to 900 K

Table 17. Predicted k_{eff} and power profile comparison in KP-AGREE to Serpent for various energy group structures. Fuel temperature set to 959 K and all other component temperatures set to 900 K. *Serpent reference k_{eff} is 1.01467± 0.00091

Energy Groups	KP-AGREE k_{eff}	Absolute Difference in k_{eff}* (pcm)	Radial power RMSE (W/cm^3)	Axial power RMSE (W/cm^3)
2	1.01129	338± 91	0.526	0.543
4	1.01258	209± 91	0.368	0.379
7	1.01428	39± 91	0.296	0.407

Reactivity temperature coefficients were calculated for the Serpent and the KP-AGREE standalone neutronics models. The steady-state multiplication factor, Fuel Temperature Coefficient (FTC), Moderator Temperature Coefficient (MTC), and Coolant Temperature Coefficient (CTC) are listed in Table 18. The reactivity temperature coeffects were calculated by perturbing the material temperatures ± 100 K of their nominal value. The CTC also accounts for the change in density as a function of temperature, according to *Table 14*. Both codes show good agreement between predicted k_{eff} and reactivity temperature coefficients in the all rods out core configuration. The reactivity temperature coefficients also agree with the reported values in the gFHR benchmark.

The grey curtain model of the control rods assumed that the material composition of the rodded and reflector region was area averaged in the azimuthal direction. This smearing of the boron number density across a larger volume predicted a significantly higher control rod worth relative to the discrete control rod model because the absorbing material was not lumped together. To correct this, the boron concentration was reduced until the eigenvalue at every insertion depth matched the discrete control rod Serpent model. Shown in Figure 51 is the calculated k_{eff} value in Serpent for the discrete control rods model, uncalibrated grey curtain model, and calibrated grey curtain model. The figure also illustrates the worth predicted in KP-AGREE from cross-sections generated in the calibrated grey curtain model.

Table 18. k_{eff} and reactivity temperature coefficients between Serpent, KP-AGREE with 7 energy groups and benchmark reference [20]**. Fuel temperature set to 959 K and all other component temperatures set to 900 K**

Parameters	Units	Serpent	KP-AGREE	Reference [20]
k_{eff}	-	1.01467± 0.00091	1.01428	1.01230 ± 0.00068
FTC	pcm/K	-4.60 ± 0.44	-4.30	− 4.56 ± 0.12
MTC	pcm/K	-0.77 ± 0.44	-0.51	− 0.40 ± 0.12
CTC	pcm/K	-1.37 ± 0.44	-1.43	− 1.20 ± 0.12

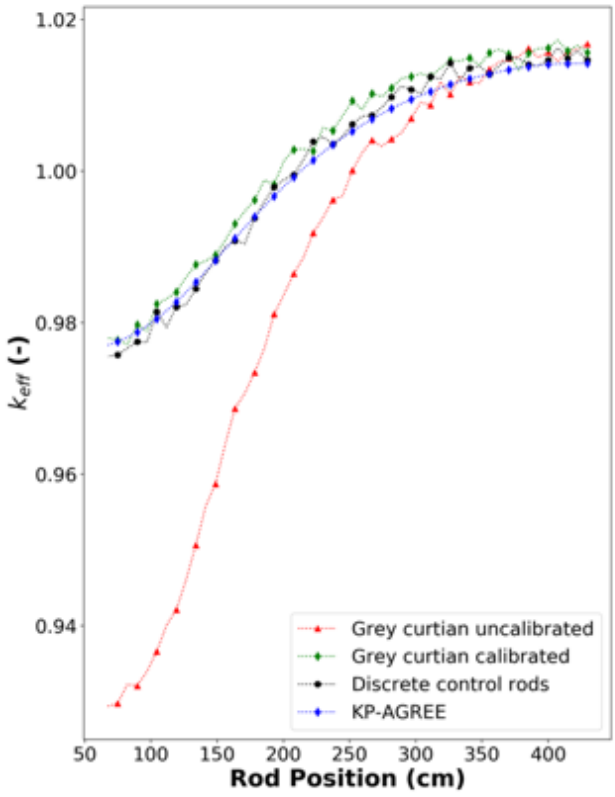

Figure 51. Control rod worth calculation for discrete control rod Serpent model, uncalibrated Serpent grey curtain model, calibrated Serpent grey curtain model, and KP-AGREE with 7 energy group homogenized cross-sections from calibrated Serpent grey curtain model. Fuel temperature set to 959 K and all other component temperatures set to 900 K

5.3.1 Steady State Coupled Neutronics and Thermal-Hydraulics

Figure 52(a) and (b) are contour plots of the gFHR fuel kernel temperature at steady state for an all rods out position and critical rod position, respectively, calculated in KP-AGREE. The coolant temperature, Figure 53, and power density, Figure 54, are lotted similarly. The critical position of the control rods was determined by performing a search on insertion depth in KP-AGREE with thermal feedback. A control rod insertion depth of 205.98 cm from the top of the upper reflector gave a k_{eff} of 0.99999. The worth of the control rod is \$2.07, which was calculated from the difference in k_{eff} from the determined critical position and all rods out core configuration when the fuel temperature was set to 959 K and all other component temperatures set to 900 K in KP-AGREE. As expected, component temperatures and power density have higher maximums and lower minimums when the control rods are inserted into the critical position because of the suppression of the neutron flux at the top of the core. The predicted maximum fuel kernel temperature in the all rods out core configuration at steady state is 1,071 K, the reported maximum average fuel matrix temperature in the benchmark is 1,072 K [20], and the maximum fuel temperature in the MELCOR model is 1,061 K [82]. These three simulations of the gFHR examine different definitions of fuel temperature. These calculations show the predicted fuel kernel temperature according to Eq. 5.5, which is scaled from the fuel matrix temperature by the local power density, the benchmark illustrates individual pebble fuel matrix temperatures, and the MELCOR model uses a lumped parameter model to find the average temperature of the fueled and unfueled regions of the pebble [82].

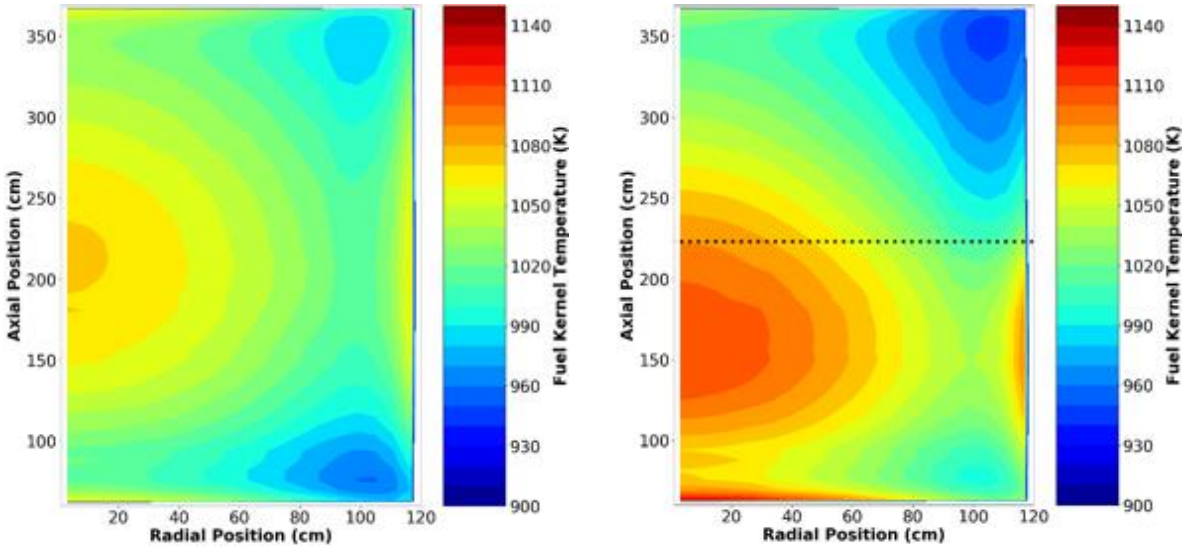

Figure 52. Steady-state fuel kernel temperature prediction in KP-AGREE for all rods out (left) and control rods inserted to the critical position (right) (control rod depth indicated by dashed line)

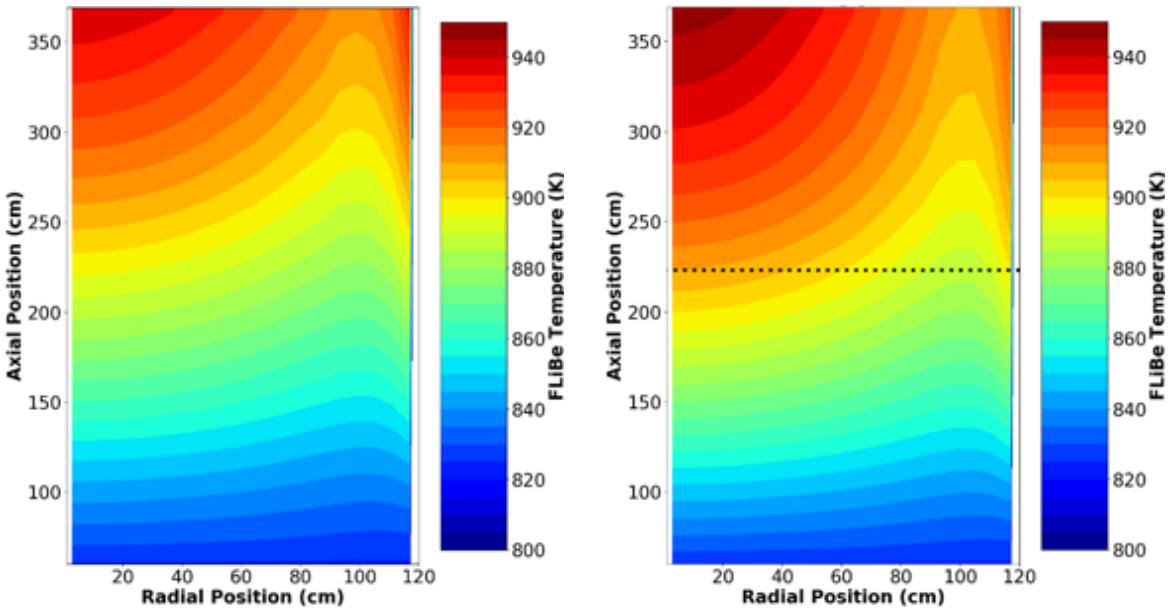

Figure 53. Steady-state coolant temperature prediction in KP-AGREE for all rods out (left) and control rods inserted to the critical position (right) (control rod depth indicated by dashed line)

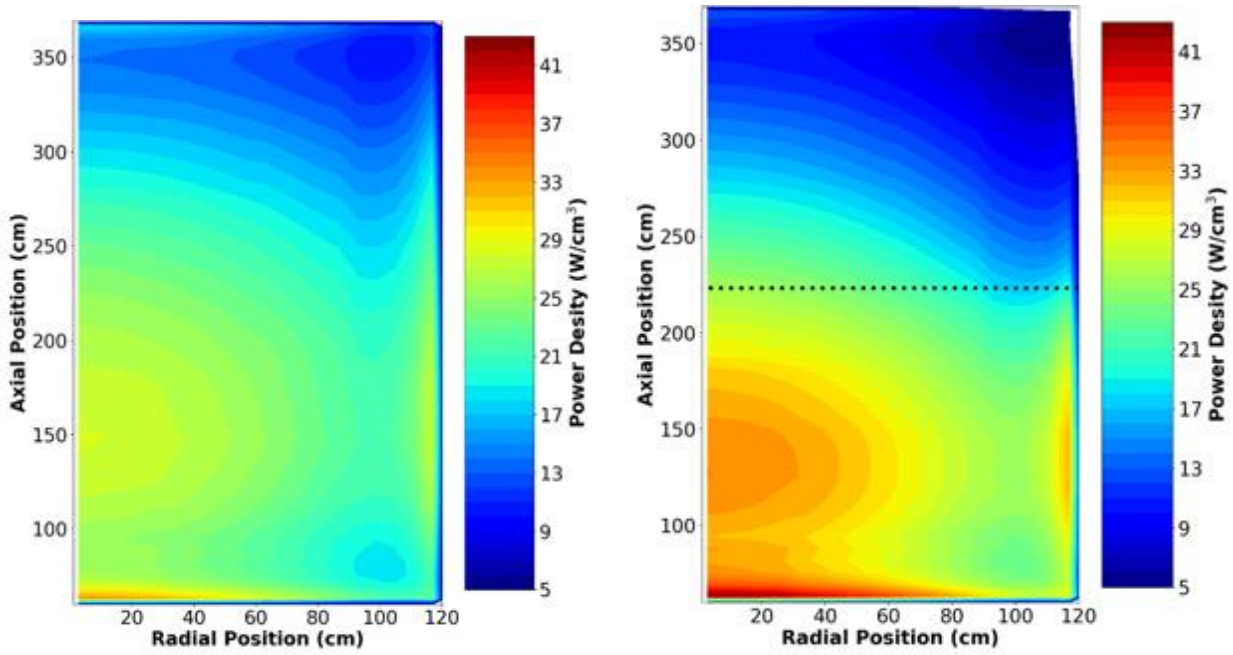

Figure 54. Steady-state power density prediction in KP-AGREE for all rods out (left) and control rods inserted to the critical position (right) (control rod depth indicated by dashed line)

For a more consistent comparison, the predicted maximum average fuel matrix temperature at steady state in the all rods out core configuration is 995K which is 77K lower than the maximum fuel matrix temperature in the benchmark. However, the benchmark used a thermal-hydraulics meshing that obtained individual pebble matrix temperatures, and only a few outlying pebbles predicted a fuel matrix temperature of around 1,072 K. The reduced order modeling in KP-AGREE is too constrained to predict these extremely localized values but is very computationally efficient for transient simulations.

The solution method between these three codes also differs, but this solution has some fundamental overlap with the benchmark model. Both KP-AGREE and the multiphysics tools used in the benchmark rely on the KTA Rule for viscous and inertial forces in the momentum equation [20] [140] as the MELCOR model relies on the Ergun equation for packed beds to determine the pressure drop [82]. Moreover, we use the fuel effective thermal conductivity listed in the benchmark model and equilibrium core distributions. Finally, both of these models and the benchmark model include thermal-hydraulic feedback effects. Satvat et al. (2021) compared average axial power densities with and without thermal feedback and determined that the relative difference in axial power density would change from +2% near the bottom of the core to -3% towards the top [20]. Different axial power density profiles would likely impact the maximum fuel temperature within the core. As for maximum coolant outlet temperature, this model predicted a value of 939 K, the benchmark predicted a value of 942 K [20], and the MELCOR model predicted a value of 923 K [82]. The difference here can likely be attributed to different solution methods as well. The MELCOR model uses a constant

specific heat capacity for FLiBe of 2,380 J/kg K [82] as the benchmark model uses 2,386 J/kg K [20]. Other measurements predict values ranging from 1,840 J/kg K with a precision of about 5% of the mean measured value [157] to 2,368 J/kg K with an accuracy of +/- 20% [158]. Exploring the sensitivity of this parameter on the predicted peak coolant outlet temperature would be of interest for external core component temperature limits, such as the reactor vessel, and remains as future work.

5.4 Transient Results

The transients simulated within this work each have a purpose in developing the understanding of FHRs and fuel behavior. A LOFA in the gFHR is simulated in KP-AGREE to compare solutions to published MELCOR results to build confidence in the transient capabilities of KP-AGREE. An overcooling ATWS is simulated in KP-AGREE to explore the impact that intrinsic safety design features of an FHR have on core power and fuel temperature. Finally, a total CRW transient is simulated to investigate intrinsic safety and design features' impact on core power and fuel temperature. The transient progression in the overcooling and CRW transient follow transient benchmark exercises for the Pebble Bed Modular Reactor (PBMR), which is a gas-cooled pebble bed reactor [149], as the progression of the LOFA transient follows the description in Kile et al. (2022).

5.4.1 Loss of Flow Accident

The LOFA results presented are compared against published MELCOR/SCALE transient models to provide confidence in the modeling of FHR transients using KP-AGREE and Serpent. The LOFA is a transient in which the primary coolant pump is

tripped and the primary heat exchanger no longer transfers heat from the primary coolant loop to the secondary loop. The FHR reactor system is designed to account for this loss of forced coolant and loss of primary heat exchanger by incorporating a Direct Reactor Auxiliary Cooling System (DRACS) that provides adequate decay heat removal if the primary heat exchanger and pump fail. The MELCOR model in Kile et al. (2022) models the primary loop including the DRACS and primary heat exchanger. The modeling of the entire primary loop is required to calculate the FLiBe natural circulation. Since the KP-AGREE model does not model any heat exchangers or pumps, we use the coolant inlet temperature and mass flow rate predicted by MELCOR during a LOFA as boundary conditions. We also use the decay heat curve predicted by Kile et al. (2022) with their neutronics tool, SCALE, for the KP-AGREE model. The decay heat in the KP-AGREE model used a fixed power profile based on steady-state prediction of the power profile. For a fair comparison, the KP-AGREE model is in all rods out configuration and the point kinetics module is used for SCRAM. The transient implemented a 0.01-second time step and was also the only simulation that used a reduced thermal-hydraulics mesh for computational efficiency, significantly decreasing the required runtime. The reduced mesh did not considerably impact steady-state maximum fuel or coolant temperatures. The decay heat, coolant inlet temperature, and coolant inlet mass flow rate used are shown in Figure 55(a) through (c). The gFHR LOFA transient progression as defined by Kile et al. (2022) is as follows:

1. (<0 seconds) Steady-state conditions
2. (0 – 1 second) Pump speed reaches 0, SCRAM occurs, and heat transfer of the primary heat exchanger reaches 0.

3. (1 second – 6 hours) No changes to input, allowing the reactor to respond to the prior changes. For KP-AGREE modeling, we use boundary conditions from LOFA results in Kile et al. (2022) to mimic the natural circulation of the coolant and decay heat of the fuel.
4. (>6 hours) LOFA simulation complete

Figure 56 is the a) overall maximum fuel temperature in the core and b) the maximum coolant outlet temperature during the LOFA transient for the MELCOR and KP-AGREE models for the first three hours of the transient. During the LOFA transient, fuel and coolant temperatures are rapidly reduced due to SCRAM. The MELCOR model predicts that the FLiBe coolant naturally circulates through the primary loop with a much lower flow rate after tripping the pump and primary heat exchanger. The decay heat can mostly be rejected through the DRACS, but the overall coolant temperature still increases. A noticeable turnaround in the coolant inlet temperature occurs when the decay heat approaches the DRACS-rated steady-state heat removal of 2.8 MW [82]. KP-AGREE results predict a higher peak fuel temperature than the MELCOR results, 1,088 K and 1,081 K, respectively, as well as a higher peak coolant outlet temperature than for the MELCOR simulation, 1,084 K and 1,076 K, respectively [82]. Both models predict that the peak fuel temperature is reached within the first hour of the transient before the fuel temperature begins to decrease, coinciding with the trend in coolant inlet temperature.

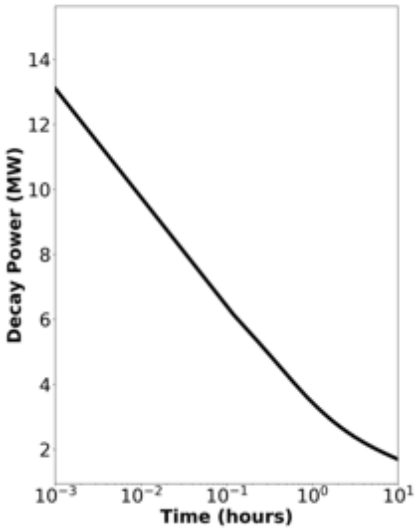

(a)

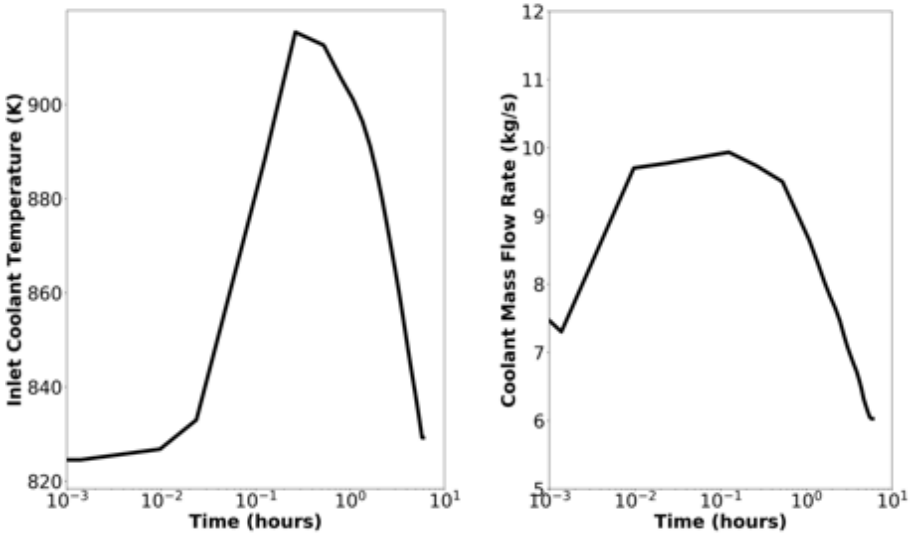

(b) (c)

Figure 55. The a) decay heat, b) inlet coolant temperature, and c) coolant mass flow rate during LOFA from Kile et al. (2022) used as boundary conditions in KP-AGREE [82]

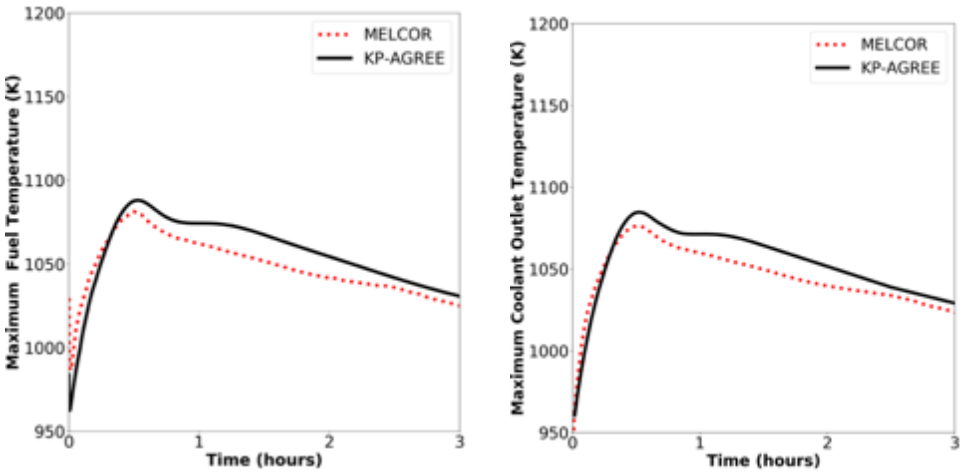

Figure 56. MELCOR and KP-AGREE predicted maximum fuel temperature (left) and maximum coolant outlet temperature (right) during LOFA

Since the power density is drastically reduced because of SCRAM, the predicted fuel kernel temperature and fuel matrix temperature are similar in KP-AGREE according to Eq. 5.5. Both the MELCOR model and the KP-AGREE model predict that the peak coolant outlet temperature briefly approaches the 1,089 K 316H stainless steel vessel temperature limit [67] [82]. This transient focuses more on code-to-code comparison between MELCOR and KP-AGREE to verify the modeling approach. The KP-AGREE model predicts these higher temperatures likely due to the differently assumed thermophysical properties in the fueled layer, FLiBe thermophysical properties, solution method, and power distributions from the MELCOR model.

5.4.2 Overcooling

An overcooling transient may occur due to the accidental triggering of a safety system or by increased heat removal of the primary heat exchanger. Perturbing the coolant temperature to a lower value from steady-state operation increases both core power and fuel temperature because of the negative core temperature feedback of the FHR. The KP-AGREE model had the control rods inserted into the critical position to provide a realistic simulation. A simulation of an overcooling accident was performed, which has a definition similar to an internationally transient benchmark for a gas-cooled pebble bed design [149]. The overcooling definition for the gas-cooled pebble bed benchmark specifies a 10% reduction in coolant inlet temperature from 500 ^{o}C to 450 ^{o}C [149]. Here, the transient definition uses the same 10% reduction for coolant inlet temperature. The overcooling definition for the gas-cooled pebble bed benchmark assumes other parameters such as the coolant mass flow rate and control rod position are

unchanged. We also incorporate these assumptions. The timestep for this transient was set to 0.005 seconds. The progression of this accident is as follows:

1. (<0 seconds) Steady-state conditions
2. (0 – 10 seconds) Coolant inlet temperature reduced from 823 K to 768 K (550 ^{o}C to 495 ^{o}C, 10% reduction)
3. (10 seconds – 300 seconds) No changes to input, allowing the reactor to respond
4. (300– 310 seconds) Coolant inlet temperature increased from 768 K to 823 K (495 ^{o}C to 550 ^{o}C)
5. (310 seconds – 3600 seconds) No changes to input, allowing the reactor to respond
6. (>3600 seconds) Overcooling simulation complete

Figure 57 shows the average coolant temperature, maximum fuel kernel temperature, and the total core power. The plots do not show the full transient simulation, as parameter values remain unchanged after eight minutes. The reduced coolant inlet temperature results in a positive increase in reactivity because of the negative reactivity temperature coefficients. The excess increase in reactivity then begins to increase overall core power and, as a result, fuel temperature increases. The increased fuel kernel temperature provides negative reactivity feedback and eventually can compensate for the excess reactivity introduced by the reduced coolant temperature. The core power, maximum fuel kernel temperature, and average coolant temperature all reach a new equilibrium shortly after the perturbation of the coolant temperature around 45 seconds.

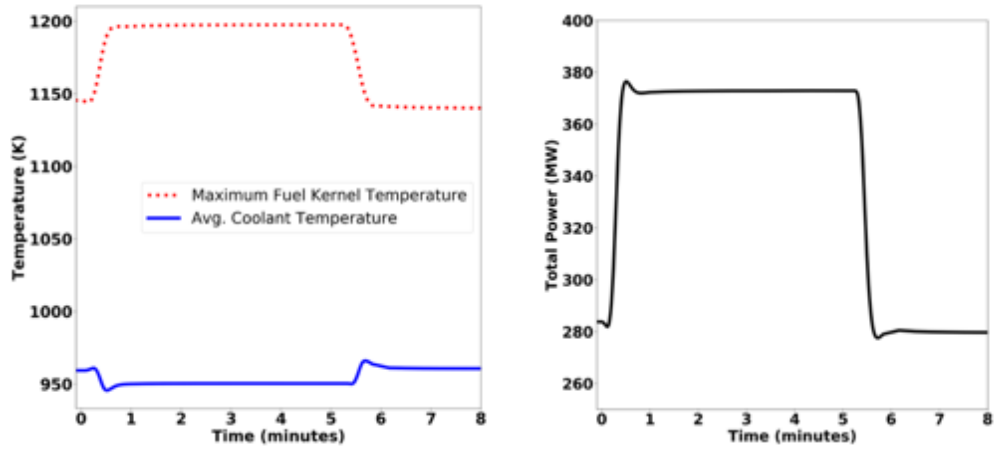

Figure 57. Maximum fuel kernel (left) and average coolant temperature and total power (right) during overcooling transient

The maximum coolant outlet temperature experiences a temperature decrease less than the coolant inlet temperature decrease due to the increase in core power and is not considered to be a significant safety concern. The maximum fuel kernel temperature increases to 1,197 K and total power rises by 32.6% between coolant temperature perturbations. This process is inverted when the nominal coolant temperature is restored and eventually all aspects of the system (power, fuel temperature, and coolant temperature) return to their steady-state value. This transient's results follow a similar response to the gas-cooled pebble bed reactor [24]. Wang (2018) predicted a similar behavior for an overcooling transient in the Mk1 PB-FHR, where a fuel temperature increase of 168 K and a total core power increase of 77.5% was predicted when the coolant inlet temperature was reduced by 100 K [125].

5.4.3 Control Rod Withdrawal

A reactivity-initiated transient is simulated by completely removing the reactivity control mechanism. We note that this CRW definition is a conservative assumption because it is total CRW and an ATWS. We explore this case to provide insight and highlight the safety response of the FHR design under conservative accident conditions. In the CRW simulation, the coolant inlet temperature and mass flow rate are unchanged throughout the transient. The initiating event considered is the inadvertent activation of the control rod drive mechanisms resulting in a slow withdrawal of the grey curtain from the critical position until fully withdrawn. Detailed information on the control rod drive mechanism for FHRs is problem dependent and sparse. Kairos Power submitted a preliminary safety analysis report detailing non-proprietary information relating to their non-power test reactor, Hermes, which included a transient definition for insertion of

excess reactivity. The limiting insertion of excess reactivity for the Hermes reactors is the continuous withdrawal of the highest control element at maximum control element drive speed [159]. The insertion of excess reactivity is bounded by the maximum hypothetical accident, which is determined by dose consequences and is significantly lower than those specified in 10 CFR 100.11 [160]. The insertion of the excess reactivity definition also includes conservative estimates on the shutdown system and initial conditions of the transient. Since the current KP-AGREE uses a grey curtain to represent the control rods and does not include a shutdown system, we elect to follow the transient definition for the PBMR-400 [149] . The focus is to exercise the transient tool and benchmark design to explore FHR accident response. The CRW transient had a timestep of 0.001 seconds. The CRW transient definition is as follows:

1. (<0 seconds) Steady-state conditions
2. (0 – 200 seconds) Grey curtain is withdrawn at a rate of 1 cm/second
3. (200 seconds – 360 seconds) No changes to input, allowing the reactor to respond to the prior changes

   (>360 seconds) CRW transient simulation complete

Figure 58 shows the maximum fuel kernel and coolant outlet temperatures and total power during the transient, respectively. The slow removal of the grey curtain inserts excess reactivity within the core, and the power slowly increases. The increased power results in an increase in the fuel kernel temperature and surrounding components, such as the moderator and FLiBe coolant. The temperature increase of core materials produces negative reactivity, which is enough to compensate for the removal of the grey curtain and limit the power increase.

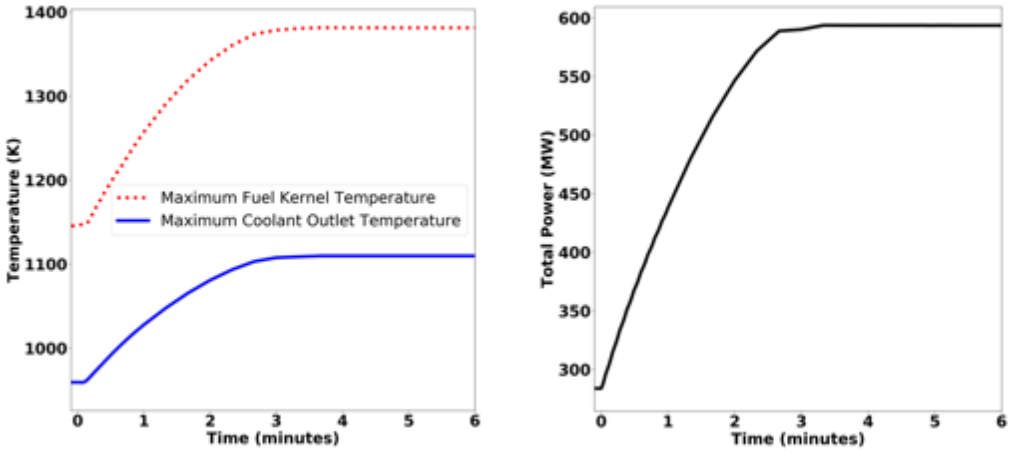

Figure 58. Peak fuel kernel and peak coolant outlet temperature (left) and total core power (right) during CRW transient

The total worth of the grey curtain was predicted to provide \$2.07 of excess reactivity, but due to reactivity temperature feedback, the maximum excess reactivity during the transient at any given point was below \$0.04, with the maximum excess reactivity of \$0.039 around the 20-second mark. Shortly after the grey curtain is fully withdrawn, the maximum fuel kernel and coolant temperatures are 1,381 K and 1,109 K, respectively. The total power increases by approximately 107.5% after completely removing the grey curtain.

5.5 Discussion

The Serpent neutronics results have a fairly good agreement with the gFHR benchmark results [20] with a slight bias in k_{eff} likely due to differences in the treatment of graphite impurities and zone-wise equilibrium fuel composition. KP-AGREE neutronics results have excellent agreement with Serpent results, verifying the selection of energy group structure and cross-section generation procedure from Serpent to KP-AGREE. Steady-state thermal-hydraulics calculations have good agreement to MELCOR calculations [82] and benchmark results [20] with slight biases in the predicted maximum fuel and coolant outlet temperatures, likely caused by thermophysical modeling assumptions. Moreover, LOFA transient results show similar results with reported values with MELCOR [82]. The general agreement in the neutronics, steady state, and transient calculations with KP-AGREE to the reported values in the benchmark and MELCOR calculations verifies the molding approach and builds confidence to explore other transient events for the gFHR.

The slow temperature increases and peak fuel temperature for the LOFA transient would not be expected to challenge fuel integrity given a TRISO temperature limit of

1,723 K [52] and peak coolant outlet temperature briefly reaching vessel temperature limits of 1,089 K [67]. However, the much more rapid fuel temperature and power changes predicted during the overcooling and CRW transient warrant further exploration. Some of the primary failure mechanisms of TRISO-coated fuel particles are buffer layer fracture, thermal decomposition of the SiC layer, kernel migration, cracking of the IPyC, and pressure vessel failure [161] [162]. Efforts have been made to enhance the modeling capabilities of TRISO fuel performance models to accurately predict failure probabilities [163] [164] and to exercise the current state-of-the-art multiphysics tools to assess SiC failure under transient conditions [165] [166]. Ghezzi et al. (2022a) performed sensitivity analyses on the SiC failure probability in BISON under reactivity-initiated accidents. They found that the Weibull modulus and characteristic stress were the most important parameters for SiC failure and that the Weibull modulus is also dependent on energy depositions directly tied to the amount of reactivity inserted [165]. Ghezzi et al. (2022b) further extend the knowledge of SiC failure by considering fuel boundary envelopes for CRE and CRW transient in an HTGR [22]. They concluded that the Weibull modulus and characteristic stress are the most important parameters, and their relative importance is dependent on energy deposition and strain rate. The fuel envelopes that Ghezzi et al. (2022b) used in their study come from Gorton et al. (2020), which only considered maximum fuel temperatures and total power. It can be shown in Figure 52 and Figure 54 that peak fuel kernel temperature and peak power density do not correspond to the exact location in the gFHR, and it would be recommended that location-specific values be used rather than global values. This can also extend to exploring SiC failure probability for different burnup regions within the core.

Shown in Figure 59 are the overcooling and CRW transient results for a) fuel kernel temperature and b) power density for the region of highest burnup, near the axial top and radial center of the core, and c) fuel kernel temperature and d) power density for the region of lowest burnup, near the axial bottom and radial edge of the core, according to Satvat et al. (2021) [20]. The local core response differs between burnup locations and between transients because of the spatial dependence of the problem definition and solution. Therefore, if available, localized parameters including temperature, power density, and burnup would be recommended for fuel performance calculation. Comparing the CRW results to Gorton et al. (2020), results on peak core power, asymptotic power, and fuel temperatures are much less severe because of the lower amount of reactivity inserted, lower rate of reactivity inserted, and more negative reactivity temperature coefficients associated with the gFHR. Ghezzi et al. (2022b) predicted that with a high-quality SiC layer, the failure probability in an HTGR CRE would be extremely low, even under the worst accident conditions. Performing fuel boundary condition envelopes for the gFHR based on transient progression and thermophysical uncertainties would provide a more credible worst-case scenario and require additional research.

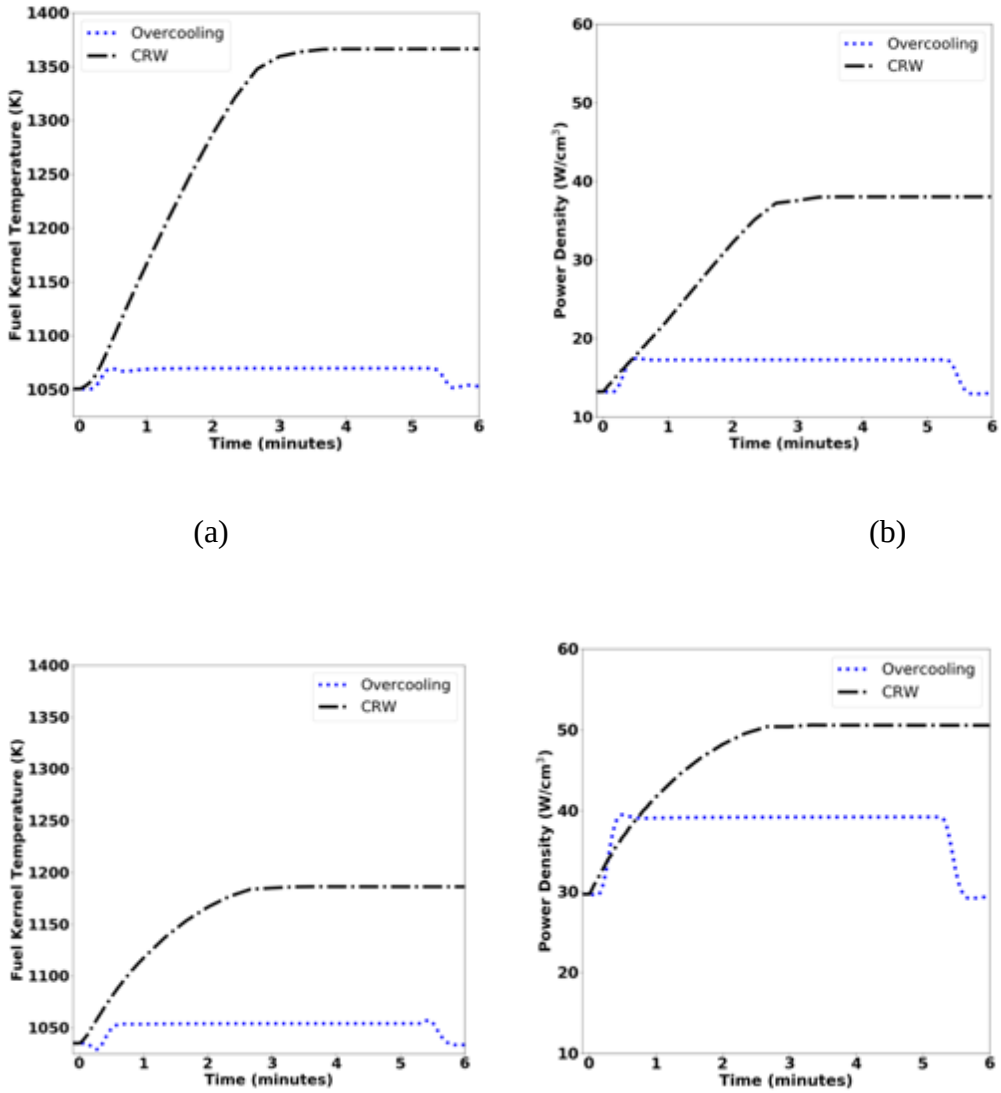

Figure 59. a) Fuel kernel temperature and b) power density at peak burnup location and c) fuel kernel temperature and d) power density at lowest burnup location for the overcooling and CRW transients.

CHAPTER 6
VERIFICATION AND VALIDATION OF MELCOR FOR THE HTR-10 STEADY STATE AND TRANSIENT BENCHMARK

6.1 Background

Pebble Bed High Temperature Reactors (PB-HTRs) is a type of advanced nuclear reactor that is designed to enhance efficiency, safety, and the economics of nuclear energy relative to the current Light Water Reactor (LWR) nuclear fleet. The design features of the gas-cooled PB-HTR have been recognized as one of the most promising reactor concepts to be used in the next generation of commercial reactors [1]. The history of the high temperature pebble bed reactor began with the initial criticality of the German AVR in 1967 [54]. The AVR proved the feasibility of the high temperature gas cooled pebble bed reactor and the larger scale THTR [55] concept soon followed.

The HTR-10 is a 10MW high temperature gas cooled test reactor built and operated by the Institute of Nuclear Energy and Technology (INET) at Tsinghua University [59], first reaching criticality in December of 2000 and fully rated power in January 2003. Prior to the construction of the HTR-10, the only operation experience on pebble bed reactors came from the German AVR and THTR, both of which had numerous problems during operation leading to concerns about public safety and prematurely decommissioned. Of the leading causes as to why the AVR was shutdown indefinitely is the unexpected high pebble temperature experienced within the pebble bed, experiencing a pebble surface temperature 200K greater than expected [167]. One answer as to why the pebble surface temperature was significantly greater than predicted is due to severe coolant flow

reduction [168]. Thus, it is paramount that thermal-hydraulics simulations are able to accurately model the phenomena within a pebble bed reactor.

Fixed fuel reactors, such as the prismatic HTGR, have well defined fuel and coolant channels in a fuel assembly. For a PB-HTR, the fuel pebbles take a packed bed configuration which leads to a non-uniform porosity distribution [24] within the core. Coolant passes through this porous media to extract heat from the fuel elements and has a complex flow path due to the nature of the packed bed. Modeling heat transfer is further complicated by the fuel elements since conduction through a pebble, conduction to localized stagnant fluid, conduction from a contacting pebble or wall, and thermal radiation to a nearby pebble or wall all contribute to the overall heat transfer from a pebble in addition to convection cooling. The necessity of modeling the complexity of the heat transfer of a PB-HTR is to accurately identify fuel hot spots that may challenge fuel integrity during the design and safety analysis of a PB-HTR concept.
Recognizing this modeling challenge and the lack of operation experience for pebble bed high temperature reactors, the International Atomic Energy Agency (IAEA) initiated a Coordinated Research Project on evaluation of HTGR Performance (CRP-5) in 1997 for the purpose of verifying and validating reactor physics and thermal-hydraulic codes for HTGRs [169]. Within a year of achieving full core power, experiments for anticipated transients without SCRAM (ATWS) were carried out in the HTR-10 by INET. These experiments generated a database for the purpose of multiphysics validation under IAEA's CRP-5. Benchmark problems under the CRP-5 were defined and multiple IAEA Member States have participated in these HTR-10 benchmark problems in the efforts to validate the multiphysics codes used for pebble bed high temperature reactor analysis.

This sort of procedure has been performed before for other HTGR concepts such as the AVR and HTTR and the thermal-hydraulic codes ZKIND, DYN-2, TINTE, ACCORD, and TAC-NC was further developed and improved for HTGR modeling [170].

Over the recent years, the NRC has taken steps to support regulatory readiness for licensing non-LWRs under Strategy 2 of the NRC's near-term Implementation Action Plans [81]. One of the most promising codes undergoing continuous development for non-LWR analysis is the systems-level thermal-hydraulics, accident progression and source term code, MELCOR. The development efforts being made to MELCOR center around the NRC action plant describing the need for new modeling capabilities such as a diffusion-based TRISO fuel radionuclide release model, pebble bed convection and radiative heat transfer models, pebble bed flow resistance model, graphite oxidation model, and graphite reflector models [81]. These code implementations have been demonstrated on the PBMR-400 concept, however, an opportunity for code validation of these new features can be realized with the IAEA CRP-5 HTR-10 benchmark. The objective of this study is to use the latest version of MELCOR to validate pebble bed HTGR modeling capabilities. An additional outcome of this work is the code-to-code comparison of MELCOR with other thermal hydraulics tools.

6.1 HTR-10 Design Description and Benchmark Problem

The HTR-10, shown in Figure 60, is based on the HTR-Module [65] concept, which was developed in German as a solution to the challenges faced from previous pebble bed reactor operations.

.

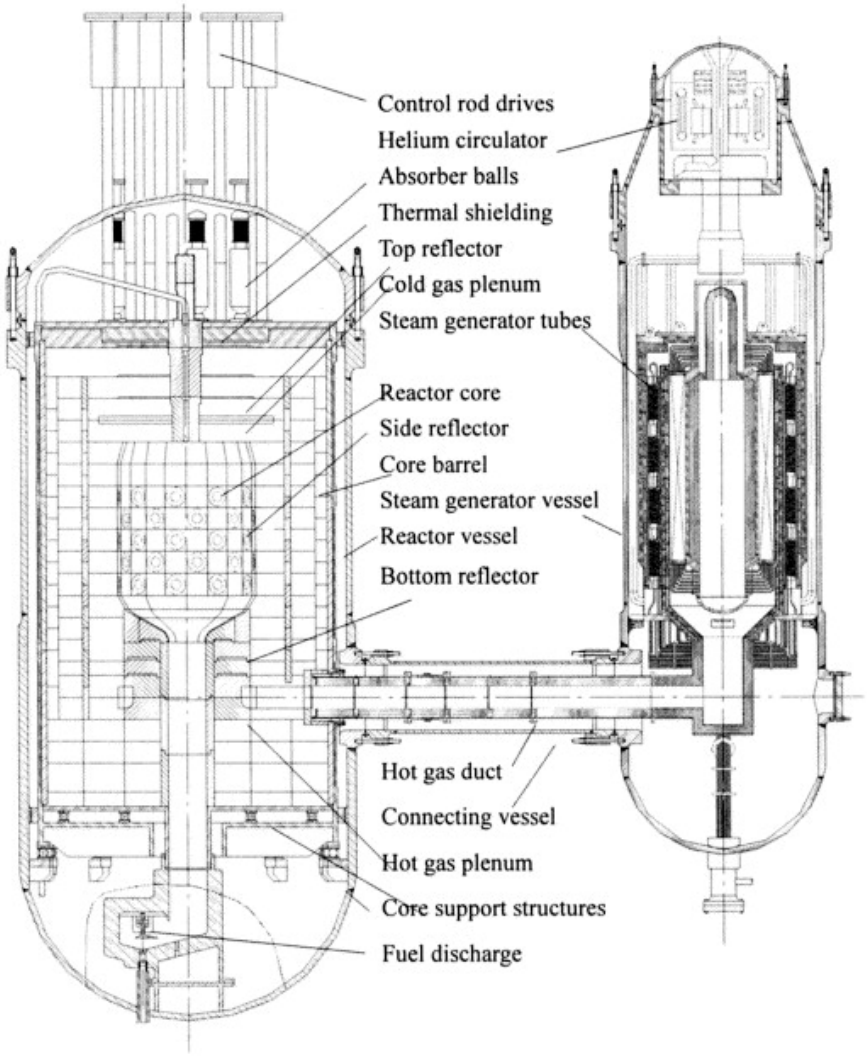

Figure 60. Image of the HTR-10 [59]

The design features of the HTR-Module focused on safe operation and accident response with some key design features being: the use of spherical elements capable of retaining all relevant fission products up to 1600°C, designed such that fuel temperatures never exceed 1600°C even during accidents, passive decay heat removal, more reliably shutdown mechanisms, separate reactor core and steam generator pressure vessel to eliminate overheating in case of primary coolant loop failure . Despite the enhanced safety of the HTR-Module relative to the AVR or THTR, it was never pursued. The HTR-10 inherits many of the same design features of the HTR-Module, but is constructed on a smaller scale and operates at a significantly lower thermal power level, since the primary objective of the HTR-10 is to demonstrate the pebble bed high temperature gas cooled reactor. The design features of the HTR-10 are listed in Table 19. The benchmark description of the HTR-10 model provides some necessary modeling information for standalone thermal-hydraulics calculations. The model also makes assumptions about the true nature of the HTR-10 and does not describe the secondary side of the reactor.

Shown in Figure 61 is the heat conduction model and convection model for the HTR-10. Referring to Figure 61, coolant enters from the inlet, volume number 16, travels through volume number 17 then 7. 1% of the coolant is expected to travel through volume number 11 and through the defueling chute while the remainder travels through volume number 8. 10% of the coolant mass flow rate bypasses the reactor entirely and travels from volume number 8, through 19, and directly to the outlet, 4

Table 19. Design feature of the HTR-10 [59]

Item	Unit	Value
Thermal power	MW	10
Reactor core diameter	cm	180
Average core height	cm	197
Primary helium pressure	MPa	3.0
Average helium temperature at reactor inlet/outlet	°C	250/700
Helium mass flow rate at full power	kg s-1	4.3
Average core power density	MW m-3	2
Power peaking factor		1.54
Number of control rods in side reflector		10
Number of absorber ball units in side reflector		7
Nuclear fuel		UO2
Heavy metal loading per fuel element	g	5
Enrichment of fresh fuel element	%	17
Number of fuel elements in core		27 000
Fuel management	Multi-pass	
Average residence time of one fuel element in core	EFPD	1080
Max. power rating of fuel element	kW	0.57
Max. fuel temperature (normal operation)	°C	919
Max. burn-up	MWd / tHM	87 072
Average burn-up	MWd / tHM	80 000
Max. thermal flux in core (E>1.86 eV)	n cm-2 s-1	3.43x10e13
Max. fast flux in core (E>1 MeV)	n cm-2 s-1	2.77x10e13

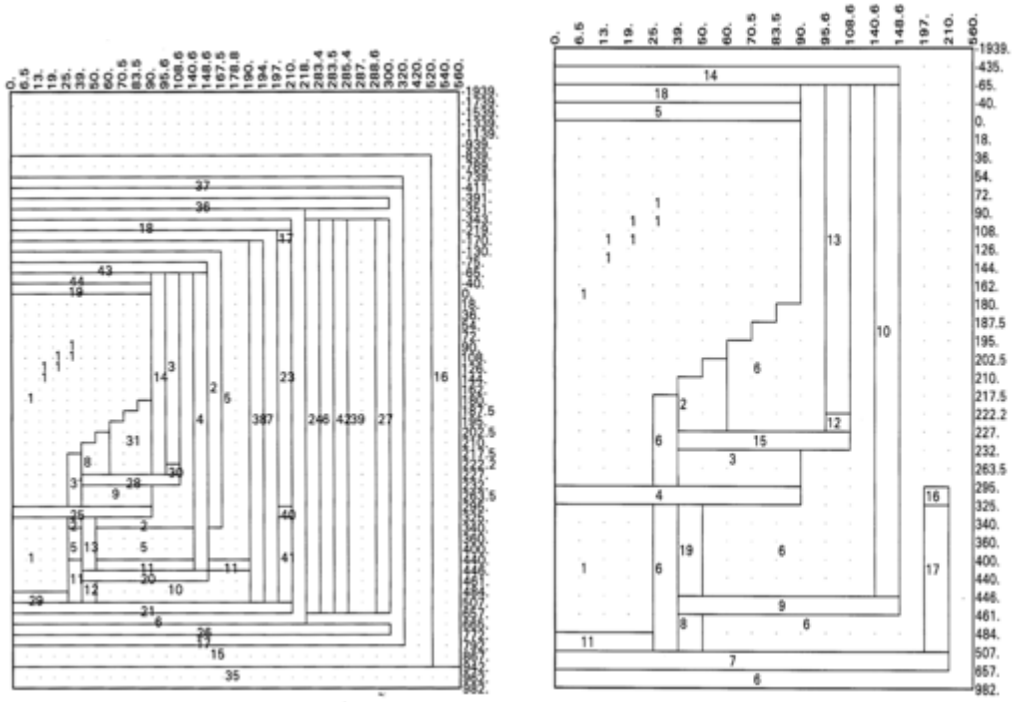

Figure 61. Nodalization from the CRP-5 report conduction model (left) and convection model (right) [169]

The remainder of the coolant mass flow rate through volume number 9, up the coolant riser (volume number 10), and to the top of the core, volume number 14. 2% of the total coolant mass flow rate travels through the control rod region, control volume 13, and the remaining 87% enters the top of the pebble bed core, control volume 5. Coolant in the pebble bed may reach the outlet by traveling down the pebble bed region and defueling chute or exit through the side reflector, control volume 2, then towards the outlet control volume. Coolant from the control rod region bypasses the pebble bed, travels through the side reflector volumes, and then reaches the outlet. The mass flow rates described at each flow path junction should be set by the porosity of the component material and the cross-sectional area of the control volume. Component information on the conduction and convection models for the HTR-10 benchmark are shown in Table 20 and Table 21, respectively. Table 22 is the initial power distribution in units of W/cc for the HTR-10 benchmark. Note, the cone region and defueling cute within the HTR-10 benchmark do not generate any power and are assumed to be unfueled. At initial full power, the fueled pebble bed region is assumed to have a ratio of 57 to 43 fueled to moderator pebbles.

6.3 The MELCOR Model

The primary objective of this work is to verify and validate the MELCOR [153] model with the results in the CRP-5. The experimental results of the CRP-5 report only report steady state temperature and power response during ATWS. As such, this study did not incorporate all of the latest features of MELCOR such as mechanistic source term evaluation or radionuclide release from TRISO particles since there is no experimental data available for comparison.

Table 20. Zones in conduction model [169]

No.	Zone	Material	Mass fraction
1	Pebble bed	Fuel elements	0.61
2	Side reflector without flow path	Graphite	1.0
3	Side reflector with control rod channels	Graphite	0.793
4	Side reflector with coolant flow paths	Graphite	0.862
5	Carbon brick insulator	Carbon bricks	1.0
6	RPV	Steel	1.0
7	Core vessel	Steel	1.0
8	Upper bottom reflector with flow paths	Graphite	0.769
9	Lower bottom reflector with flow paths	Graphite	0.932
10	Reactor bottom steel supporting structure 1	Steel	0.5
11	Reactor bottom steel supporting structure 2	Steel	1.0
12	Reactor bottom annular cold helium flow path	Helium	0.01
13	Leaking flow zone in steel structures	Steel	0.96
14	Side reflector without coolant flow path	Graphite	1.0
15	Concrete	Concrete	1.0
16	Side fluid boundary		1.0
17	Thermal insulation		1.0
18	Helium cavity inside RPV	Helium	1.0
19	Gas plenum at core entry	Helium	1.0
20	Reactor bottom gas rounding flow paths	Helium	1.0
21	Bottom helium cavity inside RPV	Helium	1.0
23	Side helium gap between core vessel and RPV	Helium	1.0
24	Air cavity outside RPV	Air	1.0
25	Hot gas plenum at core bottom exit	Helium	1.0
26	Bottom air cavity outside RPV	Air	1.0
27	Side cavity of reactor cavity	Air	1.0
28	Small plenum in bottom reflector	Helium	1.0
29	Entry throttle of cooling gas for fuel discharging tube	Graphite	0.993
30	Exit throttle of cooling gas for control rods	Graphite	0.998
31	Bottom reflector without flow paths	Graphite	1.0
35	Reactor bottom fluid boundary		
36	Top air cavity outside RPV	Air	1.0
37	Top air cavity of reactor cavity	Air	1.0
38	Side helium gap inside core vessel	Helium	1.0
39	Water cooling panels		
40	Helium entry flow path inside RPV	Helium	1.0
41	Annular flow path inside RPV	Helium	1.0
42	Air gap outside insulating plates of reactor cavity	Air	1.0
43	Helium plenum in top reflector	Helium	1.0
44	Helium flow zone in top reflector	Graphite	0.911

Table 21. Zones in Convection model [169]

No.	Zone	Void Fraction
1	Pebble bed	0.39
2	Flow zone in the upper bottom reflector	0.23
3	Flow zone in the lower bottom reflector	0.068
4	Hot helium plenum at the core bottom exit	1.0
5	Cold helium plenum at the core entry	1.0
6	Non-flowing zone	
7	Cavity of the RPV bottom closure	1.0
8	Annular coolant flow path at reactor bottom	0.99
9	Gas rounding flow path at reactor bottom	1.0
10	Coolant flow paths in the side reflector	0.138
11	Entry throttle of cooling gas for the fuel discharging tube	0.0067
12	Exit throttle of the control rod channels	0.0024
13	Control rod channels in side reflector	0.207
14	Helium plenum in the top reflector	1.0
15	Small plenum in the bottom reflector	1.0
16	Helium entry flow cavity inside the RPV	1.0
17	Annular helium flow path inside the RPV	0.99
18	Flow path zone in the top reflector	0.089
19	Gap leaking flow zone	0.046

Table 22. Power profile for the CRP-5 HTR-10 in W/cc [169]

Z/R(cm)	0	6.5	13	19	25	39	50	60	70.5	83.5	90
0	1.79	1.79	1.79	1.78	1.75	1.71	1.68	1.65	1.63	1.65	
18	2.12	2.11	2.1	2.08	2.06	2.01	1.95	1.89	1.86	1.89	
36	2.46	2.45	2.44	2.41	2.35	2.26	2.18	2.1	2.07	2.09	
54	2.61	2.6	2.58	2.56	2.49	2.43	2.33	2.27	2.22	2.22	
72	2.78	2.77	2.75	2.72	2.65	2.56	2.46	2.39	2.3	2.3	
90	2.84	2.84	2.82	2.79	2.71	2.55	2.45	2.33	2.26	2.26	
108	2.66	2.65	2.63	2.6	2.56	2.49	2.38	2.29	2.22	2.21	
126	2.49	2.49	2.47	2.44	2.37	2.29	2.19	2.08	2.01	2	
144	2.36	2.35	2.33	2.3	2.22	2.11	2.02	1.93	1.85	1.82	
162	2.33	2.32	2.29	2.25	2.16	2.02	1.93	1.83	1.73	1.66	
180	1.53	1.53	1.51	1.48	1.42	1.33	1.27	1.21	1.13	0	
187											

The model developed here only implements four types of packages from MELCOR, 1) Control Volume Hydrodynamics (CVHs), 2) Flow Paths (FPs), 3), Heat Structures (HS) , and 4) CORe package (COR). The CVH and FP packages are representative of the HTR-10 convection model in which CVH defines the coolant volumes and FP connects these volumes. The CVH volumes are defined as the volume of the node in which they resided multiplied by the porosity of the volume. The cross-sectional area for the FPs is defined as the open area between CVH multiplied by the porosity. This approach yielded a similar bypass flow to that specified within the benchmark. Each CVH that resides within the pebble bed is also connected through FPs to neighboring pebble bed CVH. The HS package is intended to describe heat transfer from one CVH to another. HSs were only used at locations physically outside the range of the COR package to describe heat transfer to boundary surfaces. Figure 62 is the MELCOR nodalization diagram for the HTR-10. The diagram is color coded based on the component and type of package used. Areas of white are air, light blue are regions of primarily helium (porosity > 0.5), dark blue is for water, green is for steel components, orange is for thermal insulators, dark grey is for reflector material, light gray is for carbon brick, dark red is for the fueled pebble bed region, and light red is for the unfueled pebble bed region. This diagram captures matches the CRP-5 convections model, although, some of the outer peripheries of the nodalization were not modeled in MELCOR since they extend beyond boundary conditions.

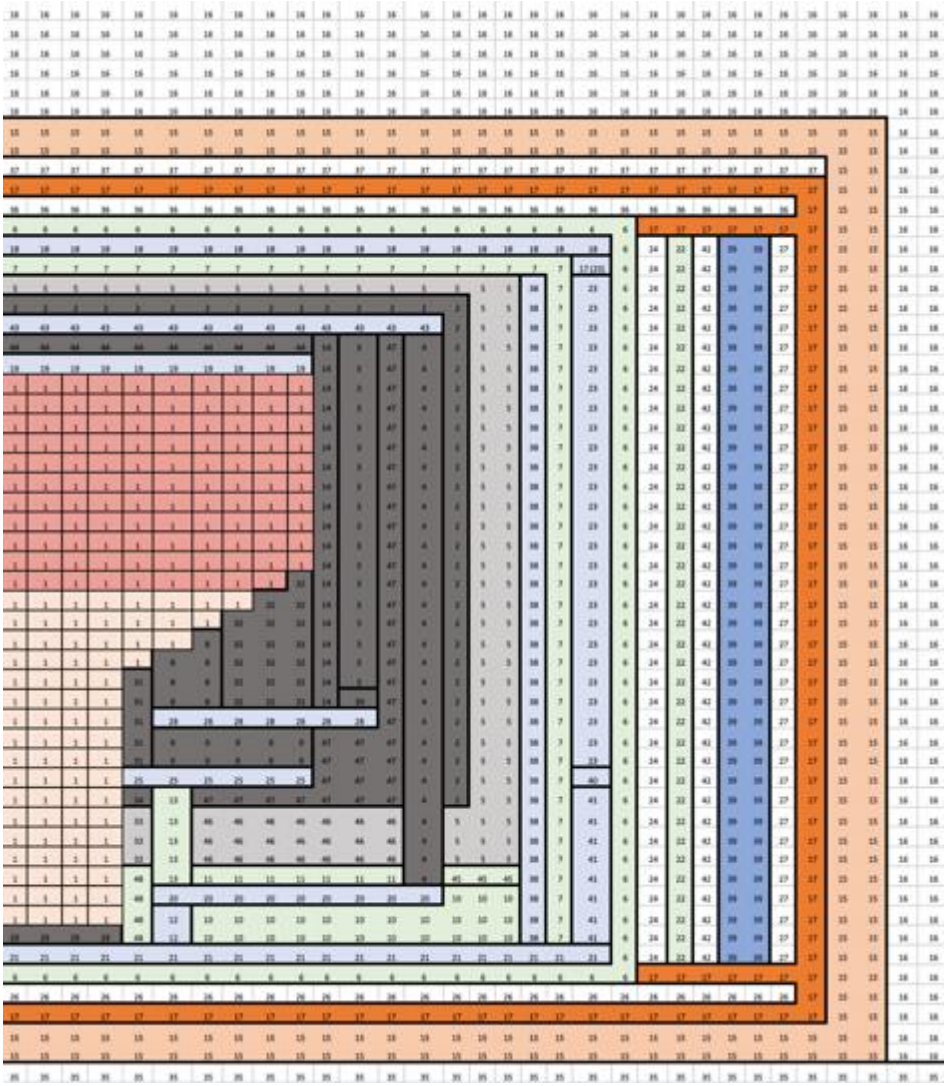

Figure 62. Full nodalization of the HTR-10 model in MELCOR

The COR package models a subregion of the overall nodalization in Figure 62 and is shown in Figure 63. Speaking generally, the types of components that can be modeled within the COR package are fuel material, graphite moderating material, reflector material, support structures, or omitted in the case of purely helium gas regions. Each of these components requires a mass and surface area, which can be easily calculated through the volume of the node and specified properties of the material according to the CRP-5 benchmark. For example, the mass of fuel within a fueled region can be calculated by multiplying the total volume of the node by the porosity and then dividing by the volume of a single pebble to obtain the number of pebbles within that zone. Then applying the fuel to moderator pebble factor to get the number of fuel pebbles within a node, and finally multiplying by the mass of fuel per pebble specified within the CRP-5 to get the total mass of fuel within the node. Surface area calculations and mass calculations of other component materials can follow this same approach [171].

Thermophysical properties for various components have been provided from the CRP-5 report, typically as functions, and provided to the MELCOR model as tabulated inputs. All of the helium thermophysical properties used in the MELCOR HTR-10 model are the default values, which are identical to the values listed in the CRP-5 report. Steel components also assumed MELCOR default stainless-steel thermophysical properties. Thermophysical values for the fuel were default values of UO_2 since the report did not list fuel thermophysical values.

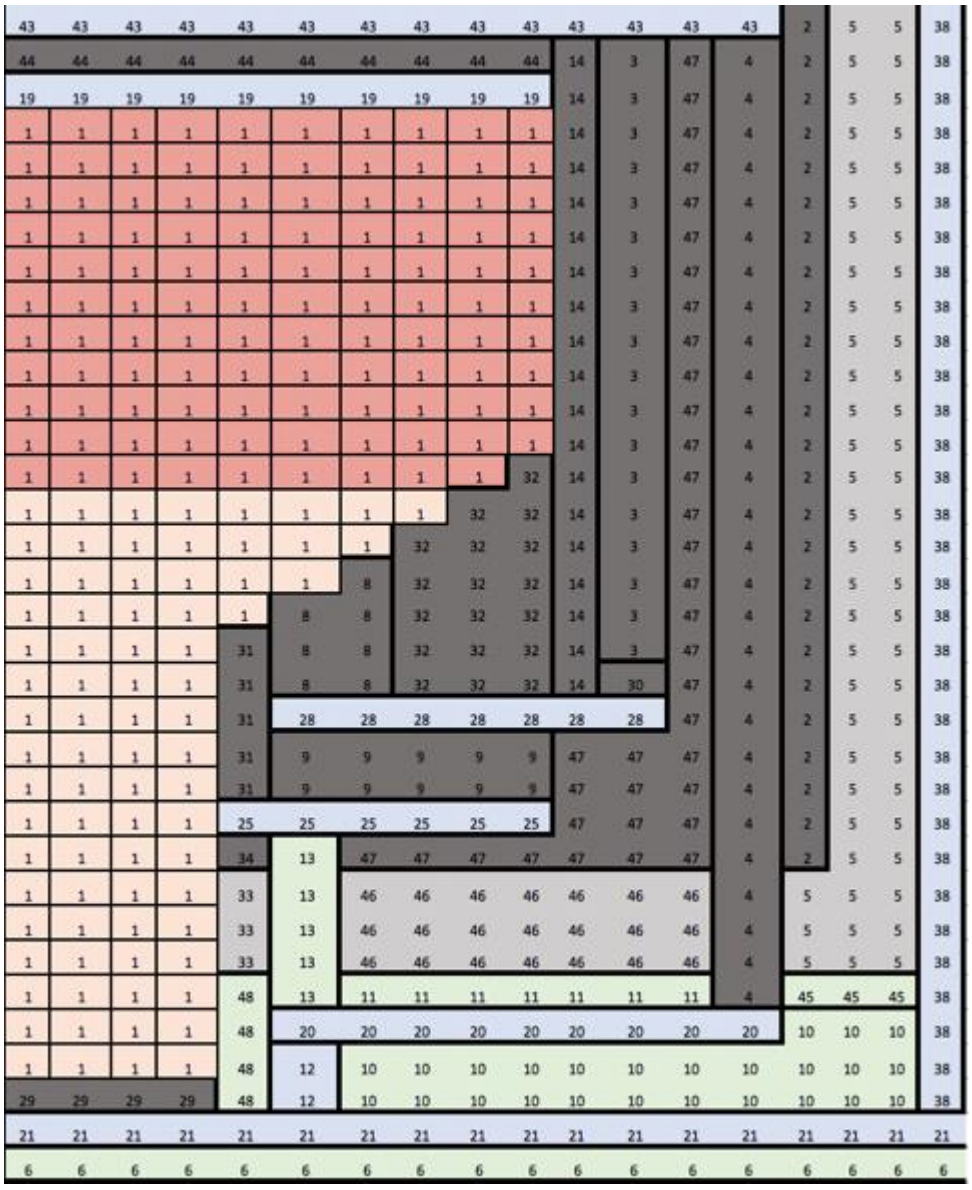

Figure 63. COR package nodalization in MELCOR

For the graphite within the fuel pebble, the density was set to 1720(kg/m^3) [169]. The volumetric heat capacity of the graphite fuel pebble was given as a temperature dependent equation,

$$C_v = 1.75(0.645 + 3.14 * 10^{-3} * T - 2.809 * 10^{-6} * T^2 + 0.959 * 10^{-9} * T^3) \ (Eq. 6.1)$$

Where C_v is the volumetric heat capacity in units of (J/cm^{3}K) and T is the temperature in units of (^{o}C) [169]. The thermal conductivity of the graphite within the fuel element is,

$$\lambda = \left(\frac{-0.3906 * 10^{-4} * T + 0.06829}{DOSIS + 1.931 * 10^{-4} * T + 0.105} + 1.228 * 10^{-4}T + 0.042\right) 1.2768 \ (Eq. 6.2)$$

Where λ is the thermal conductivity in units of (W/cm K) and DOSIS is the fast neutron irradiation dose in units of (1/10^{21}) [169]. The steady state benchmark problem states an initial core at full power so the fast neutron dose was assumed to be zero. The KTA correlation for heat transfer on a pebble was used in this MELCOR HTR-10 model. The MELCOR code does not provide the exact form for the KTA correlation but the following equation gives a similar value to the report [169] when a porosity of 0.39 is assumed,

$$Nu = 9.0 + 0.6Re^{0.7} * Pr^{0.5} \ (Eq. 6.3)$$

Where *Nu* is the Nusselt number, *Re* is the Reynolds number, and *Pr* is the Prandtl number. The equation for frictional pressure drop within the pebble bed used in the MELCOR model and described in the CRP-5 report is,

$$\frac{\Delta P}{\Delta H} = \Psi \frac{1-\epsilon}{\epsilon^3} \frac{1}{d} \frac{1}{2\rho} \left(\frac{m}{A}\right)^2 \ (Eq. 6.4)$$

Where ΔP is the change in pressure over an axial distance, ΔH. ϵ, ρ, d, m, and A are the porosity, coolant density, coolant mass flow rate, and empty cross-sectional area, respectively [169]. The coefficient for friction pressure drop is described as,

$$\Psi = \frac{320}{\left(\frac{Re}{1-\epsilon}\right)} + \frac{6}{\left(\frac{Re}{1-\epsilon}\right)^{0.1}} \ (Eq. 6.5)$$

Currently, multiple reflector materials cannot be easily modeled within MELCOR and in this model, all of the graphite ex-bed components assumed a thermal conductivity of,

$$\lambda = 1.15 * (1.5648 - 0.3162 \log(T + 100)) * F \ (Eq. 6.6)$$

$$F = \frac{F1}{Y - F2} + F3 \ (Eq. 6.7)$$

$$F1 = -0.0054705 + 0.00038214 * \frac{T}{1000} + 0.13487 * \left(\frac{T}{1000}\right)^2 \ (Eq. 6.8)$$

$$F2 = -0.013951 + 0.12064 * \frac{T}{1000} - 0.32955 * \left(\frac{T}{1000}\right)^2 \ (Eq. 6.9)$$

$$F3 = -0.07264 + 0.41459 * \frac{T}{1000} + 0.23149 * \left(\frac{T}{1000}\right)^2 \ (Eq. 6.10)$$

$$Y = \frac{DOSIS}{10} (Eq. 6.11)$$

The neutron irradiation dose, DOSIS, was assumed to be zero for these calculations. The volumetric heat capacity of all graphite ex-bed components was,

$$C_v = 1.75 * (0.645 + 3.14 * 10^{-3} * T - 2.809 * 10^{-6} * T^2 + 0.959 * 10^{-9} T^3) \quad (Eq. 6.12)$$

6.3 Steady State Results

The first benchmark problem in the CRP-5 report is for steady state full power conditions. For the MELCOR model, the set inlet temperature was 250°C and the inlet mass flow rate was set to 4.32 kg/s. A boundary condition was not set for the outlet temperature and the model predicted a temperature of 671.75 ^{o}C which is approximately 30 ^{o}C lower the specified benchmark value of 700°C [169]. Thermocouples located on the side reflector at z=4.04(m) and z=3.10(m) provide experimental data for validation that may be used for model validation. The thermocouples located at z=4.04(m) are approximately at the midpoint of the cylindrical part of the HTR-10 where power is being generated and the thermocouples at location z=3.10(m) are approximately at the bottom of the cylindrical region, just above the cone region. Note that the nodalization in the CRP-5 report defines the axial starting point at the top of the packed bed and increases in the downward direction. Here, we define the axial starting point as the bottom of the stainless-steel component shown in Figure 63 and increases in the upward direction. Redefining the axial discretization is only done for convenience and does not impact the steady state temperature comparison.

Shown in Figure 64 a) is the fuel temperature, b) the coolant temperature, and c) the pebble surface and reflector temperature for the MELCOR HTR-10 model. An edge boundary condition was assumed in this model by setting the side water coolant panels to 50 ^{o}C, located at r=2.85(m). The initial temperature field of the MELCOR model is quite similar to other predictions in the CRP-5 report [169].

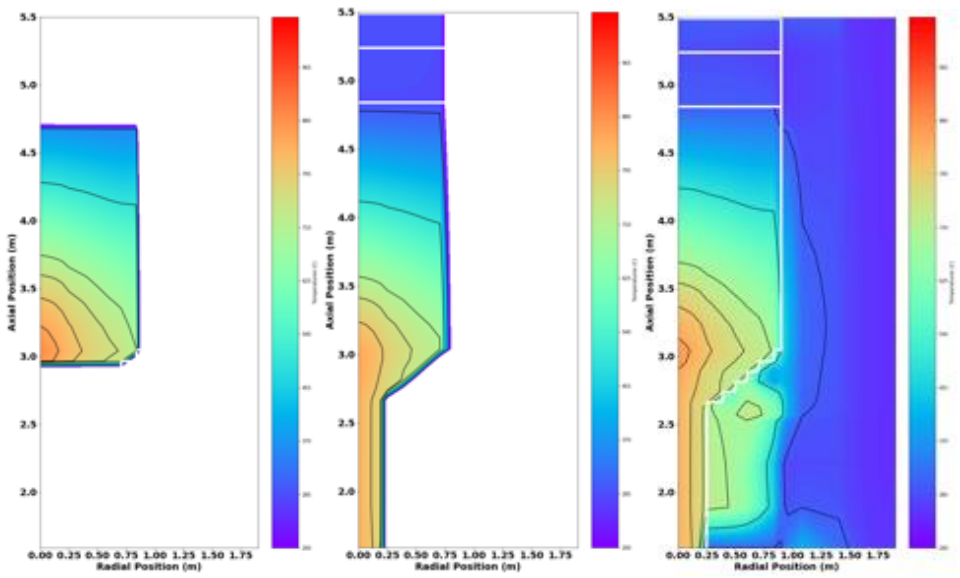

a) b) c)

Figure 64. Steady state temperatures for the a) fuel, b) coolant, and c) pebble surface and graphite reflector

Figure 65 a) and b) are the experimentally measured temperatures of the side reflector at z=4.04(m) and z=3.10(m), respectively. The calculations from other CRP-5 participants are also shown in Figure 65. Table 23 is the calculated RMSE between the calculated side reflector temperatures and the experimental data.

All participants within the CRP-5 report provided the predicted temperature at the thermocouple locations along with the radial temperature profiles. For the MELCOR results, the temperature at specific locations was linearly interpolated between radial nodes. For all calculations at z=4.04(m), all codes over predict the temperature near the pebble bed/reflector interface. For calculations as z=3.10(m), most codes have a much better agreement with the experimental data. For both axial locations, MELCOR predicts the temperature profile better than most of the participants within the CRP-5 report.

6.4 Transient Results

The next benchmark problems within the CRP-5 are ATWS, in particular, a pressurized loss of forced coolant and a control rod withdrawal with a delayed pressurized loss of forced coolant. The initial experimental conditions are different from the steady state full power experiments. Core power is reduced from 10MW to 3MW and the pressure is reduced from 3MPa to 2.5MPa. The coolant inlet temperature is identical to the steady state conditions, but the coolant mass flow rate is reduced to accommodate for the power reduction. The inlet and outlet temperatures specified for the benchmark are 250°C and 650°C. In an attempt to match these conditions by reducing the mass flow rate, the MELCOR model would begin to experience unphysical coolant flow within the pebble bed region.

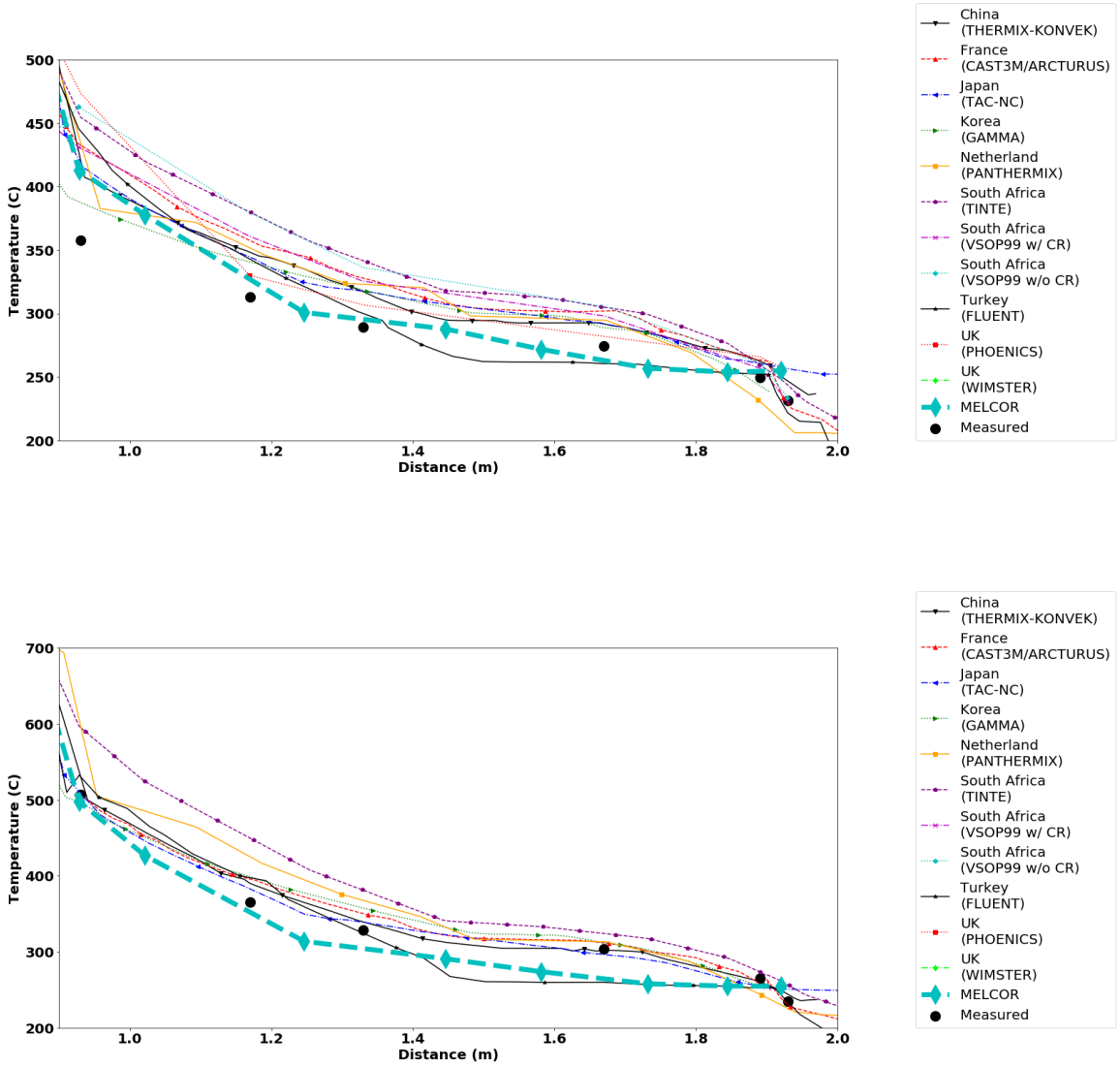

Figure 65. Steady state temperatures within the reflector for z=4.04(m) (top) and z=3.10(m) (bottom) [169]

Table 23. RMSE between measure and calculated side reflector temperatures for CRP-5 participants and this study. Ranked from lowest to highest RMSE.

z=4.04(m)		z=3.10(m)	
Participant (code)	**RMSE (ºC)**	**Participant (code)**	**RMSE (ºC)**
Korea (GAMMA)	20.93	Japan (TAC-NC)	11.77
Netherland (PANTHERMIX)	23.98	China (THERMIX-KONVEK)	12.70
This work (MELCOR)	25.47	France (CAST3M/ARCTURUS)	16.47
Japan (TAC-NC)	28.51	Korea (GAMMA)	21.20
China (THERMIX-KONVEK)	30.27	This work (MELCOR)	22.15
Turkey (FLUENT)	36.64	Netherland (PANTHERMIX)	23.18
South Africa (VSOP99 w/ CR)	40.97	Turkey (FLUENT)	25.90
France (CAST3M/ARCTURUS)	41.69	South Africa (VSOP99 w/ CR)	44.17
UK (PHOENICS)	44.97	UK (PHOENICS)	45.71
South Africa (TINTE)	54.97	South Africa (VSOP99 w/o CR)	47.13
South Africa (VSOP99 w/o CR)	55.51	South Africa (TINTE)	56.93
UK (WIMSTER)	80.57	UK (WIMSTER)	96.98

Flow reversal near the center rings would occur spontaneously prior to any accident perturbations. This would result in a drastic rise in fuel temperatures within the core. For these reasons, we increased the coolant mass flow rate enough so these spontaneous flow reversals would not occur and predicted an outlet temperature of 614.36^{o}C.

The CRP-5 reports an afterheat power vs time measurement to be used in the ATWS calculations, shown in Figure 66. The only available experimental data for these transients within the CRP-5 is the power curve during the transient, temperatures are not reported. Reactor kinetic parameters were also provided within the CRP-5 report for point kinetics. The fraction of delayed neutrons was 0.726%, the prompt generation time was 0.00168s, the fuel and moderator temperature feedback was -2.13pcm/ ^{o}C and -16.2pcm/ ^{o}C, respectively. The definition of fuel temperature reactivity coefficient was defined as the reactivity variation caused by 1°C variation of fuel temperature within the whole core and the moderator temperature reactivity coefficient followed a similar definition. The CRP-5 report does not exactly list which regions are varied in temperature to provide the specified reactivity temperature feedback. For the MELCOR model, the volume averaged fuel temperature for the highlighted regions in Figure 67 was used for fuel reactivity temperature feedback and moderator temperature feedback. Implementing reactivity temperature feedback in MELCOR was achieved with control functions and the embedded point kinetics module. At the time of publication for the CRP-5 report, many participants of the HTR-10 benchmark problems did not report on transient results.

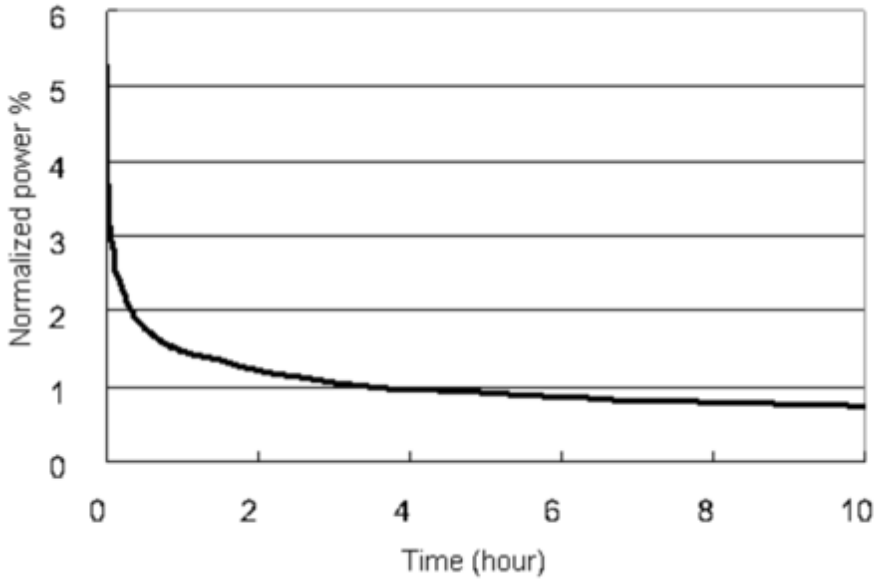

Figure 66. Decay heat curve [169]

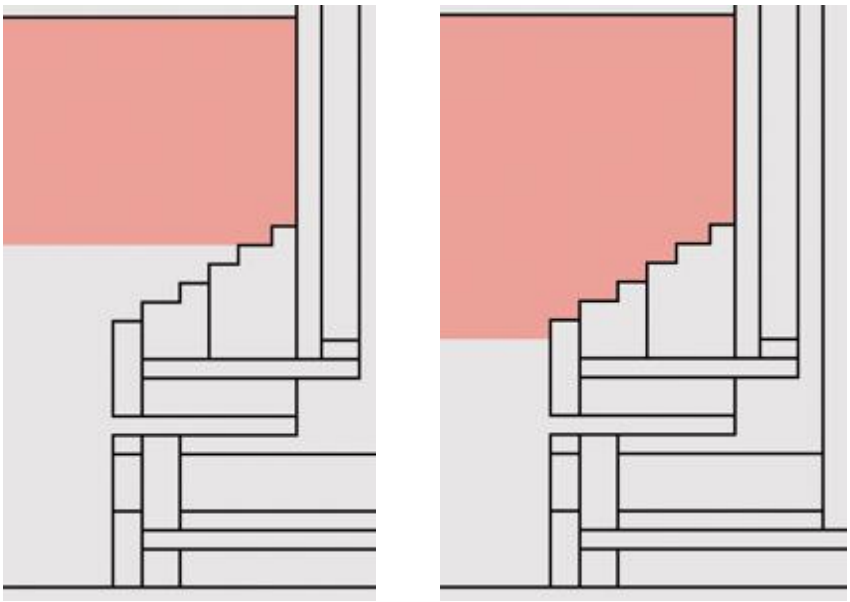

Figure 67. Region for fuel reactivity temperature feedback (left) and moderator reactivity temperature feedback (right).

6.4.1 Pressurized Loss of Forced Coolant

For the PLOFC accident, a coolant mass flow rate coast down curve over the duration of 0 to 12 seconds was implemented in the MELCOR model. The reactor is isolated from the cooling system on the secondary side of the steam generated as well, meaning no natural circulation of the coolant outside the core region. The primary mode of heat mitigation for this transient is the heat transfer through the reflector and to the set radial side boundary. After the coolant mass flow rate is decreased the moderator and fuel temperatures begin to rise and the negative temperature feedback of the components is able to completely reduce the fission power to zero at around 300 seconds, residual decay heat is still present within the core.

Shown in Figure 68 are the short term response of the PLOFC and long term response of the PLOFC. Nearly an hour after the start of the transient, the core temperatures in the HTR-10 drop below their initial temperatures due to a significantly reduced total core power and sufficient passive heat removal. The lower component temperatures introduce positive reactivity into the core and at around 4200 seconds a power peak is observed due to re-criticality. Table 24 is the calculated RMSE between the measured and predicted nominal power for all benchmark participants for the first 300 seconds, ranked from lowest to highest RMSE. Each calculation for the nominal power during the first 300 seconds has a relatively small error compared to the experimental data and ranks relatively close together.

The data used in the transient portions of this work relied on extracting the nominal power from figures within the CRP-5 report, tabulated data was not provided and inherently had some uncertainty.

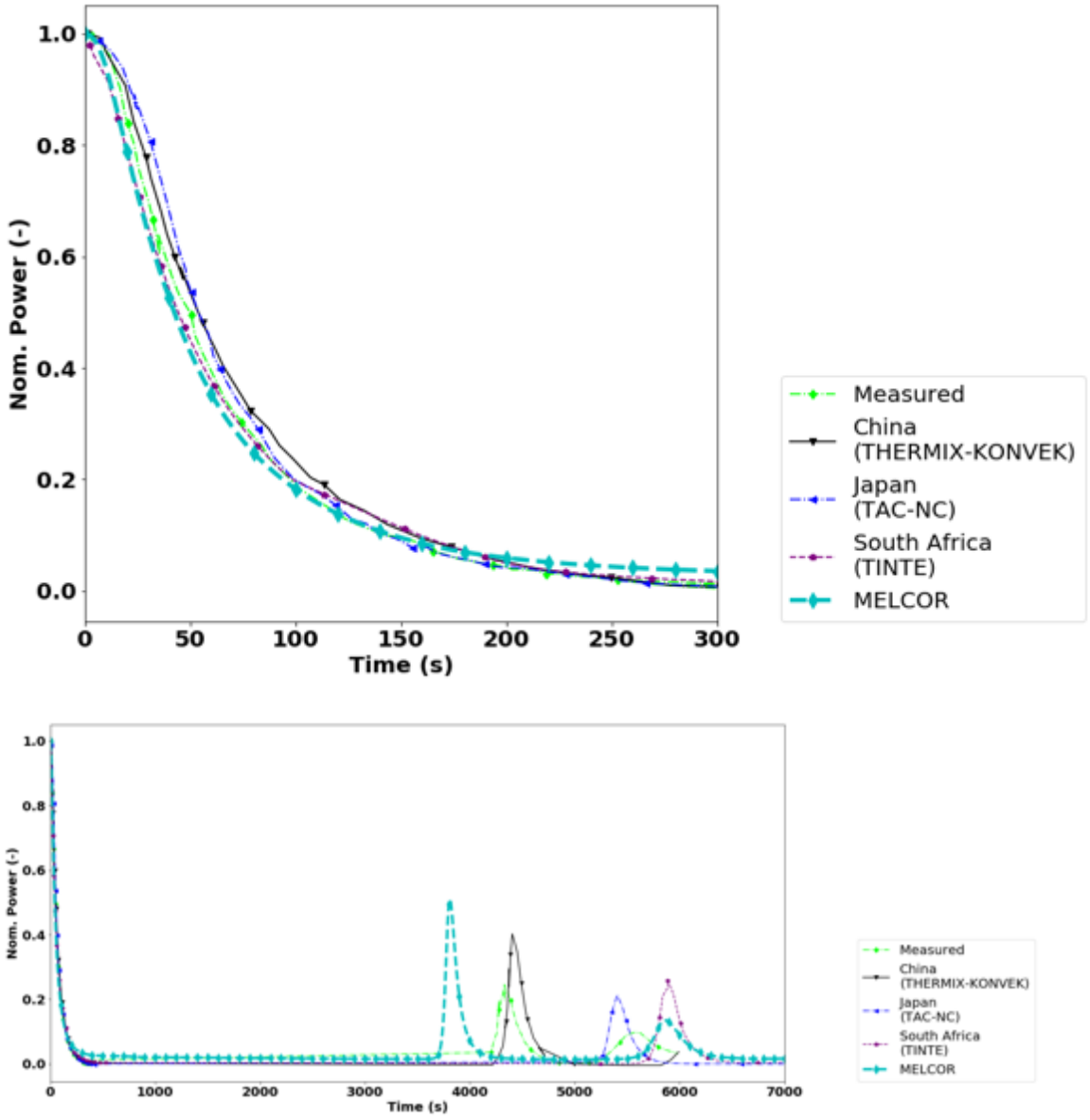

Figure 68. Normalized power during the PLOFC for short term (top) and long term (bottom)

Table 24. RMSE between measure and calculated nominal power during the first 300 seconds of the PLOFC for CRP-5 participants and this study. Ranked from lowest to highest RMSE

Participant (code)	**RMSE (Nom. Power (-))**
South Africa (TINTE)	0.0303
This work (MELCOR)	0.0358
China (THERMIX-KONVEK)	0.0366
Japan (TAC-NC)	0.0531

The long-term calculations for the PLOFC show a noticeable difference in the predicted magnitude of the re-criticality power peak and the occurrence. Each participant predicts a re-criticality peak at a later time than the measure experiment with the exception of these results using MELCOR.

6.4.2 Control Rod Withdrawal

The final benchmark problem for the CRP-5 HTR-10 was a control rod withdrawal transient. In the benchmark definition, $0.68 of reactivity is inserted over the duration of 128 seconds. At around 12 seconds, the flapper valve is closed, isolating the reactor from the rest of the primary loop and reducing the coolant mass flow rate to zero at 80 seconds [7]. The isolation of the reactor from the primary loop is a safety mechanism to mitigate the rise in core power. Just before 50 seconds, the peak power during the transient is experienced before the negative reactivity coefficients due to the rise in moderator and fuel temperature are able to reduce fission power to approximately zero at around 300 seconds. Shown in Figure 69 is a) the short-term power response during the control rod withdrawal and b) the long-term power response. In the long-term effect, a power peak due to re-criticality occurs approximately 3500 seconds into the transient.

Table 25 is the RMSE between the measured and calculated nominal power during the control rod withdrawal transient for the first 300 seconds ranked from lowest to highest. All codes predict the time of the initial power peak quite well, but there is a noticeable discrepancy in the magnitude of the initial peak power.

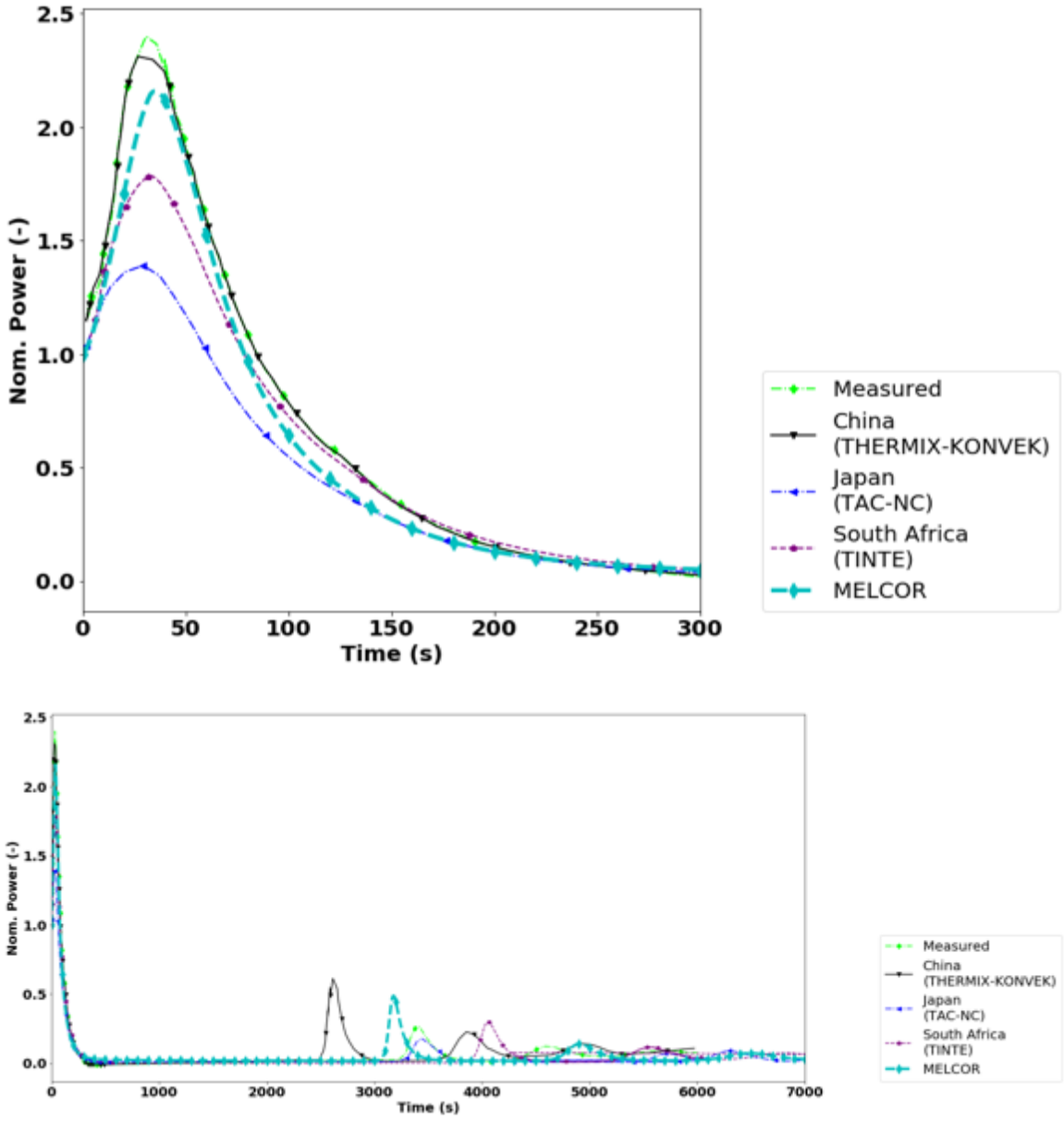

Figure 69. Normalized power during the CRW for short term (top) and long term (bottom)

Table 25. RMSE between measure and calculated nominal power during the first 300 seconds of the CRW for CRP-5 participants and this study. Ranked from lowest to highest RMSE

Participant (code)	**RMSE (Nom. Power (-))**
China (THERMIX-KONVEK)	0.024
This work (MELCOR)	0.169
South Africa (TINTE)	0.268
Japan (TAC-NC)	0.503

Again, the method for data extraction would introduce some uncertainties but the large difference between rankings in RMSE along with noticeable differences in the magnitude of the initial power peak can provide some merit on the comparative agreement between codes. Discrepancies in the magnitude and occurrence of the re-criticality power peak can also be observed between the calculations and experimental measurements.

6.4 Discussion

The MELCOR code has been used for the CRP-5 benchmark problems to assess the steady state and transient response of the HTR-10. Where available within the CRP-5 report, thermophysical properties were used to provide a more consistent basis for comparison. Steady state calculations for the HTR-10 in MELCOR demonstrated good agreement with experimentally measured side reflector temperatures. These MELCOR results had better agreement with the experimental data than the majority of participants in the CRP-5 report. Transient analysis for the HTR-10 demonstrated good agreement with the experimentally measured power for PLOFC and control rod withdrawal events.

In the steady state predictions of temperature profile within the lower region of the side reflector, all calculations within the CRP-5, and these MELCOR results, show fairly good agreement with the experimental data. Temperature predictions for the other side reflector location, which was at the axial midpoint of the pebble bed core at z=4.04m, showed a significant overprediction for all calculations relative to the experimental data. This side reflector location is only slightly higher than the peak axial power within the HTR-10. The power profile within the CRP-5 report is defined such that no power is generated below z=3.04m. The steady state benchmark problem related

to the HTR-10 assumed an Initial Core Full Power (ICFP). The power profile provided in the CRP-5 report does not explicitly mention the operational history or the exact source for the definition of the power profile, other than being provided from reactor physics calculations. One explanation for the overprediction of temperatures at the higher side reflector thermocouple location would be an overestimate of the axial power profile at this region relative to the true power profile. Steady state calculations from South Africa with VSOP99 considered two models, one with control rods inserted and the other without. VSOP99 is capable of performing reactor physics calculations and between the two VSOP99 models and benchmark, the inserted control rod models predicted a different axial power above the side reflector thermocouple location and a different axial power below the thermocouple location, relative to the uninserted control rod model and benchmark. The inserted control rod model predicted a lower temperature profile at the z=4.04m plane near the core/reflector interface and a nearly identical temperature profile for the z=3.10m plane across the entire reflector range relative to the uninserted control rod model. This direct comparison indicates the level of importance in accurately capturing the power distribution within HTR-10.

For transient calculations, all participants in the CRP-5 report, and these results in MELCOR, predicted the initial power response during the PLOFC quite well and had good agreement to experimental the data. All of the calculations in the CRP-5 report predicted a re-criticality power pulse at a later time than the measured experimental data. One parameter that was not provided for the transients was the xenon concentration or xenon reactivity during the transient. The xenon negative reactivity built up may influence the occurrence of the re-criticality power peak. Some participants elected to

calculate the xenon concentration and incorporate the effect into their transient results, but a global definition was not provided. Similarly, a decay heat curve was provided for calculation purposes but some participants used a different prediction based on their calculations. This inconstancy in xenon concentration and decay heat was acknowledged as a potential source of discrepancy between calculations [169]. In the MELCOR results, the effect of xenon was neglected and could be the source for the earlier and large re-criticality power peak. For the RIA results, all simulations underpredicted the initial power pulse. One explanation for this discrepancy that was acknowledged within the report was the definition of reactivity temperature coefficients [169]. In this model, we assumed a volume weighted average temperature for fuel and moderating material. This provided satisfactory results for the RIA benchmark problem. Other solutions did not specify exactly how the reactivity temperature coefficients were defined and applied. If a more rigorous definition of reactivity temperature coefficients would be defined it would be likely that there would be better agreement of the initial power pulse during the RIA between codes.

CHAPTER 7
CONCLUSION

7.1 Microreactor Performance

A pre-conceptual microreactor design was generated based on a HTGR platform with constraints inspired by the Pele Program to explore the performance characteristics of beryllium- and hydride-based moderators in microreactor designs. Two-phase composite beryllium- and hydride-based moderators were considered as an alternative to graphite to mitigate challenges with this material and simultaneously improve reactor performance. FCM UN TRISO fuel was considered alongside AGR UCO TRISO because of the higher fissile material density. The starting point of the microreactor designs came from scoping studies of the INL HTGTR with immediate design changes to its size to meet ISO container constraints. Changes to the fuel assembly were made to be better suited for a microreactor and enhance performance by increasing fuel density.

Parametric studies of TRISO fuel packing fraction and fuel/coolant channel lattice pitch illustrated the higher moderating capabilities of the composite moderators. The enhanced moderating power of these moderators allowed for a higher fuel efficiency than for the graphite moderated microreactor design. Longer cycle lengths and higher discharge burnups were able to be achieved for the composite moderators. The UN TRISO fuel outperformed the UCO TRISO fuel for maximizing reactor cycle length and was selected to be the fuel of choice for this pre-conceptual microreactor design due to its higher fissile material density. The beryllium- and hydride-moderated microreactors also exhibited much lower fuel cycle costs and natural resource requirements per unit energy generated when compared with the graphite design.

The design of a microreactor requires advancements to all aspects of a conventional large scale reactor design. This work demonstrates that by employing composite moderator alternatives to graphite, a much higher performance can be achieved across a variety of metrics. The composite moderators also have the potential to mitigate some of the challenges associated with irradiated graphite due to their enhanced radiation stability, although a full experimental dataset is still not available in the literature. Future work should focus on optimizing additional metrics (i.e., as opposed to only the cycle length) to design a higher performing and more competitive microreactor design.

7.2 Microreactor Safety and Design Space

Thermal-hydraulic design space calculations were performed to identify an operable steady state space for a pre-conceptual microreactor design that utilized graphite-, beryllium, and hydride-based moderators. Reactor physics calculations for power profile, thermophysical properties from experimental research performed alongside this work, maximum allowable temperature limits based on early experimental results or conservative assumptions, and other design limitations specified within the literature were all implemented to identify the design space. The higher thermal conductivity and higher allowable moderator temperature limit of the graphite system allowed for a larger operating space than for either a beryllium- or hydride-based system. The graphite system was shown to be better suited for a process heat application because of higher achievable coolant temperature, but refinement of the temperature limits for the composite moderators will expand the applicable operating window of these designs.

Calculations for EPZ confirmed that microreactors would have a much smaller size than a traditional large-scale reactor. EPZ size was shown to be much smaller for both

the beryllium and hydride moderated designs because of a more thermal neutron spectrum. Levels of key isotope released into the environment showed an expected envelope of EPZ size, and even under a conservative scenario resulting in the total release of fission products, EPZ would still be less than 2 miles for any given design. Reactor safety characteristics such as MTC and FTC were calculated to inform the thermal-hydraulic transient calculation. For all designs, the MTC was shown to be very small as the microreactor design had a high fuel density. FTC was shown to be more negative for lower moderating powers, graphite exhibiting the lowest FTC. A DLFOC accident was calculated and showed that the high volumetric heat capacity of the beryllium- and hydride-based moderators resulted in lower peak moderator and fuel temperature relative to graphite. The strongly negative FTC and high thermal conductivity of the graphite moderator resulted in a much more rapid response to temperature than for the other considered designs but the lower volumetric heat capacity of graphite also resulted in longer times at elevated temperatures.

The cumulative results of this work provide a strong argument for implementing these two-phase beryllium- or hydride-based composites in microreactor technologies. Furthermore, the postulated loss of coolant accident is not expected to challenge any fuel or moderator temperature for any microreactor design. However, the high fuel density and associated high initial excess reactivity could potentially challenge fuel integrity in an overpowered transient, such as a control rod withdrawal. Thermal conductivity of graphite degrades under irradiation while the effects of irradiation on the composite moderators are still unknown. It is likely that the two-phase composites will have some response to irradiation, but depending on how that response compares to graphite, it

could lead to a different conclusion for comparisons between design space, steady state temperature distributions, and transient analysis.

7.3 Multiphysics Modeling of a Pebble Bed Fluoride Salt Cooled Reactor

The pebble bed FHR concept is actively being pursued by industry, academia, and national laboratories. Over recent years, significant effort has been made in developing multiphysics computational tools and methods to further understand the novel reactor concept. A methodology was demonstrated to perform transient analysis on a publicly available pebble bed FHR benchmark with reactivity control mechanisms and used the continuous energy Monte Carlo code Serpent to create homogenized multigroup cross-sections for a pebble bed transient tool KP-AGREE. The approach was verified by comparing Serpent results to standalone neutronic results from KP-AGREE and illustrated with a 7-energy group structure for the KP-AGREE neutron diffusion solution, good agreement regarding power profile, core eigenvalue, and safety characteristics can be achieved. The calibrated grey curtain assumption to accurately model reactivity control mechanisms in KP-AGREE to perform transient analyses for an initially critical core configuration. The control rod worth between KP-AGREE and Serpent models showed good agreement.

This work explored three transients: a LOFA, an overcooling accident, and a CRW accident. LOFA simulation utilized boundary conditions from published MELCOR results and maximum fuel temperature as well as maximum coolant outlet temperature showed good agreement between codes but a noticeable bias between solutions could be

attributed to different modeling assumptions. Results from the overcooling transient predicted a peak fuel kernel temperature of 1,197 K and core power increase of 32.6% but fuel temperature remained below a 1,723 K TRISO temperature limit [52]. Finally, a 1 cm/sec total CRW transient was simulated following the methodology outlined in a pebble bed HTGR coupled neutronic/thermal-hydraulic benchmark. The CRW transient predicted a peak fuel kernel temperature of 1,381 K and peak coolant outlet temperature of 1,109 K, surpassing the 1,089 K core vessel temperature limit [67]. Although these simulations do not surpass fuel temperature limits, further research is needed on defining a credible worst-case scenario in an FHR and performing fuel performance analysis based on transient fuel boundary conditions to determine TRISO performance in FHRs.

7.4 Verification and Validation of MELCOR for the HTR-10 Steady State and Transient Benchmark

With the recent growing interest in pebble bed reactors, there is a noticeable paradigm shift toward extending the capabilities of the current set of reactor physics and thermal-hydraulic tools for pebble bed reactor modeling. Validating these code developing efforts requires experimental data on steady state and transient conditions. The CRP-5 initiated by the IAEA has aimed at addressing the gap in knowledge by setting benchmark problems and distilling experimental data for the efforts of verification and validation of pebble bed HTGRs. We developed a MELCOR mode to simulate steady state and transient conditions for the HTR-10 pebble bed gas cooled reactor and compared results with other solutions and experimental data. The MELCOR results

showed better agreement to measured reflector temperatures than most other simulations, including well known pebble bed thermal-hydraulic tools. A noticeable discrepancy between all calculations and experimental data was observed that may be attributed to the provided initial conditions from the benchmark problem. Transient calculations performed in MELCOR for the HTR-10 showed good agreement with experimentally measured data. Some discrepancies exist in the prediction of the long-term behavior of power during transients between MELCOR and the experimental data but may be attributed to modeling assumptions and lack of modeling data. Overall, MELCOR was able to be verified for pebble bed steady state and transient analysis.

7.5 Review of Key Questions

The set of key questions which have outlined what contributions to knowledge this dissertation aims to provide is as follows:

1. How can an existing HTGR design be modified to reduce its overall size and core power to qualify as a microreactor design and be optimized for reactor cycle length?

An existing HTGR may be modified to qualify as a microreactor primary by increasing fuel density. One of the overall most attractive features of an microreactor is its compact size and long operating cycle. A smaller assembly size is needed to increase the fueled region of a core to compensate for the maximum core size constraint. Assembly geometry should also be optimized with respect to lattice pitch which is shown to be a unique feature of the moderator, fuel loading, and fuel/coolant

configuration. High fuel packing fractions with UN TRISO fuel are recommended to maximize the cycle length of a microreactor.

2. How do composite moderators compare in terms of reactor performance relative to a graphite moderated system?

The composite moderators proposed in this preliminary microreactor design significantly outperform graphite. The shorter mean free path of the neutron in the proposed composite moderators makes them an ideal candidate for microreactors. Beryllium-based moderators can achieve over three times the cycle length of a graphite moderated system and hydride-based moderators can achieve seven times the cycle length. The composite moderators have the potential to have a fuel cycle cost that is less than half that of a graphite moderated design.

3. What is the allowable operational design space for a microreactor and how does a graphite moderated design differ from a composite moderated design?

Due to the lower moderator temperature limits of the composite moderated, the graphite moderated microreactor is shown to be able to operate across a large range of core thermal power, coolant inlet temperatures, and coolant outlet temperatures. The higher allowable coolant temperatures associated with graphite would enable higher thermal-to-electric efficiency. The graphite moderated design would also be better suited for industrial process heat applications. It should be noted that the moderator temperature limits for the composite moderators are a conservative estimate and future demonstrations of improved stability would expand the design space.

4. Would a microreactor designed to provide a long reactor cycle length have an acceptable safety performance?

The preconceptual microreactor design that has been optimized for reactor cycle length shows an acceptable safety performance for a fuel limiting loss of forced coolant accident without intervention, regardless of the moderated used. EPZ size calculations for a coolant channel blockage accident show that the smaller source term of a microreactor design would allow for an EPZ size to be less than 2.5 miles, even under the hyper conservative assumption of no radionuclide containment. The lower concentration of key radionuclides contributing to EPZ size for a composite moderated design relative to a graphite moderated design allow for a smaller EPZ size due to a more thermal neutron spectrum. Safety characteristics, such as temperature feedback, show that a zirconium hydride-based moderated designs would expect a positive moderator temperature feedback but the strong negative fuel temperature feedback is enough to compensate.

5. What accidents would be considered for a pebble bed FHR?

The types of accidents to consider within a pebble bed FHR are, loss of forced coolant accidents, overcooling accidents, and control rod withdrawal accidents. These sets of accidents span the range of postulated events that could occur within a pebble bed FHR and that may contest safety. These accidents should be considered during the early stages of reactor development since they have the most potential to cause fuel failure.

6. Could any of the postulated accidents in a pebble bed FHR contest safety?

The results from the accident considered within this work would not be expected to challenge fuel integrity since TRISO fuel temperature limits were never exceeded. Ex-core components such as coolant piping may be compromised by either a loss of forced cooling accident or a control rod withdrawal accident. The results from these two transients demonstrated a coolant outlet temperature exceeding set temperature limits.

7. Can the systems level code, MELCOR, be verified and validated for a high temperature gas cooled pebble bed reactor?

MELCOR can be verified and validated for a pebble bed HTGR given the recent developments within the code. Relative to other well-known pebble bed thermal hydraulic tools, MELCOR has better agreement to measured steady state reflector temperatures than most codes. For transient analysis, MELCOR can predict the power during the transient as well as other computational tools. Some discrepancies were observed between simulations and experimental measurements which could be attributed to the modeling assumptions used and/or the boundary/initial conditions provided for modeling. Additional experimental data would provide a more confident conclusion on the verification of MELCOR for pebble bed analysis, but this novel work presents very promising results.

REFERENCES

[1] Petti D. et al., "Advanced Demonstration and Test Reactor Options Study," Idaho National Laboratory ART Program, Idaho Falls, 2017.

[2] Shropshire D. E. & Herring J. S., "Fuel-Cycle and Nuclear Material Disposition Issues Associated with High-Temperature Gas Reactors," Miami Beach, FL, 2004.

[3] Wigeland R. et al, "Nuclear Fuel Cycle Evaluation and Screening – Final Report," US Department of Energy, 2014.

[4] Brown N. R. and Revankar S. T., "A review of catalytic sulfur (VI) oxide decomposition experiments," *International Journal of Hydrogen Energy,* vol. 37, no. 3, pp. 2685-2698, 2012.

[5] Carlson D. E. and Ball S. J. , "Perspectives on Understanding and Verifying the Safety Terrain of Modular High Temperature Gas-Cooled Reactors," *Nucl. Eng. Des.,* no. 306, pp. 117-123, 2016.

[6] Petti D. , "Implications of results from the advanced gas reactor fuel development and qualification program on licensing of modular HTGRs.," No. INL/CON-14-32127, Idaho National Lab, Idaho Falls, 2001.

[7] Hu S., Wang R., and Zuying G., "Transient tests on blower trip and rod removal at the HTR-10," *Nuclear Engineering and Design,* vol. 236, no. 5-6, pp. 677-680, 2006.

[8] K. Takamatsu et al., "Spontaneous stabilization of HTGRs without reactor scram and core cooling—Safety demonstration tests using the HTTR: Loss of reactivity control and core cooling," *Nuclear Engineering and Design,* vol. 271, pp. 379-387, 2014.

[9] Lordan-Perret R. et al, "Decommissioning the U.S. nuclear fleet: Financial assurance, corporate structures, and bankruptcy," *Energy Policy,* vol. 154, no. 112280, 2021.

[10] Testoni R. et al., "Review of nuclear microreactors: Status, potentialities and challenges," *Progress in Nuclear Energy,* vol. 138, no. 103822, 2021.

[11] Rosen S. S. ed., "HAZARDS SUMMARY REPORT FOR THE ARMY PACKAGE POWER REACTOR SM-1, TASK XVII," Mallinckrodt Chemical Works (Saint Louis, Mo.), St. Louis, MIssouri, 1960.

[12] Holland A., "Micro Nuclear Reactors: Prospects for Deploying Land-Based Nuclear Energy for the US Military.," 2019. [Online]. Available: www.jstor.org/stable/resrep19826. [Accessed 22 July 2021].

[13] Daehner E. M. et al., "Integrating Operational Energy Implications into System-Level Combat Effects Modeling: Assessing the Combat Effectiveness and Fuel Use of ABCT 2020 and Current ABCT," RAND Corporation, Santa Monica, CA, 2015.

[14] Collopy P. D., "Military Technology Pull and the Structure of the Commercial Aircraft Industry," *Journal of Aircraft,* vol. 41, no. 1, 2004.

[15] Duchnowski E. M. et al, "Reactor performance and safety characteristics of two-phase composite moderator concepts for modular high temperature gas cooled reactors," *Nuclear Engineering and Design,* vol. 368, no. 110824, 2020.

[16] Forsberg C. W. et al., "Molten-Salt Cooled Advanced High-Temperature Reactor for Production of Hydrogen and Electricity," *Nuclear Technology,* vol. 3, no. 144, pp. 289-302, 2003.

[17] Cisneros A. T. et al., "Fluoride-Salt-Cooled, High-Temperature Reactor (FHR) Subsystems Definition, Functional Requirement Definition, and Licensing Basis Event (LBE) Identification White Paper," Universiity of California, Berkely Department of Nuclear Engineering, Berkeley, California, 2013.

[18] Griveau A. et al., "Transient Thermal Response of the PB-AHTR to Loss of Forced Cooling," in *GLOBAL 2007*, 2007.

[19] Brown N. R. et al., "Preconceptual design of a fluoride high temperature salt-cooled engineering demonstration reactor: Core design and safety analysis," *Annals of Nuclear Energy,* vol. 103, pp. 49-59, 2017.

[20] Satvat N. et al., "Neutronics, thermal-hydraulics, and multi-physics benchmark models for a generic pebble-bed fluoride-salt-cooled high temperature reactor (FHR)," *Nuclear Engineering and Design,* vol. 384, no. 111461, 2021.

[21] Gougar H. et al., "Prismatic Coupled Neutronics/Thermal Fluids Transient Benchmark of the MHTGR-350 MW Core Design: Benchmark Definitio," Idaho National Laboratory, Idaho Falls, 2010.

[22] Gorton J.P. & Brown N.R., "Defining the performance envelope of reactivity-initiated accidents in a high-temperature gas-cooled reactor.," *Nuclear Engineering and Design,* vol. 370, no. 110865, 2020.

[23] Holcob D. E. et al., "Fluoride Salt-Cooled High-Temperature Reactor Technology Development and Demonstration Roadmap," Oak Ridge National Laboratory, Oak Ridge , 2013.

[24] Yang, X.T. et al., "Mechanism analysis of quasi-static dense pebble flow in pebble bed reactor using phenomenological approach," *Nuclear Engineering and Design,* vol. 250, pp. 247-259, 2012.

[25] Lu C. & Brown N.R, "Fully ceramic microencapsulated fuel in prismatic high-temperature gas-cooled reactors: Design basis accidents and fuel cycle cost," *Nuclear Engineering and Design,* vol. 347, pp. 108-121, 2019.

[26] GAIN, "Gateway for Accelerated Innovation In Nuclear," 1 July 2021. [Online]. Available: https://gain.inl.gov/SitePages/Industry.aspx. [Accessed 12 April 2022].

[27] I. BWX Technologies, 2022. [Online]. Available: https://www.bwxt.com/. [Accessed 12 April 2022].

[28] X-energy, "X-energy," 2022. [Online]. Available: https://x-energy.com. [Accessed 12 April 2022].

[29] USNC, *USNC MICRO MODULAR REACTOR (MMR BLOCK 1) TECHNICAL INFORMATION,* USNC, 2021.

[30] Stauff N.E et al., "DESIGN OPTIMIZATION OF THE HOLOS-QUAD MICRO-REACTOR CONCEPT," 2021.

[31] Snead L. L. et al, "Fabrication of Two-Phase Composite Moderators as Potential Lifetime Reactor Components," Washington, D.C., 2019.

[32] Oku T. and Ishihara M., "Lifetime evaluation of graphite components for HTGRs," *Nuclear Engineering and Design,* vol. 227, no. 2, pp. 209-217, 2004.

[33] Snead L. L. & Burchell T. D., "Thermal conductivity degradation of graphites due to nuetron irradiation at low temperature," *Journal of Nuclear Materials,* vol. 224, no. 3, pp. 222-229, 1995.

[34] Cheng B. et al., "Ceramic Composite Moderators as Replacement for Graphite in High Temperature Microreactors," *Journal of Nuclear Materials,* vol. 563, p. 153591, 2021.

[35] Snead L. L. et al., "Development and Potential of Composite Moderators for Elevated Temperature Nuclear Applications," *Journal of the Asian Ceramic Society,* vol. 10, no. 1, pp. 9-32, 2021.

[36] Cottrell, W. B. et al., "Operation of the aircraft reactor experiment.," Oak Ridge National Lab., Oak Ridge, TN, 1955.

[37] Linn F. C., "Heat Transfer Reactor Experiment Number 3: Comprehensive Technical Report," General Electric Direct-Air-Cycle Aircraft Nuclear Propulsion Program. s.l.:US Atomic Energy Commission (AEC), 1962.

[38] Karriem V. et al., "Reactor Performance and Safety Characteristics of Beryllium-Based Composite Moderators as Replacements for Graphite in mHTGRs," *Nuclear Technology,* pp. 1-12, 2022.

[39] Jordan W.H. et al., "Aircraft Nuclear Propulsion Program: Quarterly Progress Report for Period Ending December 31, 1956, Part 1 - 5," Oak Ridge National Lab. (ORNL), Oak Ridge, TN, 1957.

[40] Rosenthal M.W. et al., "MOLTEN-SALT REACTOR PROGRAM SEMIANNUAL PROGRESS REPORT FOR PERIOD ENDING FEBRUARY 28, 1969," Oak Ridge National Lab. (ORNL), Oak Ridge, TN, 1969.

[41] Stansfield O.M., "Evolution of HTGR coated particle fuel design," *Energy,* vol. 16, no. 1-2, pp. 33-45, 1991.

[42] Morris R. N. et al, "Performance of AGR-1 High-Temperature Reactor Fuel During Post-Irradiation Heating Tests," *Nuclear Engineering and Design,* vol. 306, pp. 24-35, 2016.

[43] Stempien J.D., "Tritium transport, corrosion, and fuel performance modeling in the Fluoride Salt-Cooled High-Temperature Reactor (FHR).," Diss. Massachusetts Institute of Technology, 2015.

[44] Walton N.A.W et al., "Demonstration of a random sampling approach to uncertainty propagation for generic pebble-bed fluoride-salt-cooled high temperature reactor (gFHR)," *Nuclear Engineering and Design,* vol. 395, no. 15, p. 111843, 2022.

[45] Jiang D. et al., "Fluoride-salt-cooled high-temperature reactors: Review of historical milestones, research status, challenges, and outlook," *Renewable and Sustainable Energy Reviews,* vol. 161, no. 112345, 2022.

[46] Fratoni M. & Greenspan E., "Neutronic Feasibility Assessment of Liquid Salt–Cooled Pebble Bed Reactors," *Nuclear Science and Engineering,* vol. 168, no. 1, 2011.

[47] Idaho National Laboratory, "Next Generation Nuclear Plant Licensing Basis Event Selection White Paper," Idaho National Laboratory, Idaho Falls, 2010b.

[48] Zhao H. & Peterson P. F., "Optimization of Advanced High-Temperature Brayton Cycles with Multiple-Reheat Stages," *Nuclear Technology,* vol. 158, no. 2, pp. 145-157, 2007.

[49] Blandford E. D., "Risk-informed Design Guidance for Advanced Reactor Concepts: a Case Study of the Pebble Bed Advanced High Temperature Reactor," Department of Nuclear Engineering, University of California, Berkeley , University of California, Berkeley , 2008.

[50] Scarlat R. O. et al, "Design and licensing strategies for the fluoride-salt-cooled, high-temperature reactor (FHR) technology," *Progress in Nuclear Energy,* vol. 77, pp. 406-420, 2014.

[51] Petti D. & Maki J., "The Challenges Associated with High Burnup and High Temperature for UO2 TRISO-Coated Particle Fuel," in *Conference: MIT NGNP*, Cambridge, MA, 2005.

[52] Gülol O. Ö. et al., "Performance analysis of TRISO coated fuel particles with kernel migration.," *Journal of Nuclear Materials*, pp. 168-177, 2008.

[53] Brown N. R., "A review of in-pile fuel safety tests of TRISO fuel forms and future testing opportunities in non-HTGR applications," *Journal of Nuclear Materials,* vol. 534, no. 152139, 2020.

[54] Schulten, R., "Pebble bed HTRs," *Annals of Nuclear Energy,* vol. 6, no. 8-10, pp. 357-374, 1978.

[55] Bäumer, R. et al., "Construction and operating experience with the 300-MW THTR nuclear power plant," *Nuclear Engineering and Design,* vol. 121, no. 2, pp. 155-166, 1990.

[56] Fraas, A.P. & Savolainen, A.W., "Design Report on the Aircraft Reactor Test," Oak Ridge National Laboratory, Oak Ridge, TN, 1956.

[57] McNeese, L.E., "Program Plan for Development of Molten-Salt Breeder Reactors," Oak Ridge National Laboratory, Oak Ridge, TN, 1974.

[58] Bardet, P. et al., "Design, analysis and development of the modular PB-AHTR.," in *Proceedings of ICAPP. Vol. 8*, Anaheim, CA, 2008.

[59] Wu, Z. et al, "The design features of the HTR-10," *Nuclear Engineering and Design,* vol. 218, no. 1-3, pp. 25-32, 2002.

[60] Zhang, Z. et al., "Design aspects of the Chinese modular high-temperature gas-cooled reactor HTR-PM," *Nuclear Engineering and Design,* vol. 236, no. 5-6, pp. 485-490, 2006.

[61] Cisneros, A.T et al., "Technical Description of the “Mark 1” Pebble-Bed Fluoride-Salt-Cooled High-Temperature Reactor (PB-FHR) Power Plant," University of California, Berkeley, Berkeley, CA, 2014.

[62] Koster, A. et al., "PBMR design for the future," *Nuclear Engineering and Design,* Vols. 2-3, no. 222, pp. 231-245, 2003.

[63] Moormann, R., "Fission product transport and source terms in HTRs: experience from AVR pebble bed reactor.," Science and Technology of Nuclear Installations, 2008.

[64] Zhang, Z. et al, "Current status and technical description of Chinese 2 × 250 MWth HTR-PM demonstration plant," *Nuclear Engineering and Design,* vol. 239, no. 7, pp. 1212-1219, 2009.

[65] Lohnert, G.H., "Technical design features and essential safety-related properties of the HTR-module," *Nuclear Engineering and Design,* vol. 121, no. 2, pp. 259-275, 1990.

[66] Dai, Z., "Thorium molten salt reactor nuclear energy system (TMSR)," *Molten salt reactors and thorium energy,* pp. 531-540, 2017.

[67] Blanford E. et al., "Kairos power thermal hydraulics research and development," *Nuclear Engineering and Design,* vol. 364, 2020.

[68] U.S. NRC, "Hermes - Kairos Application," 2022.

[69] Mulder, E.J. & Boyes, W.A., "Neutronics characteristics of a 165 MWth Xe-100 reactor," *Nuclear Engineering and Design,* vol. 357, no. 110415, 2020.

[70] Schulenberg, T., High performance light water reactor: design and analyses, KIT Scientific Publishing, 2014.

[71] Worley, B.A. et al., "Comparative Evaluation of Pebble-Bed and Prismatic Fueled High-Temperature Gas-Cooled Reactors," Oak Ridge Natiional Laboratory, Oak Ridge, TN, 1981.

[72] Leppänen J. et al., "Calculation of effective point kinetics parameters in the Serpent 2 Monte Carlo code," *Annals of Nuclear Energy,* vol. 65, pp. 272-279, 2014.

[73] Petti, D. et al., "The DOE advanced gas reactor fuel development and qualification program," *JOM: the journal of the Minerals, Metals & Materials Society,* vol. 62, no. 9, pp. 62-66, 2010.

[74] Bostelmann, F. et al., "SCALE Analysis of a Fluoride Salt-Cooled High-Temperature Reactor in Support of Severe Accident Analysis," OAK RIDGE NATIONAL LABORATORY, Oak Ridge, TN, 2022.

[75] INL, "RELAP5-3D Code Manuals, Volumes I-IV and Appendix A, INL/MIS-15-36723-V2," Idaho National Laboratory, Idaho Falls, 2015.

[76] Strydom G. et al., "Comparison of the PHISICS/RELAP5-3D ring and block model results for phase I of the OECD/NEA MHTGR-350 benchmark," *Nuclear Technology,* vol. 193.1, pp. 15-35, 2016.

[77] Strydom G. et al., "RELAP5-3D Results for Phase I (Exercise 2) of the OECD/NEA MHTGR350 MW Benchmark," Idaho National Laboratory, Idaho Falls, 2012.

[78] Betzler B. R. et al., "Coupled Nuclear-Thermal- Hydraulic Calculations for Fort St. Vrain Reactor," in *Proc. 14th International Topical Meeting on Nuclear Reactor Thermal-Hydraulics (NURETH-14),* Toronto, Canada, 2011.

[79] Ardiansyah H. et al., "Evaluation of PBMR-400 Core Design Steady State Condition with Serpent and AGREE," *Journal of Physics: Conference Series,* vol. 2048, no. 1, 2021.

[80] Seker V. & Downar T. J. , *KP-AGREE KAIROS POWER ADVANCE GAS REACTOR EVALUATOR USER'S MANUAL,* Ann Arbor, MI: Nuclear Engineering and Radiological Sciences University Of Michigan, 2020.

[81] Wagner K.C. et al., "MELCOR integrated severe accident code application to safety assessment of high-temperature gas-cooled reactors," *Nuclear Engineering and Design,* vol. 402, no. 112083, 2023.

[82] Kile R. F., et al, "Assessment of SCALE and MELCOR for a generic pebble bed fluoride high-temperature reactor," *Annals of Nuclear Energy,* vol. 172, no. 109107, 2022.

[83] Corson J., "Development of MELCOR Input Techniques for High Temperature Gas-cooled Reactor Analysis," Texas A & M University, 2010.

[84] Sterbentz J. M. et al., "High-Temperature Gas-Cooled Test Reactor Point Design. No. INL/EXT-16-38296.," Idaho National Lab., Idaho Falls, 2016.

[85] Office of Secretary of Defense (OSD) / Strategic Capabilities Office (SCO), "PELE PROGRAM PHASE I," Arlington, VA, 2019.

[86] Takamatsu K. et al., "Spontaneous stabilization of HTGRs without reactor scram and core cooling—Safety demonstration tests using the HTTR: Loss of reactivity control and core cooling," *Nuclear Engineering and Design,* vol. 271, pp. 379-387, 2014.

[87] Kile R. F. et al., "Transformational challenge reactor analysis to inform preconceptual core design decisions: Sensitivity study of transient analysis in a hydride-moderated microreactor," *Nuclear Engineering and Design,* vol. 376, 2021.

[88] Steinecker Containerhandel, "TECHNICAL SPECIFICATION FOR STEEL DRY CARGO CONTAINER 20' x 8' x 9'6" High Cube," 2012. [Online]. Available: http://www.steinecker-container.de/container/Container2/Spez-Container/Spez_high%20cube20.pdf. [Accessed 25 July 2021].

[89] Bartel N., "Comparative analysis of compact heat exchangers for application as the intermediate heat exchanger for advanced nuclear reactors," *Annals of Nuclear Energy,* vol. 81, pp. 143-149, 2015.

[90] Brown N. R. et al., "Neutronic evaluation of a PWR with fully ceramic microencapsulated fuel. Part I: Lattice benchmarking, cycle length, and reactivity coefficients," *Annals of Nuclear Energy,* vol. 62, pp. 538-547, 2013.

[91] Ade B. J. et al, "Candidate Core Designs for the Transformational Challenge Reactor.," *Journal of Nuclear Engineering,* vol. 2.1, pp. 74-85, 2021.

[92] Betzler B. R. et al., "Design Downselection for the Transformational Challenge Reactor," Oak Ridge National Lab. (ORN), Oak Ridge, TN, 2020.

[93] Varley F. S., "Neutron scattering lengths and cross sectioirn," *Neutron news,* vol. 3.3, pp. 29-37, 1992.

[94] Lu C. et al., "Fully Ceramic Microencapsulated fuel in prismatic high-temperature gas-cooled reactors: Sensitivity of reactor behavior during design basis accidents to fuel properties and the potential impact of the SiC defect annealing process," *Nuclear Engineering and Design,* vol. 345, pp. 125-147, 2019.

[95] Cheng B. et al., "Microstructure and Thermophysical Properties of Sintered BeO-MgO Composite Moderators," 2021.

[96] Bergeron A. et al., "ansformational Challenge Reactor Moderator Material Selection to Achieve Fuel Minimization," *Transactions of the American Nuclear Society* , no. 122, 2020.

[97] Lamarsh J.R. et al., Introduction to nuclear engineering, 3 ed., Upper Daddle River, NJ: Prentice hall, 2001.

[98] Ganda F. et al., "Nuclear energy system evaluation and screening – levelized cost of electricity at equilibrium," Department of Energy Office of Nuclear Energy Fuel Cycle Research & Development, 2013.

[99] Zhongming Z. et al., "Energy Department's Advanced Reactor Demonstration Program Awards $30 million in Initial Funding for Risk Reduction Projects," 2020.

[100] Hernandez R. et al., "Micro heat pipe nuclear reactor concepts: Analysis of fuel cycle performance and environmental impacts," *Annals of Nuclear Energy,* vol. 126, pp. 419-426, 2019.

[101] IAEA, "ACCIDENT ANALYSIS FOR NUCLEAR POWER PLANTS WITH MODULAR HIGH TEMPERATURE GAS COOLED REACTORS," International Atomic Energy Agency, Vienna, 2008.

[102] Lee H.G. et al., "Thermal conductivity analysis of SiC ceramics and fully ceramic microencapsulated fuel composites," *Nuclear Engineering and Design,* vol. 311, pp. 9-15, 2017.

[103] Katoh Y. et al., "SiC/SiC composites through transient eutectic-phase route for fusion applications," *Journal of Nuclear Materials,* Vols. 329-333, pp. 587-591, 2004.

[104] Oetting F. L. et al., "The chemical thermodynamic properties of nuclear materials I. Uranium mononitride," *The Journal of Chemical Thermodynamics,* vol. 4, no. 2, pp. 199-211, 1972.

[105] Snead L. L. et al., "Handbook of SiC properties for fuel performance modeling," *Journal of Nuclear Materials,* vol. 371, no. 1-3, pp. 397-377, 2007.

[106] Rabiti C. et al., "RAVEN User Manual, INL/EXT-15-34123," Idaho National Laboratory, Idaho Falls, 2019.

[107] Victor A. C. et al., "Thermodynamic properties of magnesium oxide and beryllium oxide from 298 to 1,200 K.," *ournal of research of the National Bureau of Standards. Section A, Physics and chemistry ,* vol. 67.4, p. 325, 1963.

[108] Slifka A. J. et al., "Thermal conductivity of magnesium oxide from absolute, steady-state measurements.," *ournal of research of the National Institute of Standards and Technology,* vol. 103.4, p. 357, 1998.

[109] Touloukian Y.S., "Thermophysical Properties of High Temperature Solid Materials. Volume 6. Intermetallics, Cermets, Polymers, and Composite Systems. Part 2. Cermets, Polymers, Composite Systems.," Elements, Macmillan, Lafayett, IN, 1967.

[110] Trofimov A. A. et al., "Thermophysical properties and reversible phase transitions in yttrium hydride," *Journal of Nuclear Materials,* vol. 542, no. 15, 2020.

[111] Uno M. et al., "Thermophysical properties of zirconium hydride and deuteride," *Journal of Alloys and Compounds,* vol. 366, no. 1-2, pp. 101-106, 2004.

[112] Mohanty S. et al., "HTGR Graphite Core Component Stress Analysis Research Program – Task 1 Technical Letter Report," Argonne National Laboratory, Illinois, 2011.

[113] Wysocki A. et al., "Transformational Challenge Reactor Accident Analysis," ANS Virtual Winter Meeting, 2020.

[114] Ma M. et al., "Decomposition kinetics study of zirconium hydride by interrupted thermal desorption spectroscopy," *Journal of Alloys and Compounds,* vol. 645, no. 1, pp. S217-S220, 2015.

[115] Collins H. E. et al., "Planning Basis for the Development of State and Local Goverment Radiological Emergency Response Plans in Support of Light Water Nuclear Power Plants," Nuclear Regulatory Commission, US, 1978.

[116] 10 CFR §. 50.47.c.2, 2021.

[117] Moe W. L., "Opportunities in SMR Empergency Planning," 2014.

[118] Cheng L. et al., "Safety Analysis Report (SAR) for License Renewal for the National Institute of Standards and Technology Reactor – NBSR NBSR 14 Appendix A," National Institute of Standards and Technology (NIST) , Upton, NY, 2004.

[119] Office of Environment, Health, Safety & Security, "Safety Software Quality Assurance - Central Registry," 2021. [Online]. Available: https://www.energy.gov/ehss/safety-software-quality-assurance-central-registry. [Accessed 18 September 2021].

[120] Homann S. G., "HotSpot: Health Physics Codes Version 3.0 User's Guide," National Atomospheric Release Advisory Center (NARAC), Livermore, California, 2014.

[121] EPA, "PAG Manual Protective Action Guides and Planning Guidance for Radiological Incidents," Office of Radiation and Indoor Air Radiation Protection Division U.S. Environmental Protection Agency, Washington, DC, 2016.

[122] Betzler, B. R. et al., "Conceptual Design of the Transformational Challenge Reactor," *Nuclear Science and Engineering,* pp. 1-26, 2022.

[123] Andreades C. et al., "Design Summary of the Mark-I Pebble-Bed, Fluoride Salt–Cooled, High-Temperature Reactor Commercial Power Plant," *Nuclear Technology,* vol. 195, no. 3, pp. 223-238, 2016.

[124] Cisneros A.T., "Pebble Bed Reactors Design Optimization Methods and their Application to the Pebble Bed Fluoride Salt Cooled High Temperature Reactor (PB-FHR)," University of California, Berkeley, Berkeley, CA, 2013.

[125] Aufiero M. & Fratoni M., "Development of multiphysics tools for fluoride-cooled high-temperature reactors," in *PHYSOR*, Sun Valley, ID, 2016.

[126] Wang X., "Coupled neutronics and thermal-hydraulics modeling for pebble-bed Fluoride-Salt-Cooled, High-Temperature Reactor (FHR)," University of California, Berkeley, 2018.

[127] Liu L. et al., "RELAP5 MOD3.2 modification and application to the transient analysis of a fluoride-salt-cooled high-temperature reactor," *Annals of Nuclear Energy,* vol. 101, pp. 504-515, 2017.

[128] O'Grady D. et al., "SAM Code Development for Transient Safety Analyses of Fluoride-salt-cooled High-temperature Reactors," Argonne National Lab. (ANL), Argonne, IL, 2022.

[129] Zhao H. et al., "Development, Verification, and Validation of an Advanced Systems Code KP-SAM for Kairos Power Fluoride Salt–Cooled High-Temperature Reactor (KP-FHR)," *Nuclear Science and Engineering,* vol. 197, no. 5, pp. 813-839, 2023.

[130] Novak A.J. et al., "Multiscale thermal-hydraulic modeling of the pebble bed fluoride-salt-cooled high-temperature reactor," *Annals of Nuclear Energy,* vol. 154, no. 107968, 2021.

[131] Leppänen, J. et al., "The Serpent Monte Carlo code: Status, development and applications in 2013," *Annals of Nuclear Energy,* vol. 82, pp. 142-150, 2015.

[132] Kairos Power LLC, *Equilibrium Core Concentrations,* 2021.

[133] Kairos Power LLC, *gFHR Reactivity Control Mechanism.*

[134] Rintala V. et al., "Modeling of realistic pebble bed reactor geometries using the Serpent Monte Carlo code," *Annals of Nuclear Energy,* vol. 77, pp. 223-230, 2015.

[135] Leppänen J. et al., "Overview of methodology for spatial homogenization in the Serpent 2 Monte Carlo code," *Annals of Nuclear Energy*, vol. 96, pp. 126-136, 2016.

[136] Seubert A. et al., "The 3-D time-dependent transport code TORT-TD and its coupling with the 3D thermal-hydraulic code ATTICA3D for HTGR applications," *Nuclear Engineering and Design*, vol. 251, pp. 173-180, 2012.

[137] Gougar H. et al., "Multiscale Analysis of Pebble Bed Reactors," in *HTR 2010*, Prague, Czech Republic, 2010.

[138] Xhonneux A. et al., "Calculation of the Fission Product Release for the HTR-10 based on its Operation History," in *Proceedings of the HTR 2014*, Weihai, China, 2014.

[139] Seker V. et al., "Modeling prismatic HTGRs with U.S. N.R.C advanced gas reactor evaluator (AGREE)," in *PHYSOR*, Knoxville, TN, 2012.

[140] The Nuclear Safety Standards Commission (KTA), "KTA Program of Standards (14.04.2008), Reactor Core Design for High-Temperature Gas-Cooled Reactor, Part 3: Loss of Pressure through Friction in Pebble Bed Cores”," KTA Standard 3102.3, 1981.

[141] Seker V., "Multiphysics methods development for high temperature gas reactor analysis," Purdue University, 2007.

[142] Park H. et al., "Tightly coupled multiphysics algorithms for pebble bed reactors," *Nuclear Science and Engineering*, vol. 166, no. 2, pp. 118-133, 2010.

[143] Novak A.J. et al., "Pronghorn Theory Manual, INL/EXT-18-44453," Idaho National Lab. (INL), Idaho Falls, ID, 2018.

[144] Novak A.J. et al., "Validation of Pronghorn friction-dominated porous media thermal-hydraulics model with the SANA experiments," *Nuclear Engineering and Design*, vol. 350, pp. 182-194, 2019.

[145] Hu R. et al., "SAM Theory Manual (Rev. 1), ANL/NE-17/4 Rev. 1," Argonne National Lab. (ANL), 2021.

[146] Zou L. & Hu R., "Recent SAM Code Improvement to Heat Transfer Modeling Capabilities, ANL/NSE-19/46," Argonne National Lab. (ANL), 2019.

[147] Nouri-Borujerdi A. & Tabatabai Ghomsheh S.I., "Porous media approach in thermohydraulic analysis of high temperature reactors in pressurized/depressurized cooldown: An improvement," *Progress in Nuclear Energy*, vol. 80, pp. 119-127, 2015.

[148] Nouri-Borujerdi A. & Tabatabai Ghomsheh S.I., "An improved porous media approach to thermal–hydraulics analysis of high-temperature gas-cooled reactors," *Annals of Nuclear Energy*, vol. 76, pp. 485-492, 2015 .

[149] The Nuclear Safety Standards Commission (KTA), "KTA Program of Standards (14.04.2008), Reactor Core Design for High-Temperature Gas-Cooled Reactor, Part 2: Heat Transfer in Spherical Fuel Elements," KTA Standard 3102.2, 1983.

[150] Reitsma F. et al., "PBMR Coupled Neutronics/Thermal-hydraulics Transient Benchmark The PBMR-400 Core Design Volume 1 The Benchmark Definition," No. NEA-NSC-DOC--2013-10. Organisation for Economic Co-Operation and Development, 2013.

[151] Ubbink O., et al., "PBMR fuel kernel model for the prediction of accurate temperature profiles," in *International Conference on Nuclear Engineering*, 2008.

[152] Novak A. J. et al. , "Pronghorn: A multidimensional coarse-mesh application for advanced reactor thermal hydraulics," *Nuclear Technology* , vol. 207.7, pp. 1015-1046., 2021.

[153] Forsberg C.W. et al., "Fluoride-Salt-Cooled High-Temperature Reactor (FHR) with Silicon-Carbide-Matrix Coated-Particle Fuel," in *ANS*, San Diego, CA, 2012.

[154] Humphries L.L. et al., "MELCOR Computer Code Manuals, Vol. 1-3.," SAND2020-0252, Sandia National Laboratories, Albuquerque, NM, 2019.

[155] Bostelmann F. et al., "Key Nuclear Data Impacting Reactivity in Advanced Reactors," Oak Ridge National Lab., Oak Ridge, TN, 2020.

[156] Walton N.A. et al., "Setup and Verification of a SCALE/KENO Platform for Generic FHR Benchmark Calculations," in *PHYSOR*, Pittsburgh, PA, 2022.

[157] Lee C. H. & Yang W. S., "Status Report on Multigroup Cross Section Generation Code Development for High-Fidelity Deterministic Neutronics Simulation System," Nuclear Engineering Division, Argonne National Lab., Argonne, IL, 2007.

[158] Lichtenstein T. et al., "Thermochemical Property Measurements of FLiNaK and FLiBe in FY 2020," Argonne National Lab. (ANL), Argonne, Il, 2020.

[159] Williams D.F., "Assessment of candidate molten salt coolants for the NGNP/NHI Heat-Transfer Loop," Oak Ridge National Laboratory, Oak Ridge, TN, 2006.

[160] Kairos Power, "Enclosure 8 Postulated Event Analysis Methodology, KP-TR-018-NP (Non-proprietary)," Kairos Power LLC, Alameda, CA, 2021.

[161] CFR2021, "10 CFR § 100.11," 2021.

[162] Verfondem K. & Nabielek H., "Triso fuel performance modeling and simulation.," 2020.

[163] Powers J.J. Wirth B.D., "A review of TRISO fuel performance models," *Journal of Nuclear Materials,* vol. 405, no. 1, pp. 74-82, 2010.

[164] Jiang W. et al., "TRISO particle fuel performance and failure analysis with BISON," *Journal of Nuclear Materials,* vol. 548, 2021.

[165] Collin B. et al., "TRISO Fuel Performance Modelling with BISON," in *HTR 2021*, 2021.

[166] Ghezzi C.G. et al, "Sensitivity analysis applied to SiC failure probability in TRISO modeled with BISON," *Progress in Nuclear Energy,* vol. 153, 2022a.

[167] Ghezzi C.G. et al., "TRISO SiC Failure Probability for Reactivity Initiated Accidents in High-Temperature Gas-Cooled Reactors," *Nuclear Science annd Engineering,* vol. 196, no. 11, 2022b.

[168] Moormann R., "A safety re-evaluation of the AVR pebble bed reactor operation and its consequences for future HTR concepts," in *In: Proc. 4th. Int. Topl. Mtg. High Temperature Reactor Technology,*, Washington, DC, 2008.

[169] Sobes V. et al., "Individual pebble temperature peaking factor due to local pebble arrangement in a pebble bed reactor core," *Nuclear Engineering and Design*, vol. 241, no. 1, pp. 124-133, 2011.

[170] Tyobeka B. et al., "Results of the IAEA CRP5–Benchmark Analysis Related to the PBMR-400, PBMM, GT-MHR, HTR-10 and the ASTRA Critical Facility.," 2010.

[171] Chen F. et al., "Post-test analysis of helium circulator trip without scram at 3 MW power level on the HTR-10," *Nuclear Engineering and Design*, vol. 239, no. 6, pp. 1010-1018, 2009.

VITA

Edward M. Duchnowski was born in Pittsburgh, Pennsylvania in 1996. He graduated from the Pennsylvania State University in 2019 with a Bachelor of Science degree in Nuclear Engineering. He went on to earn his Master of Science degree in Nuclear Engineering from the University of Tennessee, Knoxville in December of 2020. He has accepted a R&D position with Sandia National Laboratories, which he intends to begin after earning his PhD in Nuclear Engineering in December, 2023.